Aalto University
School of Chemical
Engineering

**Lotta Kleemola**

# PRECIOUS METALS REACTION MECHANISMS IN COPPER MATTE – SLAG SYSTEM

Master's Programme in Chemical, Biochemical and Materials Engineering

Major in Functional Materials

Master's thesis for the degree of Master of Science in Technology submitted for inspection

Supervisor Prof. Ari Jokilaakso

Instructors M.Sc. Lassi Klemettinen

M.Sc. Xingbang Wan

Aalto University
School of Chemical
Engineering

Aalto University, P.O. BOX 11000, 00076
AALTO
www.aalto.fi

**Abstract of master's thesis**

**Author** Lotta Kleemola

**Title of thesis** Precious metals reaction mechanisms in copper matte-slag system

**Degree Programme** Master's Programme in Chemical, Biochemical and Materials Engineering

**Major** Functional materials

**Thesis supervisor** Ari Jokilaakso

**Thesis advisor(s) / Thesis examiner(s):** Lassi Klemettinen, Xingbang Wan

**Date** 20.06.2019 **Number of pages** 106+7 **Language** English

## Abstract

The amount of WEEE generated annually is growing, and effective means of recycling are required, in order to sustainably handle the growing waste quantity. WEEE is not only considered waste, but also a secondary resource of materials, including precious metals. Electronic devices can contain precious metals more than their respective primary ores, which in many cases are depleting. Pyrometallurgical methods of WEEE recycling are advantageous, because the processes can accept many forms of scrap and there are existing facilities for WEEE smelting. Downside of pyrometallurgical recycling route is the environmental concern that arises from high level of energy consumption.

In this thesis, the time-dependent behaviour of precious metals in copper matte-slag system in simulated copper flash smelting conditions is studied. In the literature survey, the distributions of precious metals in equilibration studies were investigated. In the experimental part, the behaviour of precious metals is studied in air and argon atmospheres. Precious metals selected for this work are gold, silver, platinum and palladium. Compositional data was acquired with SEM-EDS, EPMA and LA-ICP-MS.

The analyses indicated that the precious metals favour the copper and iron-bearing phases over slag phase and that formation of precious metal droplets and migration to matte phase begin almost instantly, when the system reaches high temperature. Precious metals concentrated in the matte phase as large droplets or smaller cluster distributed in the matte. There was significant scatter in the results with 300 s and 20 min contact time in air and argon atmospheres, respectively.

For future work, it is suggested that the contact times in the proximity of 300 s in air atmosphere and 20 min in argon atmosphere are studied in more detail. The scatter in the results suggest the existence of some rate-limiting factor. In addition, the chemical dissolution behaviour of precious elements and their possible existence as sulphides in matte would require more detailed analysis. The formation of large precious metal droplets in air atmosphere should be studied further and the analysis of sample cross sections should be more extensive in order to find possible large droplets.

**Keywords** Precious metals, kinetics, WEEE, copper smelting

Aalto-yliopisto
Kemian tekniikan
korkeakoulu

Aalto-yliopisto, PL 11000, 00076
AALTO
www.aalto.fi

**Diplomityön tiivistelmä**

**Tekijä** Lotta Kleemola

**Työn nimi** Jalometallien reaktiomekanismit kuparikivi-kuona systeemissä

**Koulutusohjelma** Master's Programme in Chemical, Biochemical and Materials Engineering

**Pääaine** Functional materials

**Työn valvoja** Ari Jokilaakso

**Työn ohjaaja(t)/Työn tarkastaja(t)** Lassi Klemettinen, Xingbang Wan

**Päivämäärä** 20.6.2019 **Sivumäärä** 106+7 **Kieli** Englanti

## Tiivistelmä

Muodostuvan sähkö- ja elektroniikkaromun määrä kasvaa vuosittain ja tämän kasvavan jätemäärän kestävä käsittely vaatii tehokkaita kierrätysmenetelmiä. Elektroniikkaromua ei nähdä pelkästään jätteenä, vaan myös sekundäärisenä raaka-aineresurssina esimerkiksi jalometallien osalta. Elektroniset laitteet voivat sisältää jalometalleja enemmän kuin niiden primääriset malmit, jotka ovat monissa tapauksissa köyhtymässä. Pyrometallurgiset prosessit ovat edukkaita elektroniikkaromun kierrätysmenetelmiä, koska niiden syötemateriaalina voidaan käyttää monia eri romulajeja, ja romun käsittelyyn on jo olemassa olevia laitoksia. Pyrometallurgisten kierrätysmenetelmien haittana on suuresta energiankulutuksesta aiheutuva ympäristörasite.

Tässä diplomityössä on tutkittu jalometallien ajasta riippuvaa käyttäytymistä kuparikivi-kuona -systeemissä kupariliekkisulatusuunissa vallitsevissa olosuhteissa. Kirjallisuusosuudessa tarkasteltiin jalometallien jakautumista tasapainotuskokeissa. Kokeellisessa osuudessa jalometallien käyttäytymistä tutkittiin ilma- ja argon-atmosfäärissä. Työhön valitut jalometallit olivat kulta, hopea, platina ja palladium. Näytteiden koostumusta analysoitiin SEM-EDS:lla, EPMA:lla sekä LA-ICP-MS:lla.

Työn tulokset toivat ilmi, että jalometallit suosivat kuparikivifaasia kuonan sijaan, ja jalometallipisaroiden muodostuminen sekä jalometallien siirtyminen kivifaasiin alkavat lähes välittömästi, kun systeemi saavuttaa korkean lämpötilan. Jalometallit esiintyivät suurina pisaroina tai dispersioina jakautuneena kivifaasiin. Tuloksissa havaittiin merkittävää hajontaa 300 sekunnin ja 20 minuutin kontaktiajoilla ilma- ja argon-atmosfäärissä.

Jatkotutkimuksiksi ehdotetaan kontaktiaikojen lisäämistä 300 sekunnin (ilma-atmosfääri) ja 20 minuutin (argon-atmosfääri) läheisyydessä. Tulosten hajonta viittaa jonkin reaktionopeutta rajoittavan tekijän olemassaoloon. Lisäksi jalometallien kemiallinen liukenemiskäyttäytyminen ja jalometallien mahdollinen esiintyminen kivessä sulfideina vaatii yksityiskohtaisempaa analyysiä. Suurten jalometallipisaroiden muodostusta ilma-atmosfäärissä ehdotetaan tutkittavaksi lisää, ja useampia näytteiden poikkileikkauksia tulisi tarkastella jalometallipisaroiden löytämiseksi.

**Avainsanat** Jalometallit, kinetiikka, SER, liekkisulatus

## Acknowledgements

This Master's thesis has been actualised at Aalto University School of Chemical Engineering at the Department of Chemical Engineering and Metallurgy as a part of SYMMET project.

This thesis was supervised by Ari Jokilaakso of Aalto University's metallurgy research group. I' d like to thank him for his patient and tireless help and advice throughout my work. This work was instructed by M.Sc. Lassi Klemettinen and M.Sc. Xingbang Wan. I wish to express my gratitude to Lassi Klemettinen for all the help regarding this work, especially for the many hours he worked helping me with my sample analysis and for the insightful advice he gave me. I would also like thank Xingbang Wan for guidance in several practical issues and instructions on operating in the laboratory. I wish to extend my thanks to Petri Latostenmaa and Miikka Marjakoski at Boliden Harjavalta for participation and delivering the copper concentrate used in this work.

Also, thanks to the members of metallurgy and thermodynamic modelling research groups for their support.

Lotta Kleemola

20.6.2019

## List of symbols and abbreviations

| | |
|---|---|
| °C | Degrees Celsius |
| EDS | Energy dispersive X-ray spectroscopy |
| EoL | End-of-life |
| EoL-RR | End-of-life recycling rate |
| EPMA | Electron probe microanalyser |
| E-waste | Electronic waste |
| LA-ICP-MS | Laser ablation inductively coupled plasma mass spectrometer |
| K | Equilibrium constant |
| $L^{m/s}$ | Distribution coefficient (matte/slag) |
| OSR | Old scrap ratio |
| p | Pressure |
| PCB | Printed circuit board |
| PGM | Platinum group metals |
| ppm | parts per million |
| RC | Recycled content |
| SEM | Scanning electron microscope |
| t_e | Equilibration time |
| WEEE | Waste electronic and electrical equipment |
| wt% | Weight percentage |
| α | Activity |
| γ | Activity coefficient |

# 1 Introduction

Due to technological advances and improving economic and social conditions around the globe, the number of electronic devices in total and per capita are increasing. However, at the same time the average lifecycle of devices has shortened. This is due to the continuous technological advances, but also due to the increase in disposable income. (Cayumil, Khanna et al. 2016) The growing amount of electrical and electronic devices in the world has created an ever growing concern on how this vast entirety of devices can be properly processed and recycled as they reach the end of their product life. These waste devices are popularly known as WEEE (waste electrical and electronic devices). However, available data on WEEE is limited and the WEEE streams are not consistently defined and monitored. Therefore, estimations of the amount of WEEE generated globally need to be made. (Anindya 2012) A report by the United Nations University has estimated that for example in 2016 the global WEEE production was 44.7 million tonnes (Baldé, Forti et al. 2017) and 49.8 million tonnes in 2018 (Statista 2019a).

The recycling of precious metals from waste electronic devices is of significant interest, as the concentration of these metals can be considerably higher in the discarded devices as it would be in natural ores. It has been estimated that the value of precious metals comprises 80% of the value of electronic devices despite their small quantity. (Chancerel, Meskers et al. 2009) The natural resources of precious metals are steadily depleting, and at the same time the demand for them is growing in different sectors. Due to these large-scale trends, manufacturers, environmental agencies and governments around the globe are attempting to find systematic and environmentally sustainable ways of recycling e-waste.

However, the direct economic aspect is not the only concern with recycling WEEE. The discarded devices contain a wide range of different components and though some of them are of economic interest, a part of these elements impose severe soil,

air and water pollution problems, if they are improperly treated. Common electronic devices can contain for example lead, mercury and arsenic, which can cause diseases and tissue damage. Proper management of e-waste is therefore necessary, as the waste can pollute the ground water, acidify the soil, generate toxic fumes and gases after burning, accumulate in the municipal disposal areas and release carcinogenic substances. (Kaya 2016)

Reprocessing WEEE to recover the valuable metals is not a simple matter. WEEE is a heterogeneous mixture of metallic and non-metallic fractions, where the components containing valuable metals are strongly bonded to other components that may have little or no value. WEEE can be smelted in operations whose primary feed are copper concentrates and the reprocessing has been dominated by pyrometallurgical methods. This is expected to remain the case for many years to come. Nonetheless, the elemental composition of WEEE is often such that it can adversely affect the processing operations, for instance by changing the liquidus temperature of the slag, the viscosity of the slag, or make the slag more corrosive towards refractories. Another issue relating to WEEE smelting is that the combination of elements in WEEE does not match that in common primary mineral concentrates, for which the smelting technology has been optimised over many years and for which a large database of information has accumulated. (Anindya 2012)

To obtain the right process parameters for WEEE smelting and precious metals recovery, the thermodynamic behaviour of the valuable elements must be known and reaction mechanisms for smelting and refining step, where the secondary raw materials are processed in the smelting operations, need to be identified. Although trace element equilibrium distribution studies in flash smelting conditions have been carried out, studies on the kinetics of trace element behaviour are lacking. The target of this thesis is to experimentally measure the time dependency of trace element distribution in the pyro-processing of WEEE and investigate the chemical kinetics for precious metals present in the secondary raw materials at the primary copper smelting temperature. The thesis is divided into two sections. The first part is a

literature survey, in which equilibrium and distribution studies and literature are reviewed. In the second part the experimental procedure, equipment and analytical methods are introduced. The results are discussed and compared to the literature survey results.

# Section 1: Literature review

# 2 Annual WEEE formation and their precious metal content

Recycling of metals from secondary resources is a growing industry and there is a significant amount of secondary sources available. One of these resource categories is referred to as WEEE (waste electric and electronic equipment), which means all electrical and electronic equipment that have been discarded by their owner as waste without the intent of re-use. The definition of WEEE is very broad and it can include temperature exchange equipment, screens, monitors, lamps, large equipment (e.g. washing machines), small equipment (e.g. vacuum cleaners, microwave ovens) and small IT and telecommunication equipment.

The amount of WEEE generated was 44.7 million tonnes in 2016 (Baldé, Forti et al. 2017), 49.8 million tonnes in 2018 (Statista 2019a) and is expected to grow to 52.2 million tonnes by 2021, but only 20% of this amount is currently documented to be collected and recycled. The different categories of e-waste and their portions of the total amount are shown in Figure 1.

The total value of raw materials in WEEE was estimated at approximately 55 billion euros in 2016. (Baldé, Forti et al. 2017) The distribution of the estimated value between different elements found in WEEE is shown in *Figure 2*. According to the statistics, gold is by far the most valuable component found in e-waste in terms of economic value per mass. However, the most abundant materials found in e-waste are plastics and iron. The comparison of the volumes of different materials found WEEE is shown in Table 1.

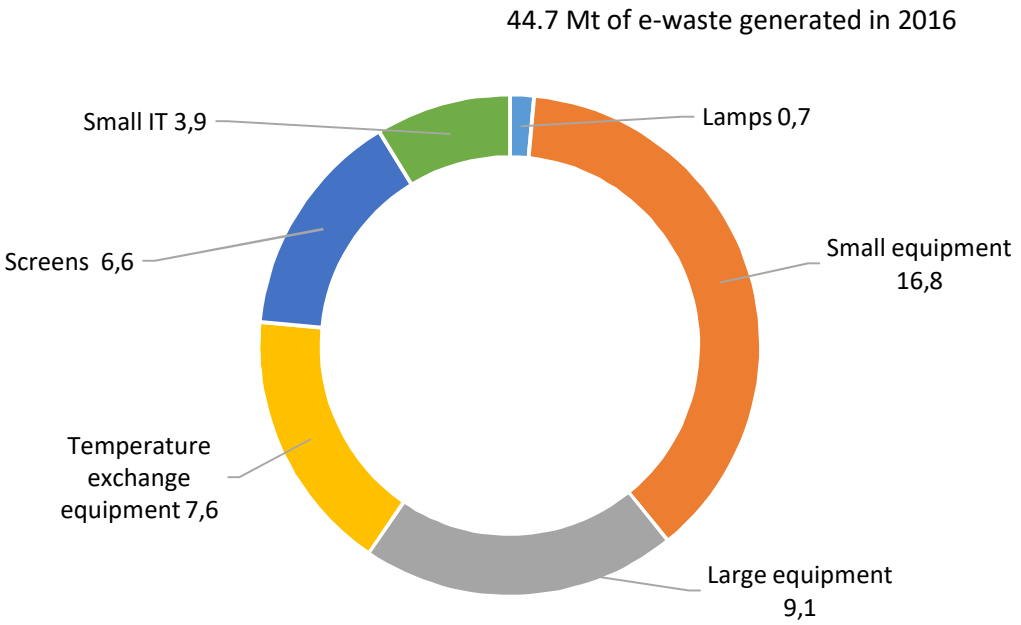


Figure 1. Estimates of the e-waste totals by category in 2016. (Baldé, Forti et al. 2017)

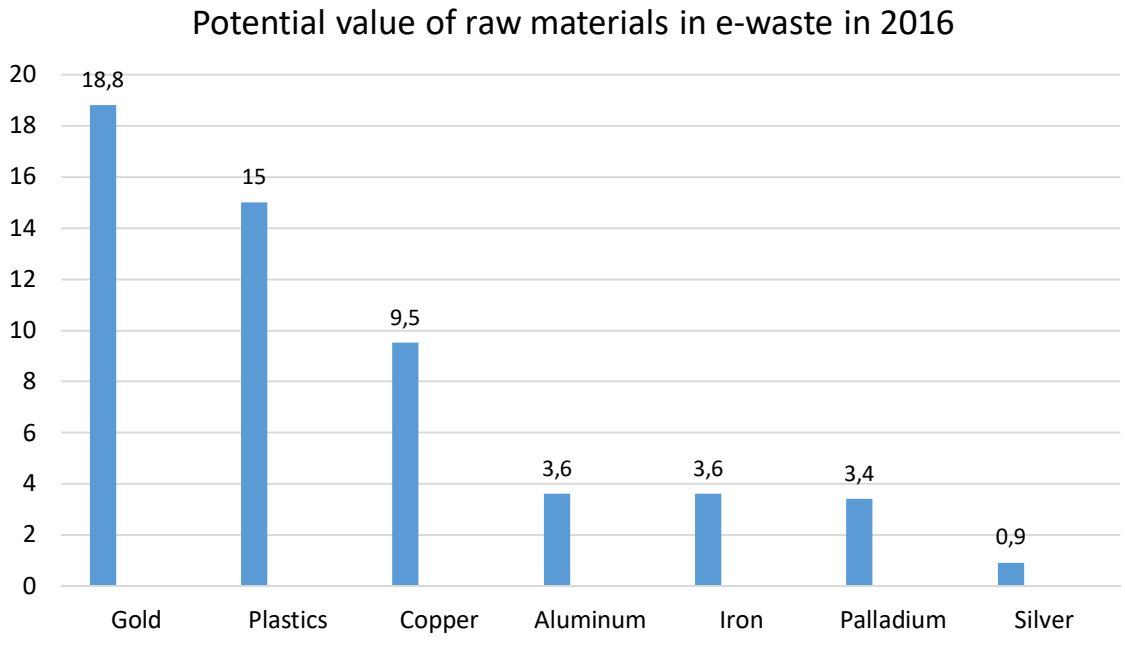


Figure 2. The estimated value of materials found in WEEE in billion euros. (Loesche 2017)

Table 1. The volume of raw materials in e-waste in 2016 (in kilotons).(Loesche 2017)

| Gold | Plastics | Copper | Aluminium | Iron | Palladium | Silver |
|---|---|---|---|---|---|---|
| 0,5 | 12000 | 2200 | 2500 | 16300 | 0,2 | 1,6 |

Comparison between the amounts of e-waste that different countries generate is made difficult by the fact that definition of WEEE varies by country. (Anindya, Swinbourne et al. 2013) In the EU, WEEE encompasses electronics, TVs, and white goods such as refrigerators and ovens. On the other hand, in North America the term 'e-waste' is more limited and does not include large household goods. The valuable metal containing fraction of WEEE that is separated and traded to smelters for processing is referred to as 'e-scrap'.

Nevertheless, WEEE is one the fastest growing segments of consumer waste and it has been estimated that the formation of WEEE continues to increase at a rate of 3-5% per annum. (Eurostat 2016) Because of the reduction in the lifetime of electronic devices, the amount of discarded devices is growing at a relatively rapid rate. The realised and estimated growth rates for different categories of e-waste are presented in Figure 3. To view this from a different angle, it has been estimated that 100 million mobile phones and 17 million computers are being discarded annually due to malfunction or obsolete technology. (Kaya 2016) E-waste is a serious problem because of the sheer volume of it, but also because of the environmental hazards that may arise from landfilling it, which causes leaching of harmful substances such as lead, mercury, arsenic and cadmium. (Anindya 2012)

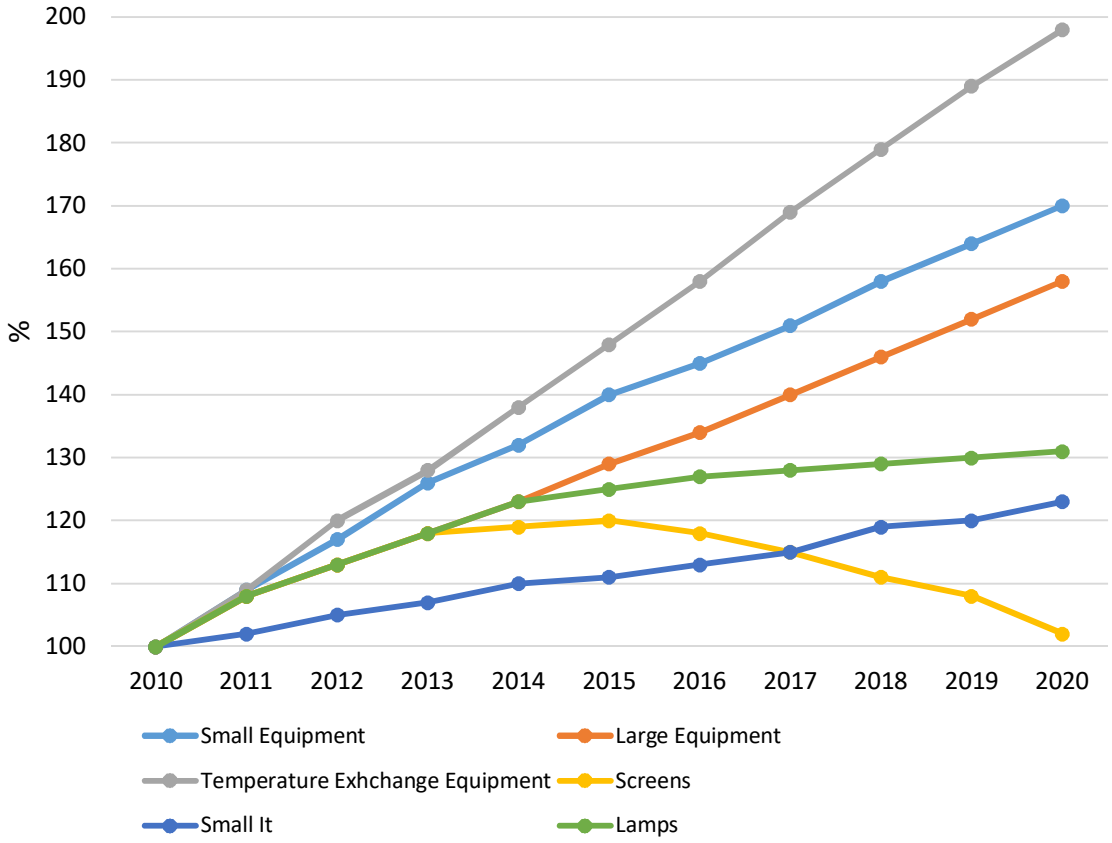


Figure 3. E-waste growth rates per category. The rates for 2017-2020 are estimates (edited). (Baldé, Forti et al. 2017)

Because WEEE consist of a wide range of materials, some of which have a very high economic value, it can be considered as an urban ore. An illustration of the elements found in electrical and electronic devices can be seen in *Figure 4*. Although it has been argued that landfilling e-waste makes the landfills the mines of the future, it disperses the materials, including the valuable elements, so widely that their recovery is practically impossible. (Reuter, Boin et al. 2005) To replace these discarded metals in the production of new devices, the materials need to be mined from primary resources, which in many cases are depleting. Therefore, the recycling of WEEE is a significant contribution to sustainability in metals production.

Electronic scrap, which is derived from discarded telecommunications equipment and computers, is a rich secondary source of precious metals. However, electronic scrap is of varying composition and it often contains approximately 30% plastics, 30%

refractory oxides and 40% metals. An overview of the materials distribution in electronic scrap is presented in *Figure 5*.

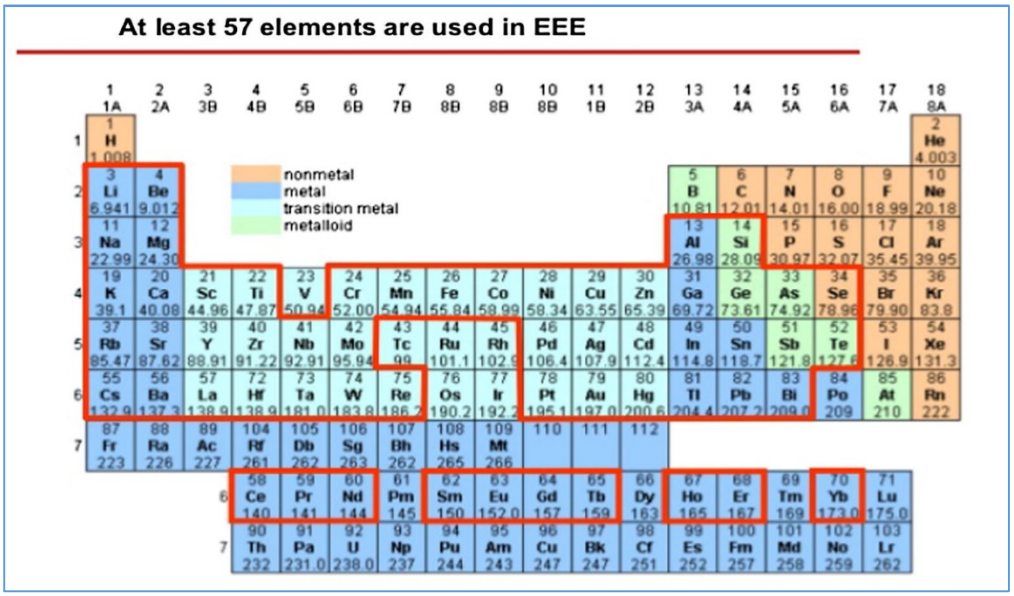


Figure 4. Listing of elements present in electrical and electronic devices. (Kaya 2016)

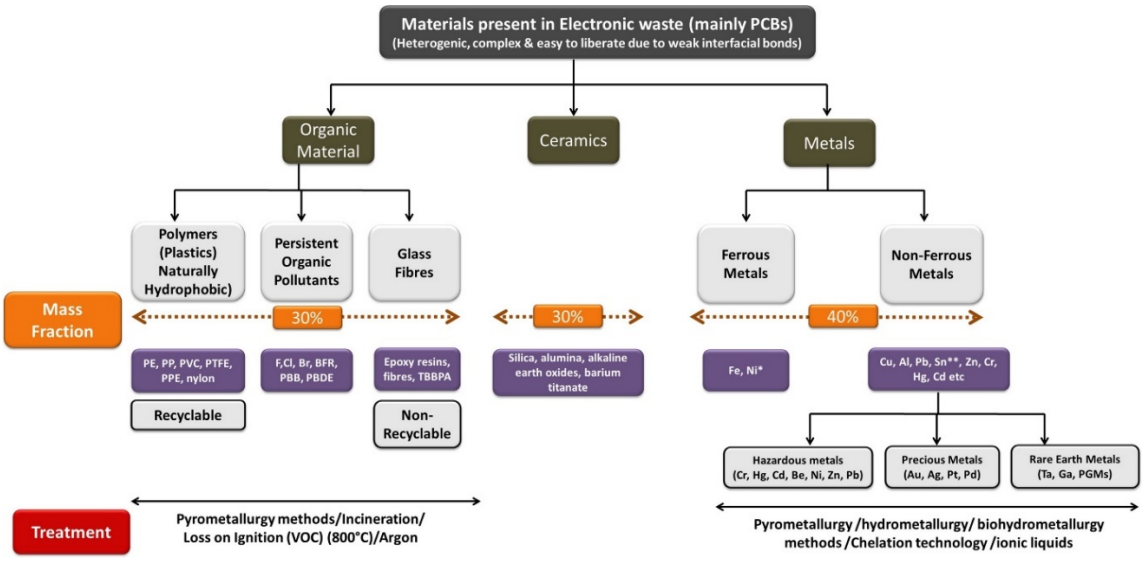


Figure 5. Compositions and mass fractions of end-of-life electronic equipment. (Kaya 2016)

For example, a mobile phone can contain over 40 different elements, including base metals such as copper and zinc and special metals such as cobalt and precious metals. (Meskers, Hageltikeni et al. 2009) The composition can vary significantly from device to device and the materials are highly interlinked. The non-ferrous metals in WEEE

can be broadly divided into two categories: those that are valuable (e.g. copper, gold and silver) and those that are hazardous (e.g. lead, cadmium, arsenic and mercury).

The precious metals in electronic scrap include gold, silver, palladium and, to a lesser extent, platinum. (Hagelüken 2010) They can be found in components such as pin connectors, contact points, silver-coated wires, terminals, capacitors, plugs, and relays. Electronic scrap recycling has been driven by the precious metal, mainly gold, content. However, the precious metal content per unit has had a downward trend in the development of new computers and, in addition to this, the newer models are smaller in size. This fact, combined with the mixed nature of the precious metals in e-waste and the variety of chemical and physical properties of the host materials, creates challenges for precious metals recovery from electronic scrap. (Rao 2006)

The concentrations of precious metals, specifically gold, silver, platinum and palladium, in printed circuit boards (PCB) are essentially higher than in their respective primary sources. It has been estimated that the waste PCBs count for 3 wt% of the globally produced WEEE. As mentioned earlier, the concentrations vary from device to device and establishing a typical concentration of precious metals in PCBs is difficult. As the concentrations have also decreased due to development of smaller and more efficient devices, generalisations of the precious metals concentrations need to be made. An example of precious metals content in WEEE is given in *Table 2* and 3 and in *Figure 6*. In Figure 6, the analysis of the composition is based on estimates made in 1991, whereas in Table 2 and Table 3 the concentrations are collected from more modern sources. As it can be seen from these data, there is significant scatter in the estimations and the precious metals content is dependent on the age of the e-scrap. In Table 3 the reported gold content of memory modules is unusually high and inconsistent with other reported results. A study by (Charles, Douglas et al. 2017) reported the average gold content of PC DRAMs to be 932 ppm, and a study by (Khaliq, Rhamdhani et al. 2014) concluded that the typical gold content of PCBs can vary between 20—1000 ppm.

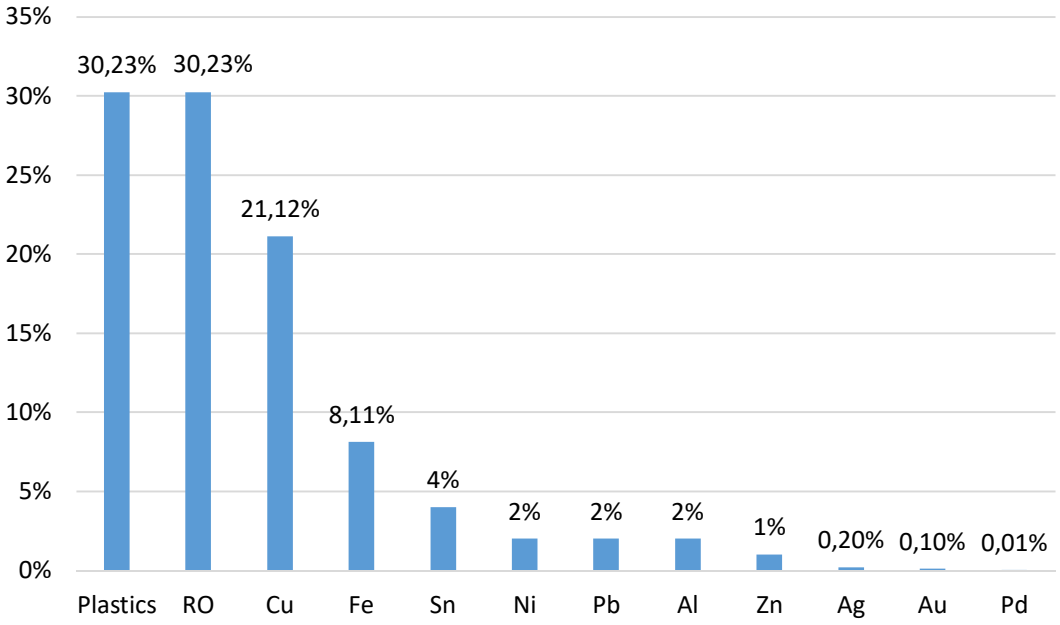


Figure 6. An example of a typical material composition of WEEE (edited). RO=refractory oxides. (Gramatyka 2007)

Table 2. Weight distributions of selected metals in e-waste. (Tesfaye, Lindberg et al. 2017, Habib Al Razi, Khadankar 2016)

| E-waste | Fe (wt%) | Al (wt%) | Cu (wt%) | Plastics (wt%) | Ag (ppm) | Au (ppm) | Pd (ppm) |
|---|---|---|---|---|---|---|---|
| TV-board | 28 | 10 | 10 | 28 | 280 | 20 | 10 |
| PC board | 7 | 5 | 20 | 23 | 1000 | 250 | 110 |
| Mobile phone | 5 | 1 | 13 | 56 | 3500 | 340 | 130 |
| Portable audio | 23 | 1 | 21 | 47 | 150 | 10 | 4 |
| DVD-player | 62 | 2 | 5 | 24 | 115 | 15 | 4 |
| Calculator | 4 | 5 | 3 | 61 | 260 | 50 | 5 |
| Average EEE | - | - | 13,8 | - | 1009 | 127 | 51,6 |
| Ore/mine | - | - | 0,6 | - | 215,5 | 1,01 | 2,70 |

Table 3. Waste drives containing the selected precious metals. (Habib Al Razi 2016)

| Component | Weight (g) | Gold (g/kg) | Silver (g/kg) | Palladium (g/kg) |
|---|---|---|---|---|
| CPU slot | - | 0.008 | 0.045 | 0.01 |
| CD drive | 788 | 0.012 | 0.105 | 0.02 |
| Floppy drive | 262 | 0.001 | 0.014 | 0.003 |
| HDD drive | 508 | 0.013 | 0.087 | 0.014 |
| PCBs of HDD drives | 84 | 0.013 | 0.087 | 0.014 |
| Memory modules | 20 | 823 | 0.79 | 0.05 |
| PCI cards | 62 | 0.015 | 0.073 | 0.01 |
| Motherboards | 459 | 0.067 | 0.35 | 0.089 |
| Power boards | 2000 | - | 0.68 | - |

# 3 Primary production of precious metals and recycling rates

Recycling metals from WEEE can decrease the need for the production of metals from primary resources and it can thereby conserve the scarce, depleting resources. The production of metals, especially precious metals where the ore grade is typically low, significant amounts of waste water, carbon dioxide and sulphur dioxide are created. The mining also requires large areas of land and consumes massive amounts of energy. The total $CO_2$ emissions from the production of metals used in WEEE is estimated to be 23.4 million tonnes per year. It has also been shown that recycling metals creates less emissions than their production from primary resources. (Gunn 2013)

The main environmental issues associated with the mining and processing of sulphide-bearing ores of any type, including platinum group metal (PGM) ores, include: the generation of acid mine drainage from mine workings, ore dumps, treatment plant and tailings, release of associated trace elements which may be harmful to human health and the environment (e.g. arsenic, lead, antimony), discharge of chemicals used in the mining and processing of the ores and concentrates and gaseous emissions (chiefly sulphur dioxide) associated with the smelting and refining processes. (Kaya 2016)

## 3.1 Gold and silver

Unlike many other materials, most of the gold that has ever been mined is still in use. It has been estimated that approximately 85% of historically produced gold is still in use and available for recycling, i.e. between 133,000 and 153,000 tonnes. (Muller, Frimmel 2010) It has traditionally been used for purposes such as money, to back currency, jewellery-making and dentistry. Nowadays it is used in many kinds of electronic applications because of its high electrical conductivity. On top of

electronics, gold nanoparticles are increasingly being used as industrial catalysts. Gold is also favourable because of its chemical stability and corrosion resistance. Gold does not react with water, dry or humid air and most corrosive reagents so it is well suited as a protective coating, for example. (The Royal Society of Chemistry 2019a)

The current estimate of world's remaining gold reserves is 51,000 tonnes. The ore grade has been falling globally and the current mean ore grade in the world is in the order of 3-4 g/t Au. It has been suggested that the decrease continues in a similar fashion and that in 2050 the grade will have fallen to about 1 g/t Au. (Norgate, Haque 2012). The gold mine production in 2017 was approximately 3,269 tonnes and the total amount of recycled gold from all recycling chains was 1,160 tonnes. The demand for gold in electronics manufacturing was in the order of 265 tonnes. (Chou 2018) The downward trend in the gold ore grades brings an incentive to utilise gold resources found in WEEE.

Like gold, silver has also historically been used in jewellery and coins, but nowadays its main uses are industrial. Silver is considered precious, because it is rare and valuable, and it is also a noble metal as it can resist corrosion and oxidation. It is widely used in electrical applications, because it is the best thermal and electrical conductor. Its malleability and ductility also make it attractive for many industrial applications. Silver is relatively abundant, which makes it much less expensive than gold.

Most of the world's silver comes as a by-product from lead, zinc, copper and gold mining, and only 20% of silver production is from primary silver resources. (The Silver Institute 2018) In 2017, the global silver production from mines was approximately 25,000 tonnes. It has been estimated that the world's silver reserves as of 2017 are approximately 551,000 tonnes. In 2017 the total demand for silver was 28,900 tonnes and the demand from electrical and electronics manufacturing was 6,900 tonnes. The global supply for silver was 23,400 tonnes, from which 3,900 tonnes (17%) was from silver scrap. (Statista 2018a)

## 3.2 Palladium and platinum

Platinum group metals have a significant role in modern technology since they are used in important applications including information technology, consumer electronics and sustainable energy production, such as photovoltaics and fuel cells. Platinum and palladium are commercially the most important ones. All platinum group metals are chemically similar and they have strong siderophile and chalcophile tendencies, preferentially bonding with iron, nickel, copper and sulphur rather than oxygen. (Gunn 2013)

Platinum is highly corrosion-resistant and stable at high temperatures. The main uses of platinum are in automotive catalytic converters and it is also prominently used in jewellery. In 2017 7.29 tonnes of the global platinum demand was by electronics manufacturing and it is expected to steadily grow during the coming years, as well as the total demand. The global production of platinum for 2017 was 200 tonnes (Statista 2018b) and according to statistics, 1,020 kg of platinum was recycled from the electrical industry in 2018. (Statista 2019b)

The estimated reserves of platinum worldwide are 69,000 tonnes. The production of platinum from primary resources is very capital and labour intensive as it can take up to 7-12 tonnes of ore to produce one troy ounce (31.135 g) of pure platinum. Platinum is always found alongside other platinum group metals. (Bell 2018)

The concentration of platinum group metals in virgin ore is low, approximately 3-20 ppm and because of this, most of them are recovered as by-products from copper and nickel smelting. Palladium has been found uncombined in nature, but mostly it is found in sulphide minerals. (The Royal Society of Chemistry 2019b) Global supply of palladium in 2017 was 254 tonnes. Its main use, approximately 83%, is in automotive catalytic converters and 16 % is in electrical engineering applications. (Statista 2011) It is widely used in electronics industries in the manufacturing of multi-layer ceramic capacitors, hybrid integrated circuits, hydrogen storage materials, connective plating,

gas sensors and photovoltaics. In terms of physical appearance, palladium is silvery white, dense, soft and ductile. (Shuva, Rhamdhani et al. 2017)

## 3.3 Recycling rates of precious metals from WEEE

The definition of recycling rate is not a straightforward matter and it can be approached from different angles, such as product-to-metal ratio, metal-in-product ratio and it can be defined for many different life stages. In some studies the term is left undefined. A metals recycling report by UNEP (UNEP 2011) states that the efficiency of the end-of-life (EoL) recycling can be measured at three levels:

1. How much of the scrap enters the recycling chain as opposed to being landfilled,
2. recycling process efficiency, i.e. the efficiency of any given recycling process in the chain and
3. the end-of-life recycling rate.

In this consideration the EoL recycling rate refers to functional recycling, in which the physical and chemical properties that made the material desirable in the first place are fully retained. Non-functional recycling refers to recycling in which the collected metal becomes an impurity, such as copper in a steel alloy.

The UNEP recycling report concluded that exact metrics for recycling rates are not specified and the rates are evaluated in five ranges when enough data for the metal in question is available. The efficiency ranges for the selected elements are shown in Table 4. EoL-RR refers to End-of-Life recycling rate, RC to recycled content in the fabricated metal and OSR to old scrap ratio, which describes the fraction of old scrap in the recycling flow. The EoL-RR from the electronics industry and the relevance of the end use sector (electronics industry's demand-% of the total gross metal demand) are also shown.

Table 4. Recycling efficiency ranges for selected precious metals.

| | Au | Ag | Pd | Pt |
|---|---|---|---|---|
| **EoL-RR** | >50% | >50% | >50% | >50% |
| **RC** | >25-50% | >25-50% | >25-50% | >25-50% |
| **OSR** | >50% | >50% | >50% | >50% |
| **EoL-RR from electronics** | 10-15 % | 10-15 % | 5-10% | 0-5% |

The numbers on recycling rates of precious metal vary depending on the source. According to (Hageluken 2012) the annual recycling rate of platinum group metals from WEEE is 5-10%. The recycling rate of gold is approximated at 26% by (Reck, Graedel 2012). On the other hand, other estimates of the recycling rates from waste electronics in Table 4 imply that the rates are significantly lower. Precious metals are generally considered sufficiently valuable to make their recycling economically viable, except for some cases when they are used in very small amounts, such as platinum in computer hard disks.

A relatively high EoL-RR may lead to a notion that the material in question is being recycled more efficiently than materials with lower EoL-RR. However, the high EoL-RR tends to be reflected from a large amount of products and applications where the material is present in an easily recoverable form. A high value of the target material is also mirrored in the recycling rates. In Table 4 the total recycling rates include recycling of coins and jewellery from which the metals are easily recovered. On the other hand, when the material is used in small quantities and the recycling techniques are more complex, as is the case for precious metals in WEEE, recycling rates tend to be lower.

# 4 Pyrometallurgical treatment of WEEE

## 4.1 Primary copper production

Copper is present in the Earth's crust as copper-bearing minerals and gangue minerals. The commonly used raw materials for copper production are copper-iron-sulphur ores chalcopyrite ($CuFeS_2$), bornite ($CuFeS_4$) and chalcocite ($Cu_2S$). Some other minerals of copper such as carbonates, oxides, silicates and sulphates also exist, but these are less commonly used as a source of copper. Currently approximately 80% of the global copper production is carried out through pyrometallurgical methods, where the sulphide copper ores are treated by smelting and converting to make blister copper. The total smelter production of copper worldwide in 2015 was 18.5 million tonnes. The generic process flow of primary copper production is presented in *Figure 7*.

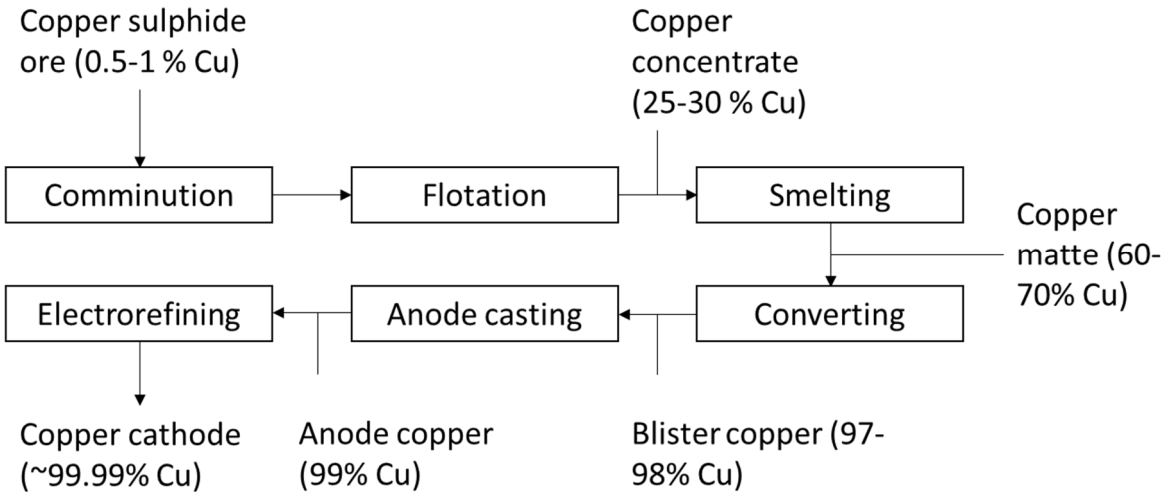


Figure 7. Flow sheet of primary copper production through pyrometallurgy (edited). (Shuva 2017)

## 4.2 Matte smelting

The primary purpose of matte smelting is to turn the sulphide minerals in the solid copper concentrate into three products, molten matte, molten slag and off-gas through the overall equation (1):

$$\mathrm{CuFeS_2 + O_2 \rightarrow (Cu, Fe, S)_{matte} + FeO_{slag} + SO_2} \quad (1)$$

A major constituent of the concentrate is chalcopyrite ($CuFeS_2$). The stoichiometry of reaction (1) can vary depending on the amount of chalcopyrite and other sulphide minerals in the concentrate and the oxidation degree of Fe. $Cu_2S$ and FeS form the Cu-Fe-S matte.

Smelting process involves some trade-offs, most significant of which is that between matte grade (mass% of Cu in matte) and recovery. A large oxygen input in equation (1) will result in more iron oxidising in the concentrate and hence creating a higher matte grade. However, the oxidising environment also enhances the oxidation of copper and the resulting copper oxide dissolves in slag.

The matte formation is followed by partial oxidation of S into $SO_2$, FeS into magnetite ($Fe_3O_4$) and FeO. Sulphur and FeS oxidise through reactions

$$\mathrm{S_2 + 2\ O_2 \rightarrow 2\ SO_2} \quad (2)$$

$$\mathrm{3\ FeS + 5\ O_2 \rightarrow 3\ Fe_3O_4 + 3\ SO_2} \quad (3)$$

$$\mathrm{FeS + \frac{3}{2} O_2 \rightarrow FeO + SO_2} \quad (4)$$

The silica flux, unreacted FeS and magnetite form the FeO-$SiO_2$ system:

$$3\ Fe_3O_{4(s)} + FeS_{matte} + 5\ SiO_{2(s)} = 5\ Fe_2SiO_{4(slag)} + SO_{2(g)} \quad (5)$$

$$3\ Fe_3O_{4(s)} + FeS_{matte} \rightarrow 10\ FeO_{slag} + SO_{2(g)} \quad (6)$$

FeO content of the slag is important to smelter operations, because when the activity of FeO in the slag is too high, it will react with the $Cu_2S$ in the matte by the following reaction

$$FeO_{(slag)} + Cu_2S_{(matte)} \rightarrow FeS_{(matte)} + Cu_2O_{slag} \quad (7)$$

If the activity of FeO in the slag is high and the activity of FeS in the matte is low, higher activity of $Cu_2O$ in the slag is caused. FeO also reacts with oxygen to form solid magnetite $Fe_3O_4$. As a result, lowering the activity of FeO in the slag is crucial, and it is done by controlled additions of silica as a flux.

In addition to FeO and silica, other commonly found oxides in slags include ferric oxide $Fe_2O_3$, alumina ($Al_2O_3$), calcia (CaO) and magnesia (MgO). Small quantities of sulphides may dissolve into the slag as well. The slag oxides are divided into three groups: acidic, basic and neutral. Silica and alumina are the best-known acidic oxides. When melting, these oxides polymerise and form long polyions, which give the acidic slags high viscosities. Basic oxides like magnesia and calcia break the polyions into smaller units when added to acidic slags, lowering the viscosity of the slag and increasing solubility for acidic oxides. FeO and $Cu_2O$ are neutral oxides with low melting points, resulting in lower melting point of the slag and lower viscosity.

## 4.3 WEEE treatment

The two main routes for recovering precious metals from scrap are pyrometallurgical and hydrometallurgical extraction methods. Here the focus is on pyrometallurgical methods.

An appropriate recycling chain for metals extraction from WEEE includes collection, dismantling and metal recycling. (Tesfaye, Lindberg et al. 2017) Collection determines the availability of the recyclable material and it is therefore a crucial step in the recycling chain. Collection of waste is technically logistics, but it also requires much awareness of the consumers who are in the stage of recycling their EoL devices. Therefore efficiency in municipal waste collection plays an important role in urban mining.

Dismantling in this case means mechanical separation that is carried out to liberate the valuable components and to remove and safely treat the hazardous materials. The fractions obtained from the pre-processing stage are enriched in certain materials and are directed to further treatment depending on their following pyrometallurgical process. (Rao 2006) Components such batteries, capacitors etc. are treated in a more dedicated facility, for these contain toxic heavy metals. Having disassembled the hazardous components, different operations such as shredding, crushing and grinding can be used to remove the metallic parts from the cladding material, namely resin, fiberglass and plastics. (Anindya 2012)

Pyrometallurgical techniques, including incineration, smelting in plasma arc furnace, blast furnace or copper smelting furnace, have become a traditional way of recovering both non-ferrous as well as precious metals from electronic waste in the past decades. (Cui, Zhang 2008) In these processes the crushed scrap is burnt in a furnace or in a molten bath to remove plastics, and the refractory oxides form a slag phase with metal oxides. Depending on the process, the scraps can be fed into process at different steps.

Reprocessing of WEEE is dominated by pyrometallurgical methods, but because secondary copper has no sulphur in it, it is a net energy consumer. (Schlesinger, King et al. 2011) However, in the case of WEEE recycling, smelting furnaces are preferred over converters due to the plastic content of WEEE. This is due to two reasons. Firstly, the plastic parts in electronic scrap have fuel value, which provides heat for smelting. Secondly, when plastics are burned intermittently they often give off organic compounds that can cause risks. However, high temperature oxygen smelting completely avoids this problem. When burned in a sealed smelting furnace, the potential particulates are efficiently captured by dust collection devices.

Pyrometallurgy is advantageous in the recovery of precious metals from WEEE in the sense that the processes can accept any forms of scrap. A major proportion of waste PCBs are treated in smelters rather than through mechanical processing and the waste PCBs can be used as a part of raw material to recover copper alongside precious metals. The downside of pyrometallurgical techniques in the recovery of precious metals is the high energy consumption of the process and the environmental concerns that arise from it. The process itself also creates gas emissions and the e-waste recycling facilities require extensive emission control system for environmental protection. (Ghosh, Ghosh et al. 2015)

# 5 Precious metals distributions in matte-slag systems

Literature on the kinetics of precious metals in matte smelting conditions has not been found and, therefore, there are few literature sources for accurate evaluation of the experimental results. Equilibrium studies in matte-slag system have been conducted and the information on equilibrium distribution behaviour of precious metals is reviewed in this chapter.

## 5.1 Thermodynamic behaviour of valuable elements in copper

In pyrometallurgical processing of copper the minor elements distribute themselves between different phases: slag, matte, copper and gas. The distribution behaviour does not directly provide information on the kinetics of precious metals in matte-slag system, but it does give insight on their behaviour. Understanding this distribution behaviour also provides information for developing optimum process conditions to recover the precious metals. The equilibrium distribution for a trace element Me between matte and slag having a valence of 2n can be expressed by equations (8)-(9) (Yazawa 1974, Avarmaa 2015)

$$[\mathrm{Me}] + \frac{\mathrm{n}}{2}\mathrm{O}_{2(\mathrm{g})} = (\mathrm{MeO_n}) \tag{8}$$

$$[\mathrm{Me}] + \frac{\mathrm{m}}{2}\mathrm{S}_{2(\mathrm{g})} = (\mathrm{MeS_m}) \tag{9}$$

The equilibrium constant *K* for the above reaction is expressed by the activities of metal oxide and metal distribution-ratio:

$$K = \frac{\alpha_{\mathrm{MeO_n}}}{\alpha_{\mathrm{Me}} p_{\mathrm{O_2}}^{\mathrm{n}/2}} \tag{10}$$

The distribution ratio of Me between matte and slag is defined as

$$L_{\mathrm{Me}}^{\mathrm{s/m}} = \frac{(\mathrm{Me})}{[\mathrm{Me}]} \tag{11}$$

where the parentheses ( ) and [ ] denote the concentration of the element in slag and matte phases, respectively. Takeda et al. showed that the distribution ratio can be presented as

$$L_{\mathrm{Me}}^{\mathrm{s/m}} = \frac{K(\mathrm{n_T})[\gamma_{\mathrm{M}}]p_{\mathrm{O_2}}^{\mathrm{v/2}}}{[\mathrm{n_T}](\gamma_{\mathrm{MO_n}})} \tag{12}$$

where *K* is the equilibrium constant for Reaction (10), $n_T$ is the total number of moles in constituents in the relevant phases, $\gamma_M$ is the activity coefficient of M in the metal, $\gamma_{MO_n}$ is the activity coefficient of metal oxide $MO_n$ in the slag and $p_{O2}$ is the oxygen partial pressure. For a particular temperature the terms on the right side of the equation (12) are constant except for $p_{O2}$ and the following relationship can be established

$$\log L_{\mathrm{M}}^{\mathrm{s/m}} = \log \mathrm{B} + \left(\frac{\mathrm{v}}{2}\right) \log p_{\mathrm{O_2}} \tag{13}$$

From the linear relationship the degree of oxidation of solute element v/2 in the slag can be determined. The activity coefficient of the $MO_v$ in the slag can be calculated, if the activity coefficient of the element M in liquid metal phase is known. It has been stated by (Yazawa 1974) that the trace element behaviour in primary copper processing can be presented by the following reactions:

$$[\mathrm{M}]_{\mathrm{s,l}} + \frac{1}{2}\mathrm{S}_2 = (\mathrm{MS})_{\mathrm{s,l}} \quad (14)$$

$$[\mathrm{M}]_{\mathrm{s,l}} + \frac{1}{2}\mathrm{O}_2 = (\mathrm{MO})_{\mathrm{s,l}} \quad (15)$$

## 5.2 Equilibrium and distributions

The distribution of elements between the matte and slag phase is of interest, as it indicates the efficiency at which the desirable metals are retained in the matte phase. The distribution studies also generate important data on the amount of impurities which go forward with the matte to the metal production stage. (Tavera, Davenport 1979)

## 5.3 Ag

The distributions of precious metals between matte and slag are not very well known. However, some reports of studies on this topic have been found. (Nagamori, Mackey 1978) assumed that the behaviour of silver in fayalitic slags is monoatomic as the sulphides and oxides of silver are unstable at smelting conditions. The equilibrium distribution of precious metals between $FeO_x$-$SiO_2$ slag and Cu-matte has been studied by (Avarmaa, O'Brien et al. 2015). The temperature range was 1250-1350 °C and $p_{O2}$, $p_{SO2}$ and $p_{S2}$ were controlled. It was reported that the Ag distribution ratio (matte/slag) increased slightly with increasing matte grade, as the distribution coefficient of silver was $L^{m/s}[Ag]$ = 200 to 300 in the matte grade range of 50 to 70 % Cu. It has been reported by (Louey, Swinbourne et al. 1999) that the distribution ratio

of silver between Cu-matte and $FeO_x$-$SiO_2$ slag at 1250 °C and $p_{O2}$ $10^{-11.5}$ atm was found to be 120 ± 40.

The volatilisation of Ag occurs at high temperatures and the temperature dependency of the silver solubility was found to be significant. It was observed that the silver content decreased in both matte and slag phases with increasing temperature. If considering the slagging, the silver concentration in the matte should decrease by the same amount as it increases in the slag. It was suspected that the silver is volatilised at increasing rate during this temperature change, or at least it migrates increasingly somewhere but not the slag. (Avarmaa, O'Brien et al. 2015) In comparison, distribution of silver between metal and matte have been studied and no dependency on temperature was found. (Schlitt, Richards 1975)

The effects of slag basicity on silver solubility have been studied. It has been reported that the solubility of silver decreases as the basicity of the slag increases. (Park, Min 1999)

## 5.4 Au

Gold is known to exist in compounds in the oxidation state of $Au^{3+}$, is unknown to exist in state $Au^{2+}$ and is believed not to occur in the $Au^{+}$ oxidation state. The solubility of gold in slags has always been assumed very low, because the Gibb's free energy of formation for gold (III) oxide $Au_2O_3$ is very positive ($\Delta G^\circ$ = +378·17 kJ/mol at 1200 °C). (Nagamori, Mackey 1978)

It has formerly been stated by (Nagamori, Mackey 1978) that the distribution coefficient of gold in copper-matte, copper-slag or matte-slag systems is not a function of oxygen or sulphur partial pressure. They assumed that gold dissolves as neutral atoms in slag since metals may occasionally exist in slags as neutral atoms.

However, it has later been reported that gold dissolves in slags probably as $Au^{+}$ ions and the solubility of gold in iron-silicate slag is a function of oxygen partial pressure. (Swinbourne, Yan et al. 2005) have reported that the solubility of gold in iron-silicate

slag is the same as in calcium ferrite slags and significantly lower in slags than previously assumed. Their experiments were conducted by varying oxygen partial pressure for iron-silicate slag between $10^{-9}$ and $10^{-7}$ atm at 1300 °C. They also stated that the gold content of the slags in smelting and converting are expected to be dominated by matte or copper entrainment rather than solubility of gold in slag.

(Avarmaa, O'Brien et al. 2015) also investigated the distribution of gold. They reported that the distribution coefficient $L_{\mathrm{Au}}^{\mathrm{m/s}}$ varied from approximately 400 to 3000 with matte grade ranging between 50-70%. The temperature was varied between 1250 °C and 1350 °C. The distribution coefficient showed no dependence on temperature.

In comparison, (Avarmaa, O'Brien et al. 2016) studied the equilibrium of gold between molten copper and $FeO_x$-$SiO_2$-$Al_2O_3$ slag in WEEE smelting at 1300 °C. They reported the results for the distribution ratio of gold in copper in terms of oxygen partial pressure. They found the distribution ratio at $p_{O2}=10^{-5}$ atm to be $10^5$ and over $10^6$ for pressures between $10^{-6}$ and $10^{-10}$. As for the slag, they reported that the slag composition is highly dependent on the oxygen partial pressure. In comparison, the concentration of gold in the copper alloy phase stayed constant as a function of $p_{O2}$.

## 5.5 Pd & Pt

The distribution ratios of platinum and palladium have been studied between copper matte and $FeO_x$-$SiO_2$ slag, at 1300 °C and at fixed $p_{SO2}$ by (Henao, Yamaguchi et al. 2006). It was observed that the distribution ratio remained constant up to the matte grade of 60% and decreased from thereon as matte grade increased. It was reported that the distribution coefficient (matte/slag) for palladium was 1000 and 100 for platinum.

A same kind of study was made by (Avarmaa, O'Brien et al. 2015), where the distributions of palladium and platinum were investigated between $FeO_x$-$SiO_2$ slag and Cu matte. The temperature was within the range 1250-1350 °C and they reported

an increase in the distribution ratio (matte/slag) as the matte grade increased. For palladium, the distribution ratio was 1000 with 50% Cu matte grade, but increased to 2000-3000 with 70% Cu matte grade. They also reported that the effect of temperature on distribution coefficient is less pronounced than the effect of matte grade. The distribution behaviour of palladium with increasing matte grade seems to be contradictory in these two studies; in Henao's study, the distribution coefficient decreased along with the increasing matte grade, whereas in Avarmaa's study the distribution coefficient increased.

It was suggested by (Avarmaa, Johto et al. 2016) that the precious metals replaced copper and/or iron in the molten matte structure, and that they are probably dissolved as sulphides in copper mattes in equilibrium with silica-saturated iron silicate slags under 0.1 atm $p_{SO2}$. It has also been found that the solubility of platinum and palladium increased with increasing temperature and increasing $p_{O2}$. This has been explained to happen because palladium and platinum exhibit deviation from the Raoultian behaviour in dilute Cu-Pt and Cu-Pd systems. (Shuva 2017)

The effect of basicity on the solubility of platinum in oxide melts has been studied by (Nakamura, Morita et al. 1998). Their conclusion was that the behaviour of platinum is amphoteric, as it exists as platinum cation in acidic fluxes and as a platinate ion in basic fluxes.

As palladium forms a divalent oxide PdO which is mildly basic, a less-acidic slag (low in $SiO_2$) and a reducing atmosphere with higher temperature is suggested to decrease the palladium deportment to the slag. It has also been reported that the solubility of palladium is strongly dependent on the optical basicity of the slag. Temperature has some effect on the palladium distribution, as palladium is less stable at higher temperatures and palladium mostly moves to the copper-bearing phase. (Shuva, Rhamdhani et al. 2017)

# Section 2: Experimental procedure and analysis

# 6 Raw materials and sample preparation

## 6.1 Synthetic slag

A synthetic slag was prepared by mixing hematite powder (Alfa Aesar, 99.99% purity) and silica powder (Umi-core, 99.99% purity). The powders were first mixed by the mass ratio of 65% $Fe_2O_3$ and 35% $SiO_2$ and ground in a mortar to obtain fine and even composition. After grinding, the mixture was heated in a furnace at 1300 °C for more than 8 hours in air atmosphere. This resulted in the formation of solid magnetite and solid silica grains, which simulates the conditions in the flash smelting furnace when the concentrate particles and silica flux descend from the reaction shaft and hit the slag layer. (Jokilaakso, Suominen et al. 1991) During the experiment, the concentrate will mix with the $Fe_3O_4$ and $SiO_2$ system, and start to produce liquid slag.

## 6.2 Concentrate

Industrial copper concentrate from Boliden Harjavalta was used in the experiments. Elemental composition results from two different chemical analysis methods are shown in *Table 5*.

Table 5. Chemical analyses of the copper concentrate in weight-%.

| Boliden Harjavalta XRF | | | | | | |
|---|---|---|---|---|---|---|
| **S** | **Fe** | **Cu** | **Zn** | **SiO2** | **Pb** | **CaO** |
| 33.17 | 27.36 | 27.34 | 3.77 | 2.53 | 0.13 | 0.09 |
| **Cr** | **Ni** | **Bi** | **Cl** | **Sb** | **As** | |
| 0.012 | 0.004 | 0 | 0 | 0 | 0.026 | |
| Boliden Harjavalta Semiquantitative | | | | | | |
| **S** | **Cu** | **Fe** | **O** | **Zn** | **Si** | **Mg** |
| 33.43 | 28.63 | 27.47 | 4.94 | 4.17 | 0.66 | 0.35 |
| **Ca** | **Al** | **Ba** | **Ag** | **Mn** | **Cd** | **As** |
| 0.065 | 0.053 | 0.051 | 0.025 | 0.018 | 0.016 | 0.014 |
| P | Se | K | Ni | Pb | | |
| 0.004 | 0.004 | 0 | 0.013 | 0.107 | | |

## 6.3 Precious metals

The details of the precious metals used in this work are shown in Table 6.

Table 6. Producers and product details of precious metals.

| Metal | Supplier | Form | Purity |
|---|---|---|---|
| Gold | Alfa Aesar | Powder, APS 1.5-3.0 micron | 99.96% |
| Silver | Alfa Aesar | Powder, -60+80 mesh | 99.99& |
| Platinum | Alfa Aesar | Powder, -200 mesh | 99.98& |
| Palladium | Alfa Aesar | Powder, -60 mesh | 99.9% |

## 6.4 Gas

The experiments were conducted in air and argon atmospheres. For the experiments conducted in air, no gas flow was used; the bottom end of the furnace was left open so that the work tube was filled with air from the surrounding atmosphere. For argon experiments, the work tube was sealed from the bottom and 400-500 mL/min argon (AgA Linde, 99.999% purity) flow was used.

## 6.5 Sample preparation

The concentrate and slag powders were weighed to obtain samples of 0.5 g. The slag to concentrate ratio was chosen to be 1.116 according to industry standards, which corresponds to $SiO_2$/Fe flux ratio of 0.533 or 0.517, depending on which analysis results from Table 5 are used. With this ratio the slag would be silica-saturated (Wan, Jokilaakso et al. 2019), and have the orthosilicate composition, which has been showed to be optimal for minimising the valuable metal losses into the slag. (Hellstén, Klemettinen et al. 2019) Precious metal powders were added to the mixture of slag and concentrate and the amount of each precious metal (gold, silver, palladium, and platinum) was measured to be 2.5 wt% of the amount of concentrate. This percentage was chosen to obtain a reasonable detectability with the analysis methods used. All the powders were ground together in a mortar to obtain a homogenous slag-concentrate-precious metal mixture. Having reached a fine, uniform structure, the powder was transferred to cone-shaped silica crucibles (Finnish Special Glass, Finland).

# 7 Equipment and experimental procedure

## 7.1 Equipment

An illustration of the experimental setup is shown in Figure 8. The experiments were conducted in a Lenton LTF 16/450 single phase vertical tube furnace, which was equipped with four silicon carbide heating elements. The heating elements were positioned close to the alumina working tube (Frialit AL23, Friatec AG, Germany) with inner diameter of 35 mm. A smaller alumina tube was installed within the working tube, with inner diameter of 22 mm. The working tube extended from the top of the furnace to the bottom, whereas the inner tube extended from the top to approximately 20 mm above the horizontal centreline of the furnace. The bottom end of the inner tube was located in the experimental hot zone, which was held at 1300 °C. The furnace temperature was controlled with a Eurotherm 3216 PID controller. Hot-zone temperature was measured with a calibrated S-type Pt/Pt-10Rh thermocouple (Johnson-Matthey Noble Metals, UK) connected to a Keithley 2700 multimeter (Keithley, USA). The cold junction temperature was measured with a Pt100 resistance thermometer connected to a Keithley 2000 DMM multimeter (Keithley, USA). Temperature was data logged with LabVIEW software.

## 7.2 Procedure

### 7.2.1 Air

The silica crucible, filled with sample material, was placed into a platinum wire basket. The basket was attached to the platinum/platinum-rhodium wire hanging from the top of the furnace, and it was lifted to the hot zone between the heating elements of the furnace by pulling the platinum-rhodium wire upwards from the top of the furnace. The experiments were started with the use of platinum wire, but its strength was found insufficient and it was changed to platinum-rhodium wire. The outer diameter of the crucible basket was deliberately made wider than the inner tube to prevent the crucible from moving any higher than the hot zone and having a fixed position. The contact times studied in this work were chosen to be 10, 20, 30, 60, 150, 300 and 600 seconds. After the chosen contact time, the platinum-rhodium

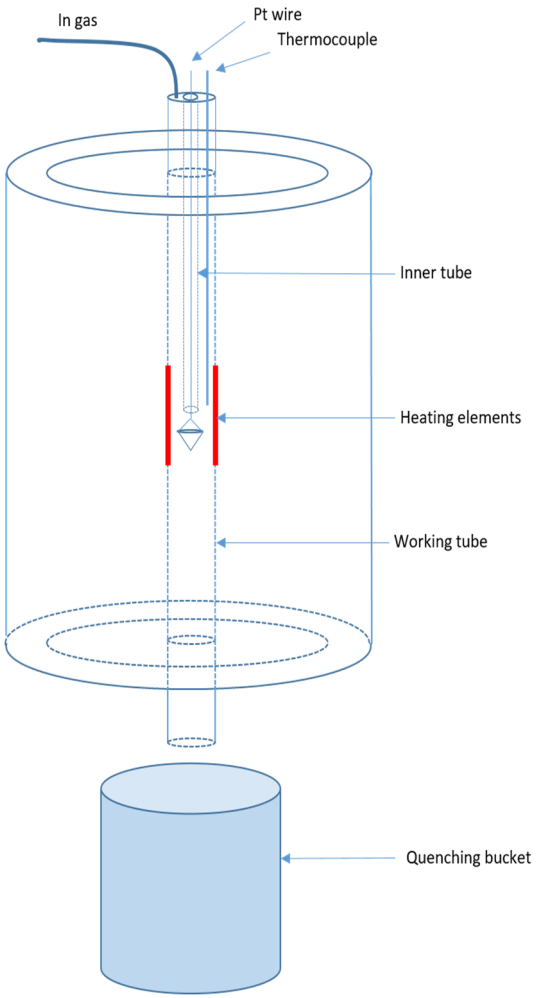


Figure 8. Schematic illustration of the furnace and crucible position

wire was pulled sharply from above, causing the loosely-held platinum-rhodium wire to detach, and the crucible and basket were dropped to the quenching bucket filled with ice water. The sample was then collected for analysis. Since the experiments were conducted in air, oxygen is constantly available in the reactions.

### 7.2.2 Argon

The experiments in argon atmosphere were performed in similar manner as the air atmosphere experiments, but with some alterations. Argon gas flow was directed into the furnace from the gas inlet on top of furnace, and the sample was firstly positioned in the cool zone at the bottom of the furnace. The bottom end of the working tube was then closed with a plug that had tubing in it to allow the gas flow through it. The furnace was then flushed with argon gas for 20 minutes to ensure an inert atmosphere for the experiments. After the argon flushing the sample was lifted to the hot zone. The contact times chosen for argon experiments were 5, 10, 20 and 40 minutes. Shortly before the end of the chosen contact time the bottom end of the working tube was immersed in ice water and the plug was removed below the water level to prevent air from entering the furnace. The end of the working tube was kept below the water level and the samples were quenched directly into the ice water without air contact.

# 8 Analytical procedure

The analytical techniques used in this work are presented in this chapter. The overall quality and microstructure of the samples were studied with SEM-EDS (scanning electron microscopy-energy dispersive X-ray spectroscopy). The trace element concentrations in the slag were analysed by using LA-ICP-MS (laser ablation-inductively coupled plasma-mass spectrometer) and the concentrations in matte were analysed with EPMA (electron probe micro analyser). The SEM-EDS analyses were performed at the Aalto University Department of Chemical and Metallurgical Engineering. The LA-ICP-MS and EPMA analyses were carried out at GTK (Geological Survey of Finland).

## 8.1 Preparation of polished sections

The crucibles were mounted in epoxy resin, cut in half and mounted in epoxy resin again. The cross-section was ground and polished with silicon carbide papers (P120, P240, P400, P800, P1200 and P2500) and diamond polishing (3 µm, 1 µ). The cross-section surfaces were carbon-coated for SEM and EPMA.

## 8.2 SEM-EDS

The primary elemental analysis of the samples was carried out by using SEM-EDS. EDS is a technique that is based on the collection and energy dispersion of characteristic X-rays. The system includes a source of high-energy radiation, in this case electrons, a sample, a solid state detector and signal processing electronics. X-rays that enter the detector are converted to signals that are processed to produce an X-ray energy histogram. This spectrum consists of a series of peaks that are representative of the type and relative amount of each element in the sample. The number of counts in each peak are further converted into elemental weight concentration by comparison with standards. (Glaeser 2012)

All of the experiments performed in this work were firstly analysed with Tescan MIRA 3 SEM (Tescan, Brno, Czech Republic) equipped with an UltraDry Silicon Drift Energy Dispersive X-Ray Spectrometer and NSS Microanalysis Software (Thermo Fisher Scientific, Waltham, MA, USA) to make sure that the microstructures and phase compositions were as expected. For the major element concentrations in the slags, only EDS analysis results were used.

## 8.3 EPMA

EPMA (Electron probe microanalysis) is a technique used for non-destructive chemical analysis of minute solid samples. Its operating fundamentals are similar to those of SEM, and it can be used to acquire elemental analyses at very small spot sizes. In EPMA the sample is bombarded with an accelerated and focused electron beam. The interaction between the material and electron beam generate heat, and ejected secondary and back-scattered electrons and X-rays, which can be used for surface imaging and obtaining the average composition of the sample. (Goodge 2017)

The EPMA used in this work was a Cameca SX100 electron microprobe equipped with five wavelength dispersive spectrometers (Cameca SAS, Gennevilliers, France). Accelerating voltage was 20 kV, beam current 60 nA and beam diameter 100 µm. Analysed lines and standards (Astimex) used were as follows: Fe $K_\alpha$ and O Kα(hematite), Mg $K_\alpha$ (diopside), S $K_\alpha$ (pentlandite), Cu $K_\alpha$ (Cu), Zn $K_\alpha$ (sphalerite), Pd $L_\alpha$ (Pd), Ag $L_\alpha$ (Ag), Pt $L_\alpha$ (Pt), Pb $L_\alpha$ (galena) and Au $L_\alpha$ (Au). The detection limits are presented in Table 7.

## 8.4 LA-ICP-MS

The trace element concentrations in the slags were analysed by using LA-ICP-MS, which is an analytical technique that enables sensitive elemental and isotopic analysis of solid samples. It provides major, minor, and trace element information with a wide

elemental coverage and excellent limits of detection. In this technique, the sample surface is irradiated with deep-UV output from a laser. The high-intensity pulsed UV beam is focused onto the sample surface in a helium-purged ablation chamber, causing ablation of the sample. The UV beam diameter can be set by software-controlled apertures to produce spot sizes varying from < 5 µm to 300 µm depending on the application.

As the pulsed laser beam causes fine grains of material to detach from the sample surface, the resulting laser-induced aerosol is then transported to the inductively coupled plasma in a helium carrier gas stream. This stream is mixed with argon gas before entering the argon plasma. In the plasma, the aerosol is decomposed, atomised and ionised. The ionised particles are then extracted from the plasma and directed to the mass spectrometer vacuum system, where they are separated according to their mass-charge ratio and detected with an ion-detector. (Neufeld 2004, Limbeck, Galler et al. 2015, Klemettinen 2017)

The equipment used in this work was a Photon Machines Analyte Excite laser ablation system with 193 nm wavelength 4 ns ArF excimer laser (Teledyne CETAC Technologies, Omaha, USA) coupled to a NuAttoM single collector sector field ICP-MS (Nu Instruments Ltd., Wrexham, UK), housed at GTK. The laser spot size was selected as 65 µm for the air experiments, and 40 µm for the argon samples due to the very limited size of slag areas available, as shown in **Error! Reference source not found.**. The laser was fired at 10 Hz frequency and the energy was set to 27.9% of 4 mJ, resulting in a fluence of 2.5 J/cm$^2$ on the sample surface. The analysis procedure consisted on 5 pre-ablation pulses to remove carbon coating and possible contamination from the surface, followed by 20 second pause, 20 second gas background analysis, and 400 (air) or 300 (argon) pulses of sample analysis.

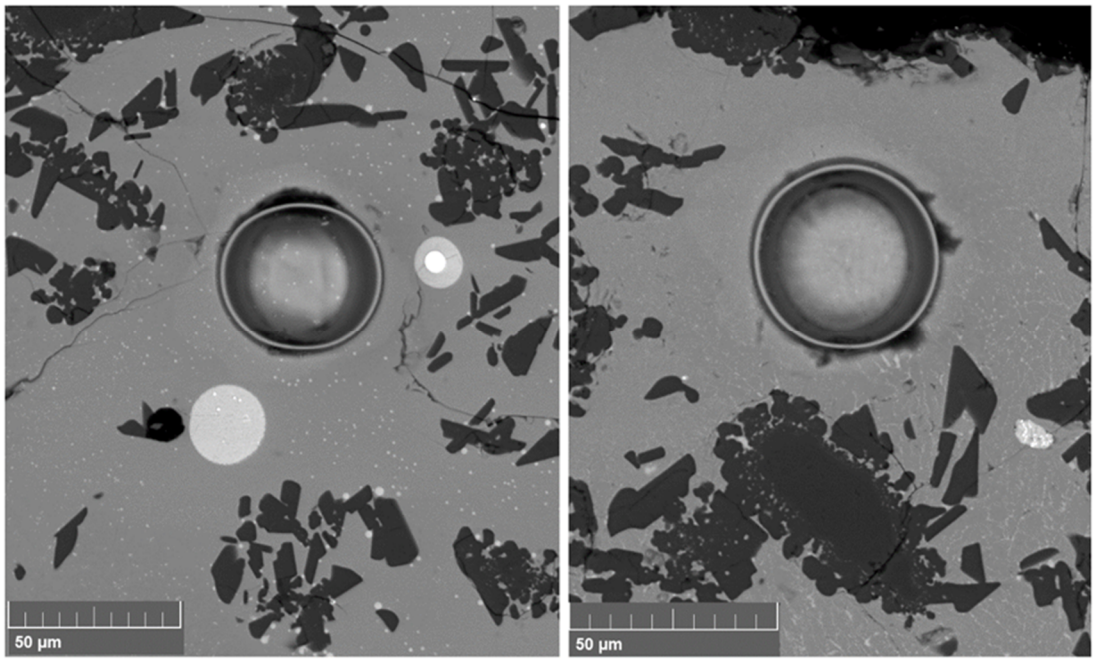


Figure 9. SEM-BSE images of laser ablation pits in a sample reacted in argon atmosphere for 5 minutes. The dark grey grains within the slag are tridymite (silica).

NIST 610 SRM (Jochum, K. P., Weiss et al. 2011) was used as the external standard and $^{29}$Si as the internal standard, with concentration values obtained from EDS. NIST 612, USGS BHVO-2G and BCR-2G (Jochum, Klaus Peter, Willbold et al. 2005) glasses were analysed as unknowns for monitoring the hardware conditions and analysis quality. The mass spectrometer was operated in FastScan mode with low resolution ($\Delta M/M = 300$) for maximum sensitivity. Data reduction was performed with Glitter software (Van Achterberg, E. et al. 2001). For the precious metals of interest in this work, $^{104,105,106,108,110}$Pd, $^{107,109}$Ag, $^{194,195,196}$Pt and $^{197}$Au isotopes were analysed.

With LA-ICP-MS, palladium has been found to be a problematic element from analytical viewpoint. (Sukhomlinov, Klemettinen et al. 2019) Its most commonly used isotope for quantification in the ICP-MS technique is $^{105}$Pd, but significant mass interference exists with copper argide ($^{40}Ar^{65}Cu^{+}$) formed in argon plasma of the ICP when copper containing samples are analysed. Therefore, $^{104}$Pd was chosen for the analysis. For Ag and Pt the different isotopes showed congruent results in the analysis, and $^{107}$Ag and $^{195}$Pt were chosen to represent the samples. For Au, the only

stable isotope is $^{197}Au$, which was used for concentration quantifications. The obtained detection limits are shown in Table 7.

Table 7. EPMA and LA-ICP-MS detection limits in ppm.

| | O | Si | S | Fe | Cu | Zn | Pd | Ag | Pt | Pb | Au |
|---|---|---|---|---|---|---|---|---|---|---|---|
| EPMA (matte) | 1499 | | 138 | 221 | 338 | 397 | 248 | 448 | 797 | 1274 | 1196 |
| LA-ICP-MS (slag) | | | | | | | | | | | |
| 65µm spot (air) | | 3.8 | | | | 0.3 | 0.03 | 0.005 | 0.002 | 0.002 | 0.001 |
| 40µm spot (Ar) | | 8.6 | | | | 0.6 | 0.09 | 0.01 | 0.003 | 0.004 | 0.002 |

Figure 10 and Figure 11 show the time-resolved laser analysis signals for samples with 20 s and 150 s contact time in air atmosphere. When the element of interest is chemically dissolved into the slag, homogeneously within the ablated area, the signals should look smooth, without any significant higher peaks. As is evident from Figure 11, the signals obtained from several analysis points in two 150 s air atmosphere samples look fairly smooth, indicating homogeneous chemical solubility in the analysed area. In the case of 20 s samples, the signals show clear peaks, which can be interpreted as mechanically entrained areas (for example matte droplets) with locally higher gold concentrations. In general, the elements studied in this work dissolved more homogeneously into the slag when the contact time was longer. Some inhomogeneities were, however, observed after the longer contact times as well. The analysis signals were individually treated in Glitter software to eliminate the effect of the peaks, i.e. mechanical entrainment, whenever possible.

At short contact times, the effect of mechanical entrainment was quite significant. After longer contact times, for example 150s shown in Figure 1, the obtained concentration values can be almost entirely attributed to chemical solubility of the PGM's into the slag. In general, the experiments conducted in argon atmosphere

showed smoother analysis signals, i.e. more homogeneous PGM solubility, compared to the air atmosphere experiments.

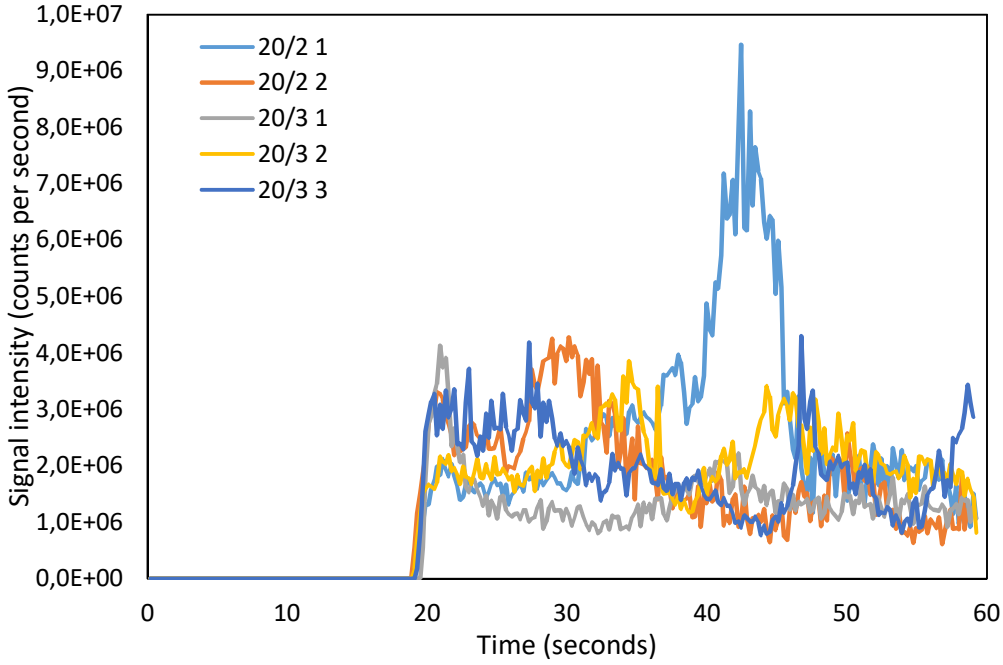


Figure 10. Time-resolved laser analysis signal for gold in a sample with 20 s contact time in air atmosphere.

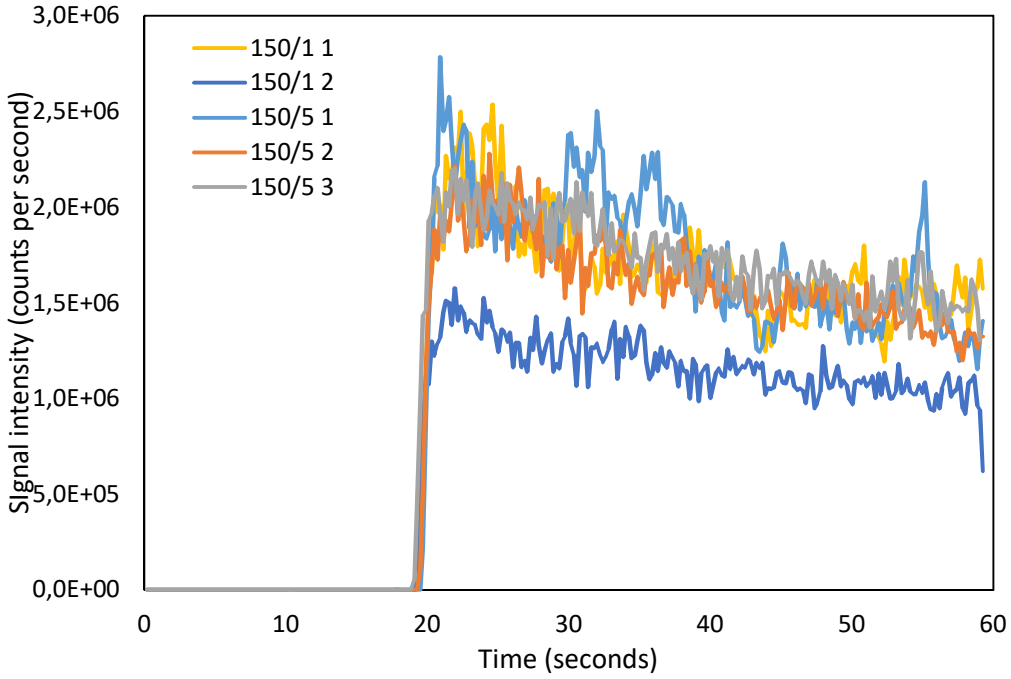


Figure 11.Time-resolved laser analysis signals for gold in samples with 150 s contact time in air atmosphere.

# 9 Results and discussion

The experimental parameters in this work were chosen based on earlier experiments conducted by the research group. The sulphidic phase did not reach copper contents high enough in the experiments with contact time less than 300 s to be actually classified as matte. However, for the sake of clarity, the phases are referred from now on as matte and slag.

## 9.1 Air atmosphere

### 9.1.1 SEM analysis

In Figure 12**,** a polished cross section of a sample after 10 seconds of contact time is shown. The structure is highly inhomogeneous at this point. The experiment of 10 s contact time was repeated several times unsuccessfully, indicating that 10 s was not enough time for the sample to reach a high enough temperature. There is significant amount of unmelted silica present in the sample, as shown by C in the figure. The liquid fayalite slag phase has not started to form at this point, as there are mainly iron oxides present at areas such as B. The concentrate seems to have started to melt. Platinum is found in clusters with smaller amounts of copper, iron and precious metals as pointed out by A.

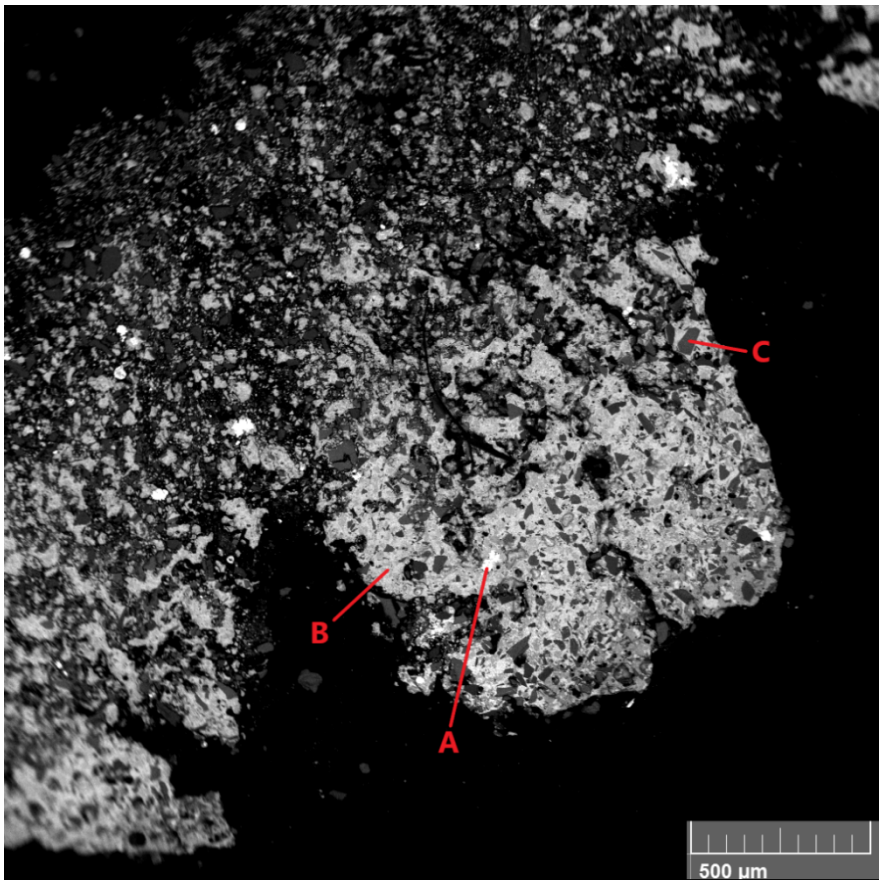


Figure 12. Sample after 10s contact time in air atmosphere.

In Figure 13, a sample after 20 seconds contact time is shown. The light grey areas (A) are matte, the darker areas (B) are slag and the darkest grey areas (C) are unreacted silica. The fayalite slag phase is gradually forming and is starting to segregate from the matte phase, but the matte is rather randomly distributed, which shows that the coagulation and settling have not taken place at this point. Magnetite was observed in the sample. There is still a significant amount of unreacted silica present. Platinum is forming a metallic phase with copper and iron enclosed within the matte phase. There are also smaller clusters of precious metals, copper and iron

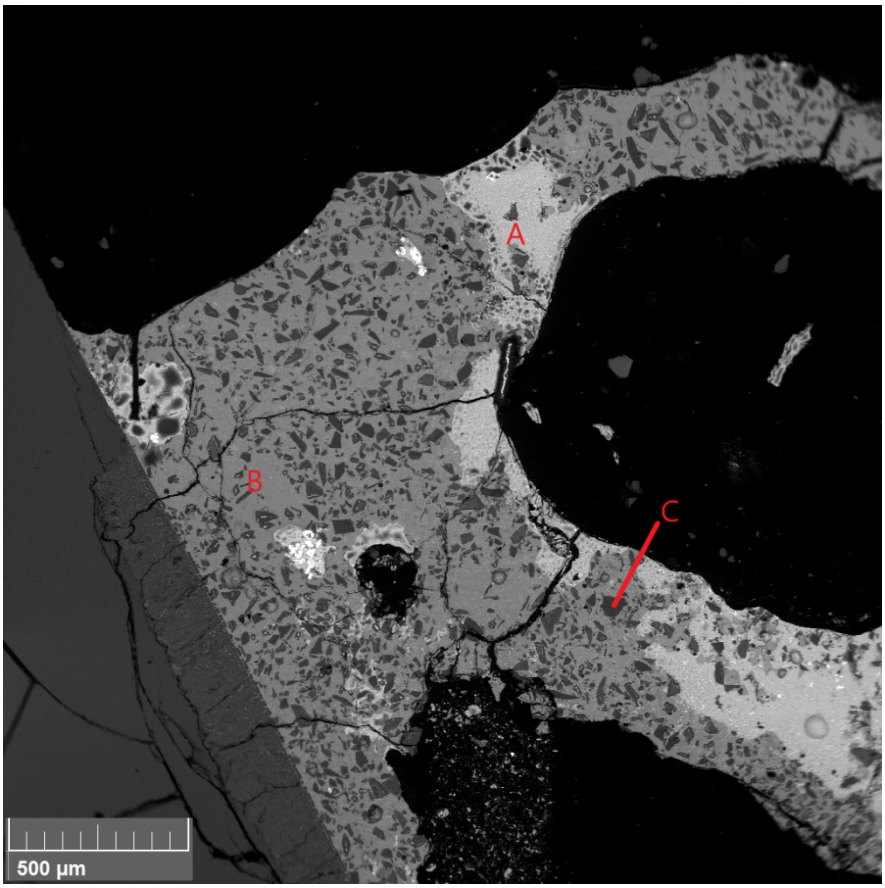


Figure 13.Sample after 20s contact time in air atmosphere.

within the slag. Gold, silver and palladium disperse more evenly into the matte phase, though part of them are precipitated as their own clusters in matte and slag phases.

Figure 14 shows the structure of a sample after 30 seconds contact time. At this point the structure is already significantly different from the samples with shorter contact times. The amount of unreacted silica has decreased noticeably and the slag and matte have been separated to a larger extent. Individual droplets of matte are found in the slag phase. The precious metals are found mostly in the matte phase at this stage.

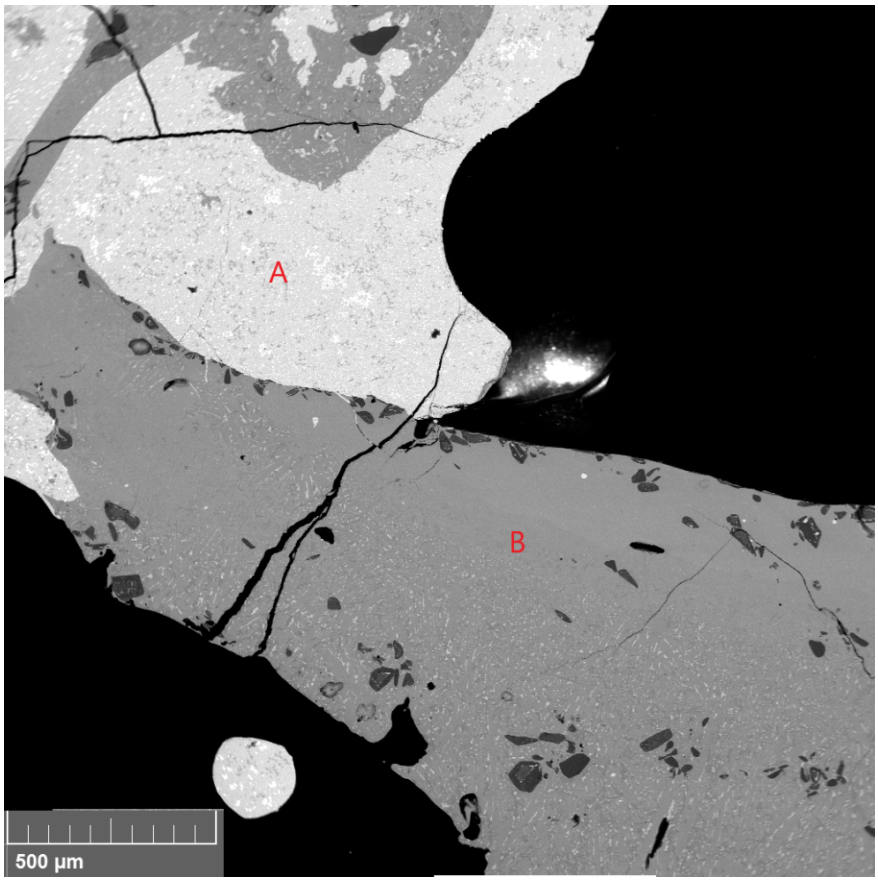


Figure 14. Sample after 30s contact time in air atmosphere.

After 30 seconds contact time the remaining unmelted silica reacted quickly. In Figure 15, the situation after 60 s contact time is shown, and it can be seen that only small amounts of unreacted silica are present in the slag phase. In Figure 16 and Figure 17 samples after 150 s and 300 s contact time are presented. After 300 seconds contact time there was no unreacted silica left and by visual inspection the sample seems similar to that of 150 s. The silica crucible was dissolving into the slag, expectedly causing silica saturation of the slag. The precious metals were found in the matte phase where they were dispersed or separated. The slag was found to have fayalitic composition. Some matte droplets were found entrained in the slag and attached to the interface between silica and slag. Platinum formed platinum-rich areas with smaller amounts of gold, palladium, copper and iron in them.

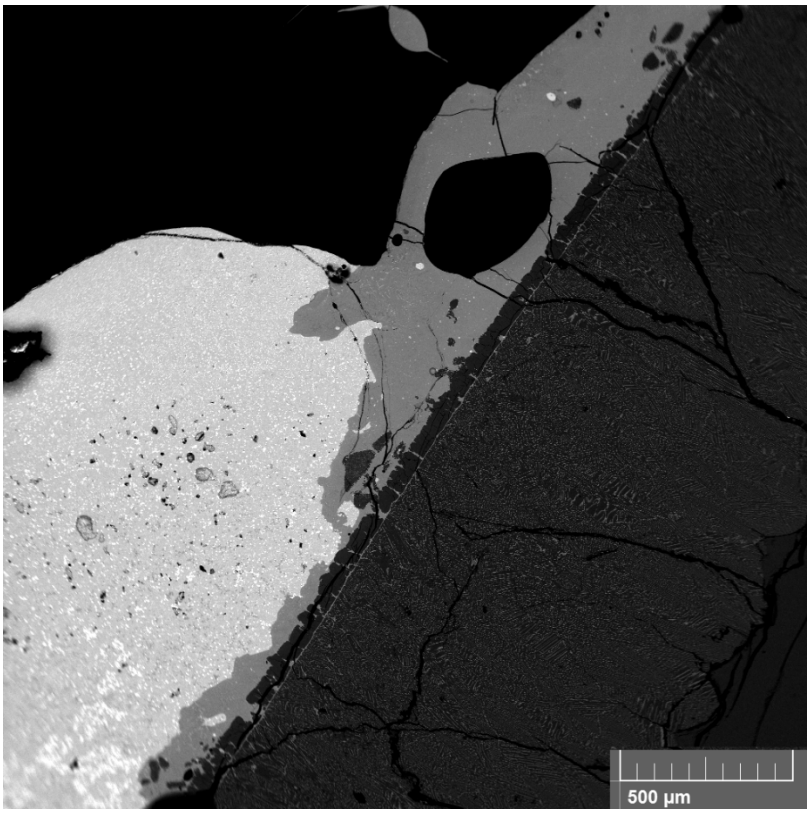


Figure 15. Sample after 60s contact time in air atmosphere.

In samples after 150 s and 300 s contact time, the precious metals formed significantly larger clusters containing precious metals, copper and iron. These are shown in Figure 18 and Figure 19. In the 150 s sample an area of high platinum and gold content was found. In the 300 s sample a large cluster with a platinum core was formed. Platinum core was surrounded by a shell of precious metals with copper and iron. Droplets of copper sulphide were confined within precious metal-copper-iron alloy.

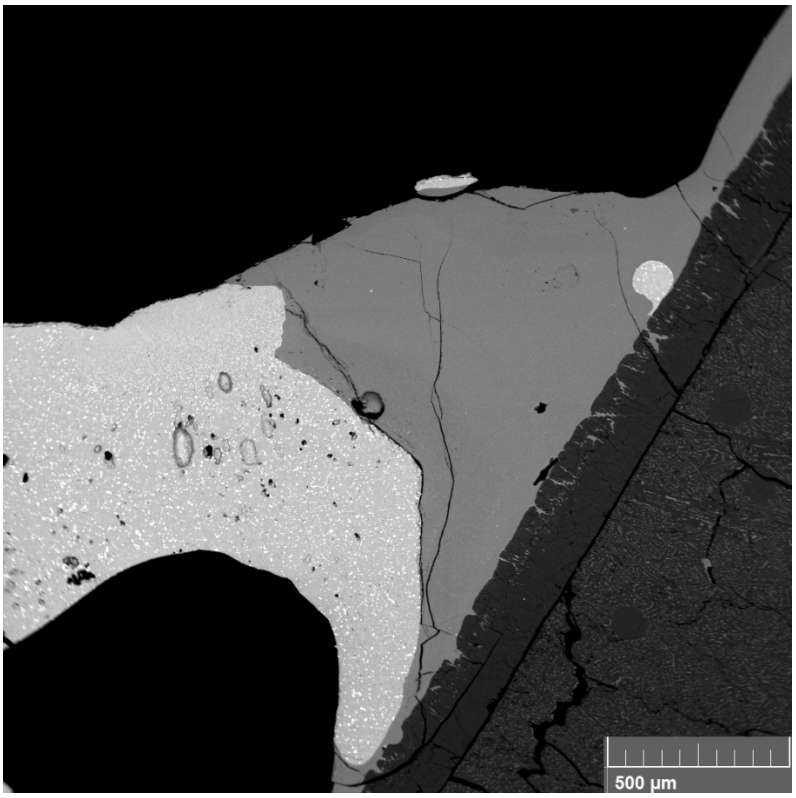


Figure 16. Sample after 150 s contact time.

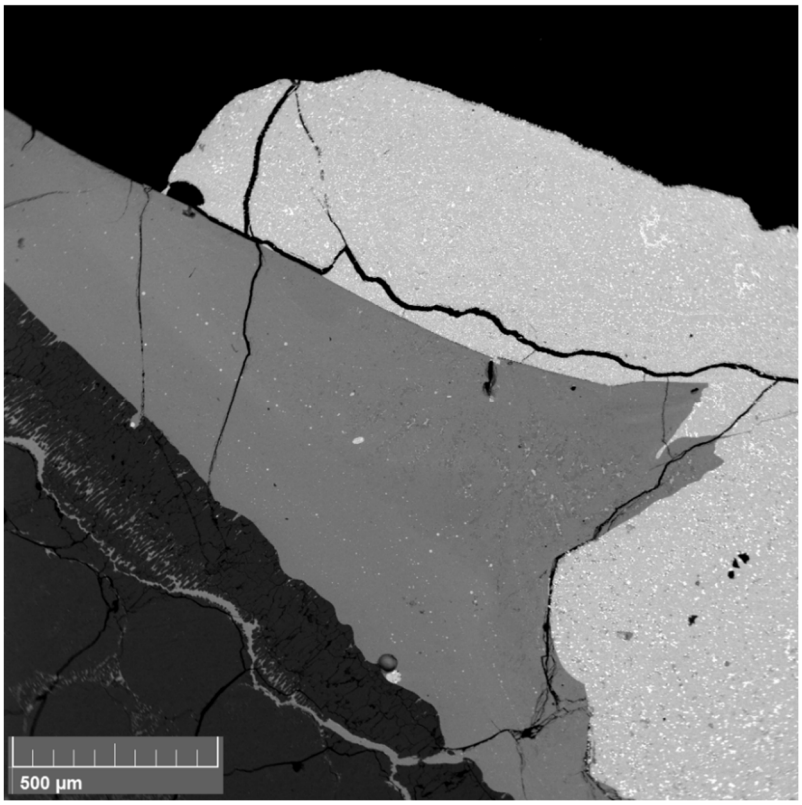


Figure 17. Sample after 300s contact time in air atmosphere.

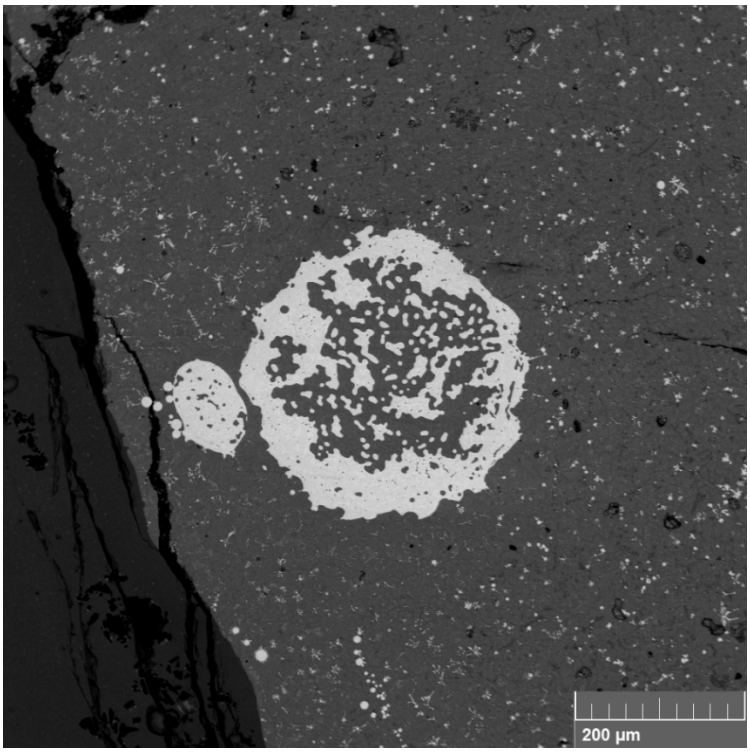


Figure 18. A sample after 150 s contact time with a platinum- and gold-rich cluster.

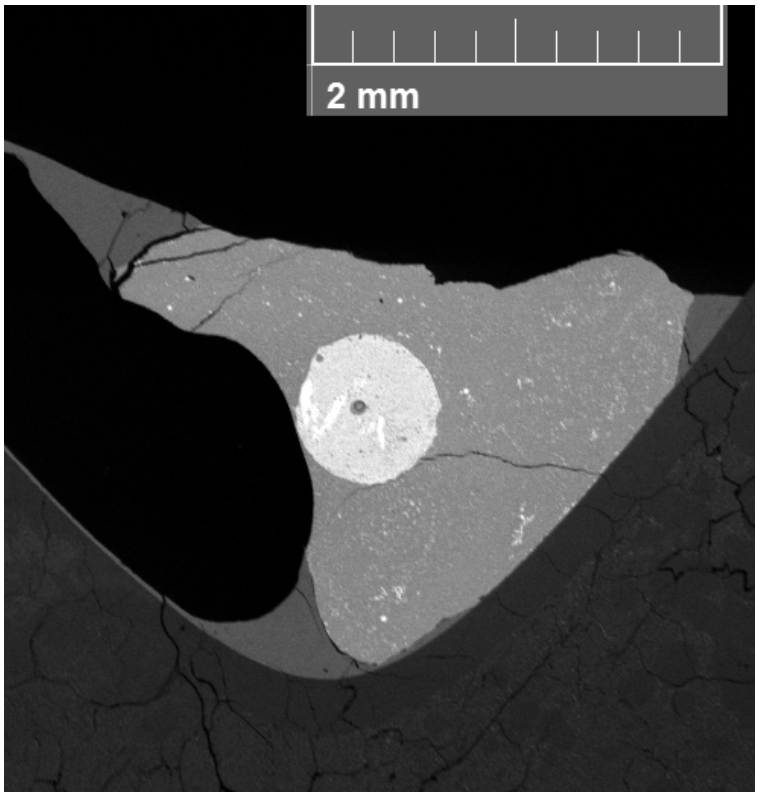


Figure 19. A sample after 300 s contact time, showing a large precious metals-copper-iron cluster.

In Figure 20 the EDS results for iron and silicon in slag are shown. There was very little deviation in the analysis results, and it was observed that the concentrations of iron and silica in slag stabilised very quickly. The error bars are the standard deviations of the results, but they are too small to be distinguished from the symbols.

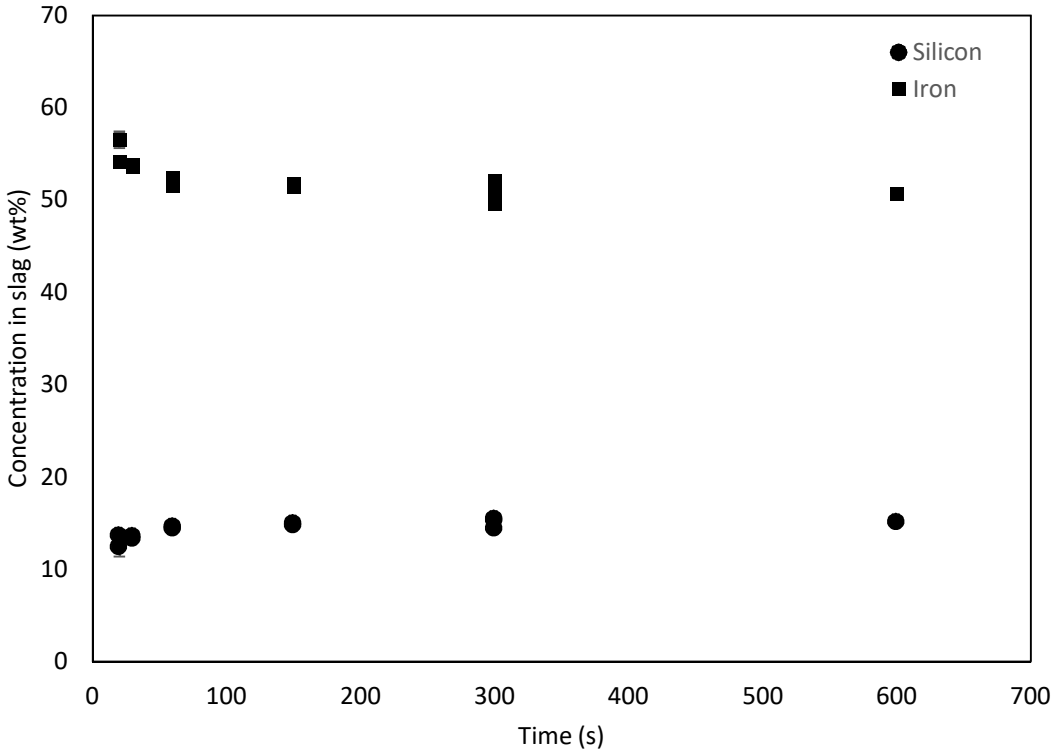


Figure 20. Concentrations of iron and silicon in slag as a function of contact time in air atmosphere.

### 9.1.2 EPMA results

In this section the results of the EPMA analysis of the matte are presented. The results contain the analysis of two samples for each time point, except 300 s where three samples were analysed and 600 s where only one experiment was performed and analysed. The error bars in the graphs are the standard deviations of the results.

In Figure 21 the copper content of matte is presented as a function of time. The copper content increased slowly up to the contact time of 150 s, but with longer contact times the results differ significantly from one another. The copper content is increasing with longer contact times, but it should be noted that in these experiments the matte grade increases more slowly compared to earlier experiments. (Guntoro, Jokilaakso et al. 2018, Wan, Jokilaakso et al. 2019)

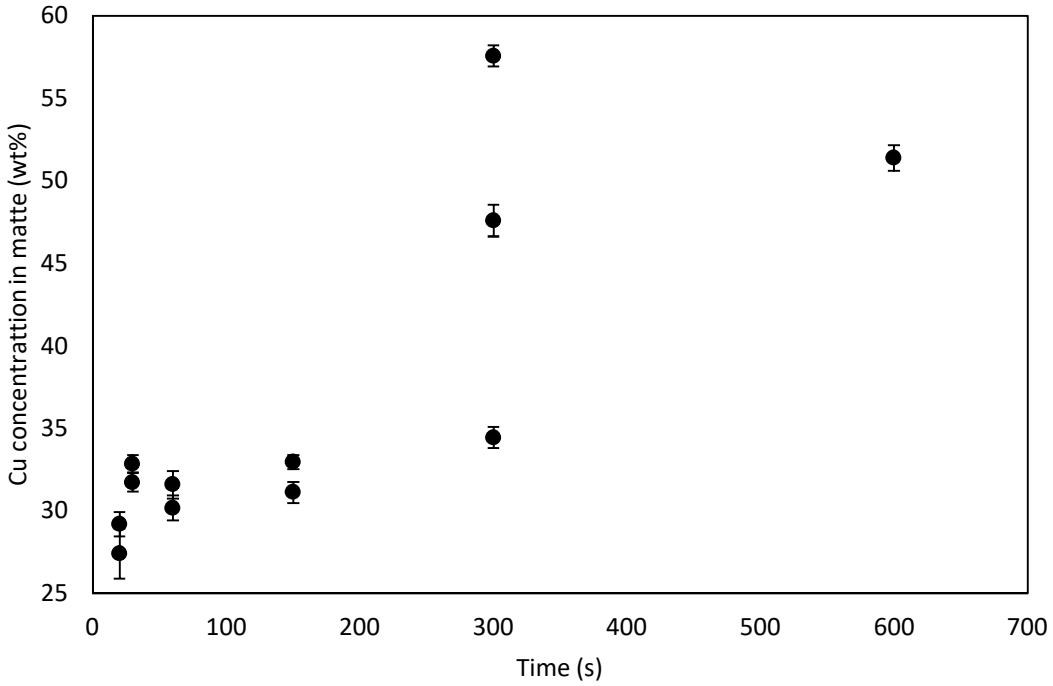


Figure 21. Concentration of copper in matte as a function of contact time in air atmosphere.

The iron concentration in matte is shown in Figure 22. Like copper, the iron concentration remained relatively stable during contact times up to 150 s, showing

only slight decrease. At 300 s the iron content shows the same kind of deviation as copper, with copper-richer samples containing less iron.

The sulphur content of the matte at different contact times is shown in Figure 23. Similarly to iron, sulphur content showed a slight decrease as a function of contact time. As in the case of iron, sulphur content showed very little deviation in the analysis at 150 s contact time.

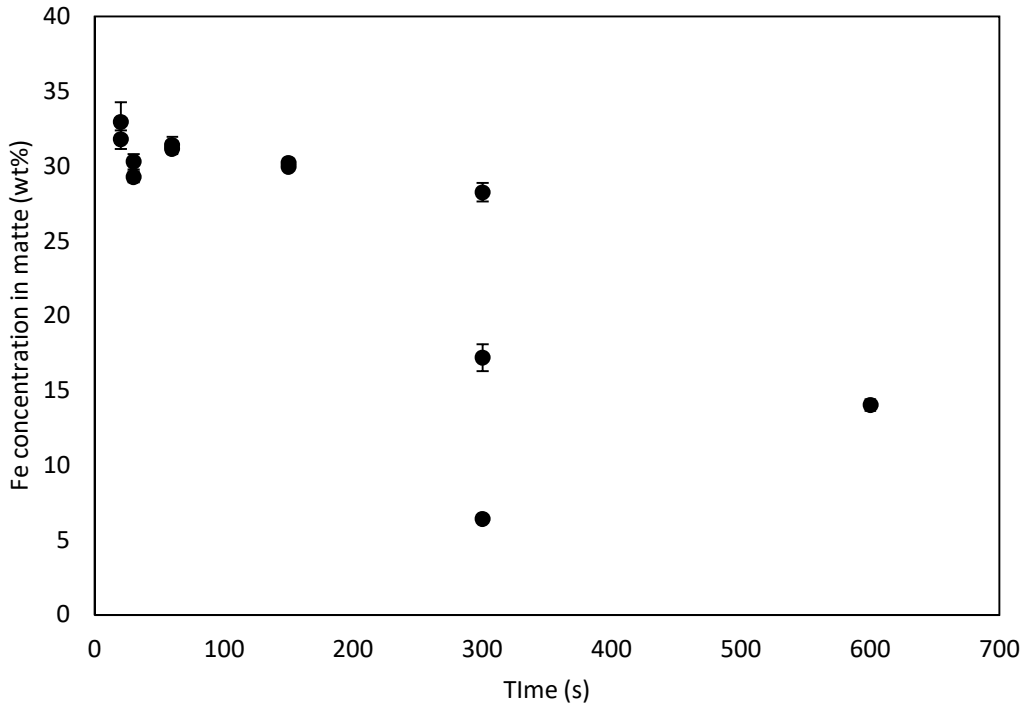


Figure 22. Concentration of iron in matte as a function of contact time in air atmosphere

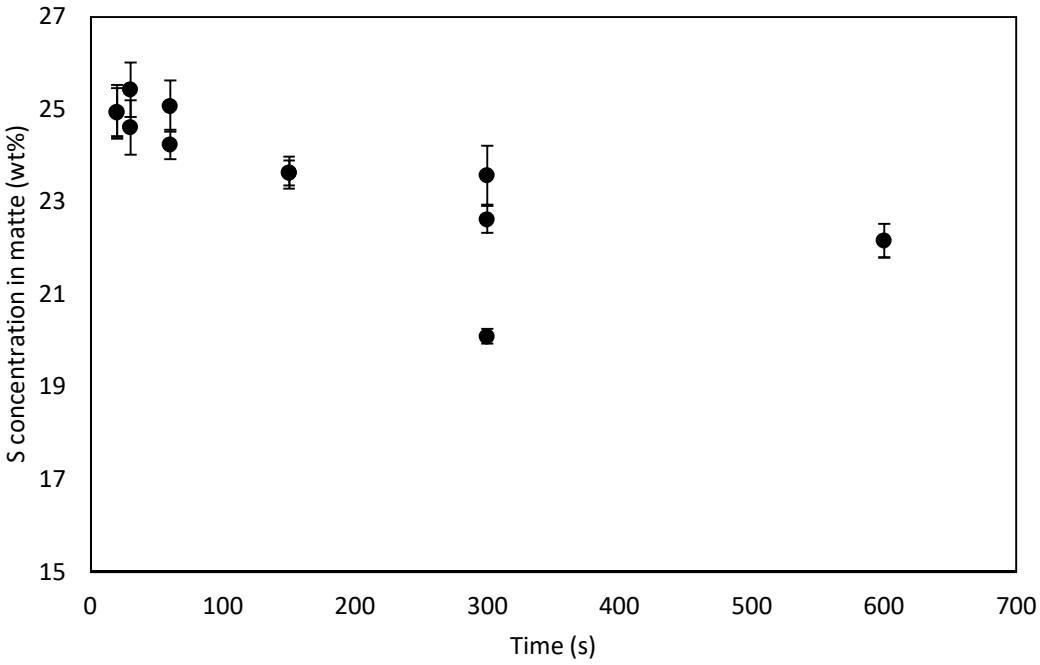


Figure 23. Concentration of sulphur in matte as a function of contact time in air atmosphere.

The results for the palladium concentration in matte are shown in Figure 24. As the variation in the copper concentration increased also the variation in palladium concentration increased. The silver concentration in matte reached higher levels compared other precious metals, as shown in Figure 25.

.

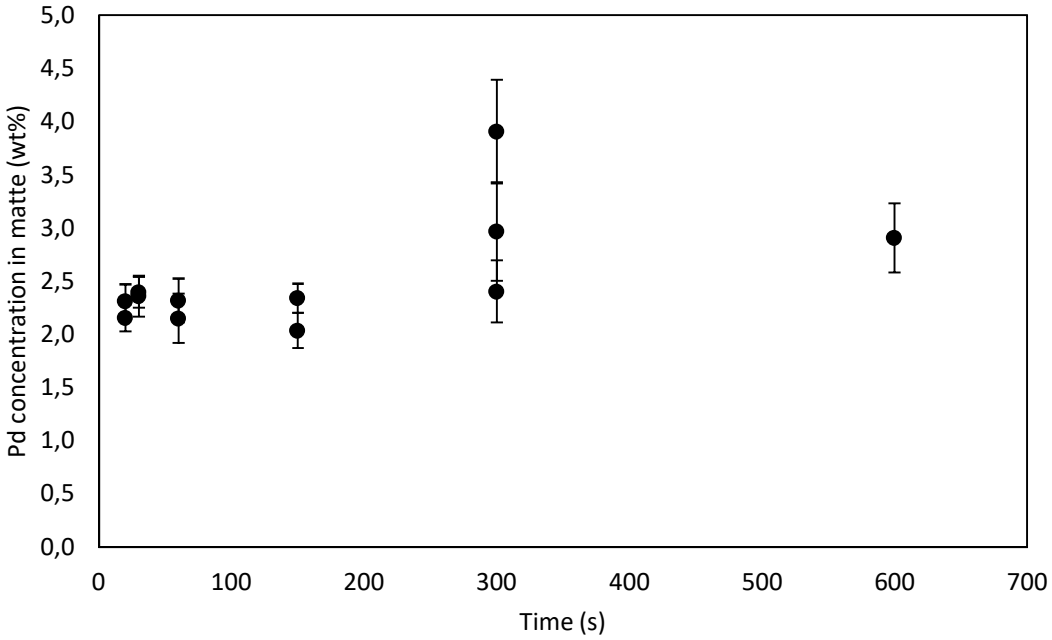


Figure 24. Palladium concentration in matte as a function of contact time.

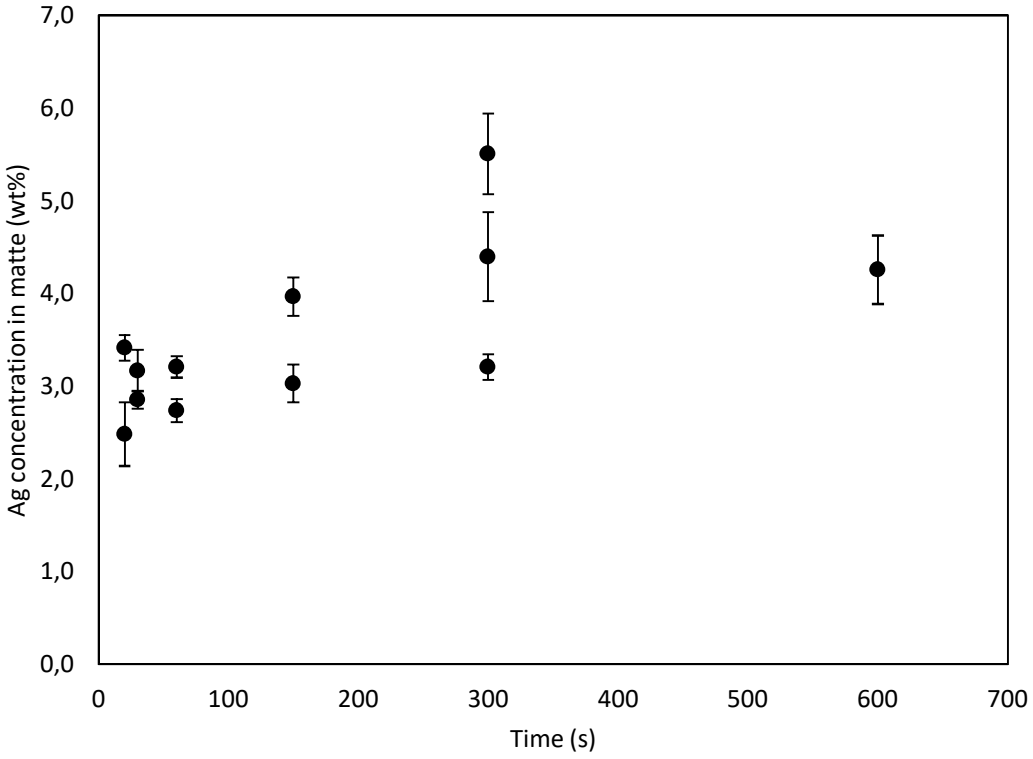


Figure 25. Silver concentration in matte as a function of contact time.

The results for platinum concentration in matte showed significant deviation, as can be seen from Figure 26. Platinum concentration in matte was noticeably lower than that of other precious metals. This can be due to the observation that platinum tended to form metallic phase areas within the matte phase, with smaller amounts copper, iron and other precious metals. Therefore its concentration varied significantly between different analysis sites.

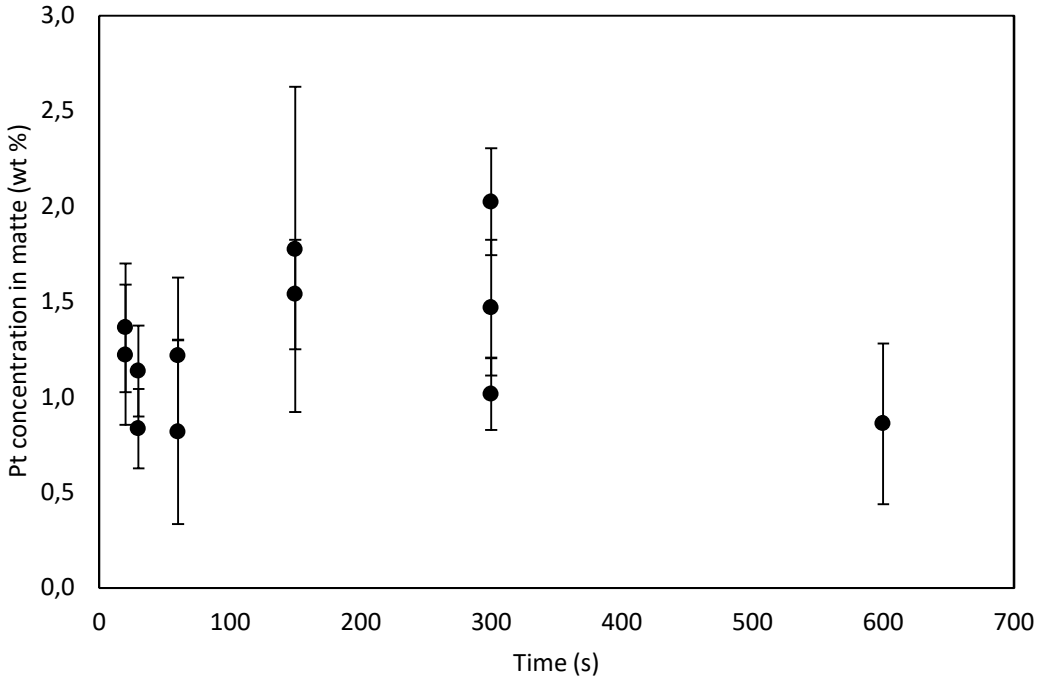


Figure 26. Concentration of platinum in matte as a function of contact time in air atmosphere.

The gold concentration in matte as a function of contact time is shown in Figure 27. It seemed to remain relatively constant during different reaction times up to 150 s. At 300 s contact time the gold concentration showed a clear increase along the increased copper content. The results varied between analysis points as described by the error bars, but the deviation between the analysis results remained relatively stable.

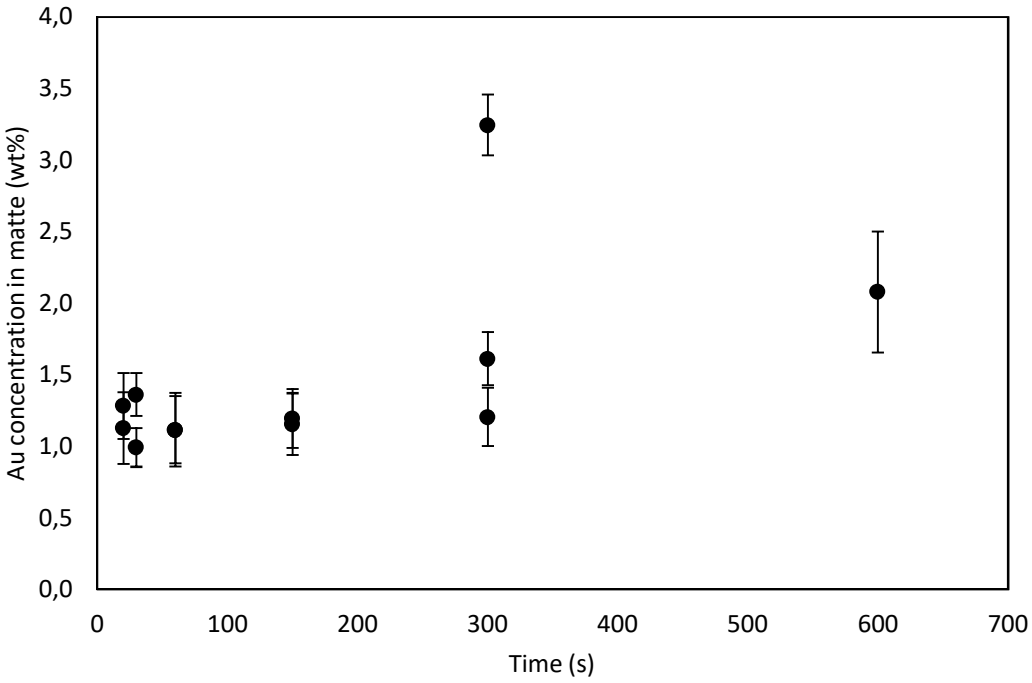


Figure 27. Concentration of gold in matte as a function of contact time in air atmosphere.

### 9.1.3 LA-ICP-MS results

In this section the LA-ICP-MS results in air atmosphere are presented in Figures 28-31. For each contact time there are analyses from two samples, except for 300 s time, for which there are three samples, and one sample for 600 s. This is the case for all LA-ICP-MS precious metal analyses in air. The error bars in the analysis results are the standard deviations of the LA-ICP-MS results. In the 10 s sample, no liquid slag was formed, therefore it was left out of these analyses. The copper concentration of the slag was not analysed with laser, but based on the results from EDS analyses it can be assumed low (< 1 wt%). The palladium (Figure 28), platinum (Figure 30) and gold (Figure 31) concentration in the slag had similar kind of downward trend. The silver concentration (Figure 29) showed no clear trend as a function of contact time.

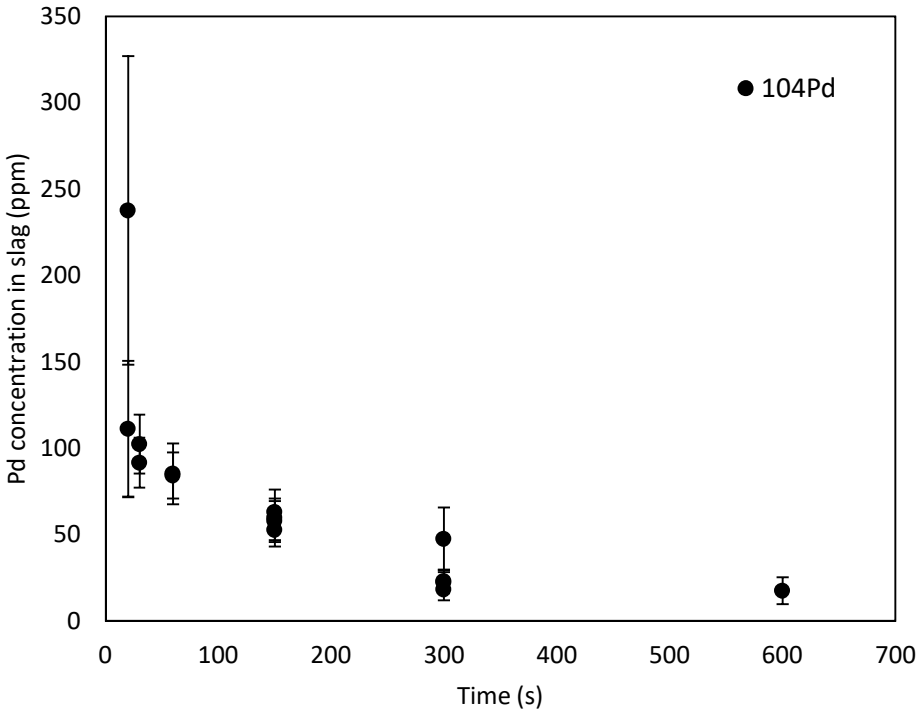


Figure 28. Concentration of palladium in slag as function of contact time in air atmosphere.

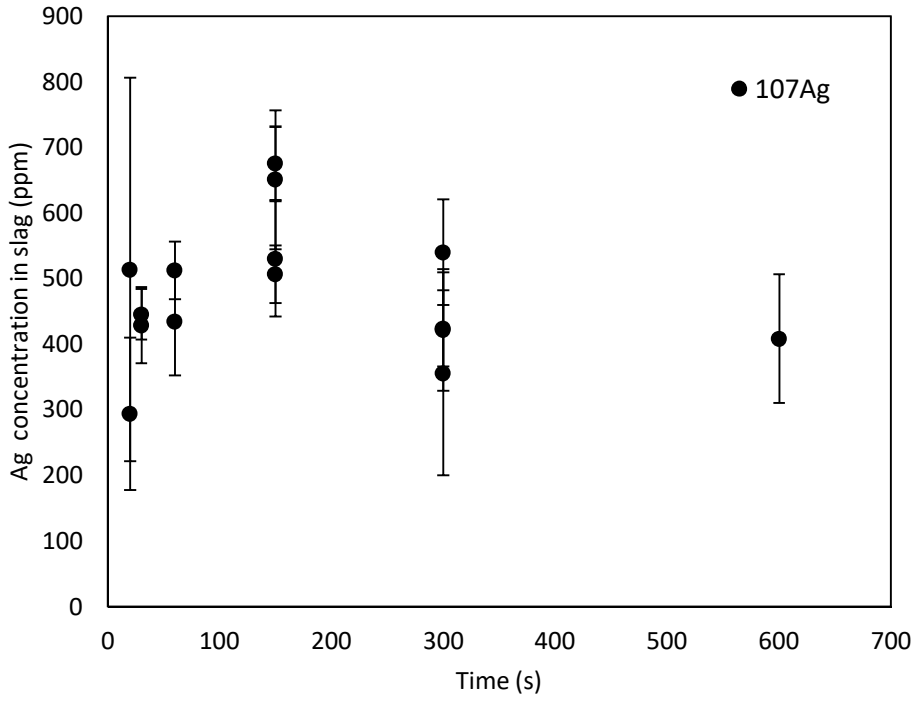


Figure 29. Concentration of silver in slag as function of contact time in air atmosphere.

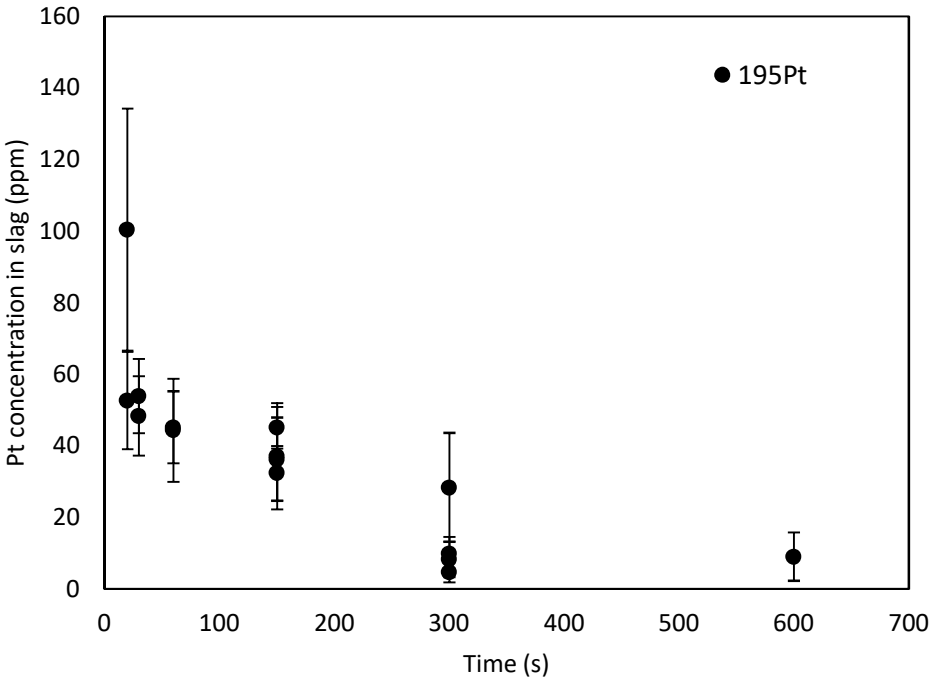


Figure 30. Concentration of platinum in slag as function of contact time in air atmosphere.

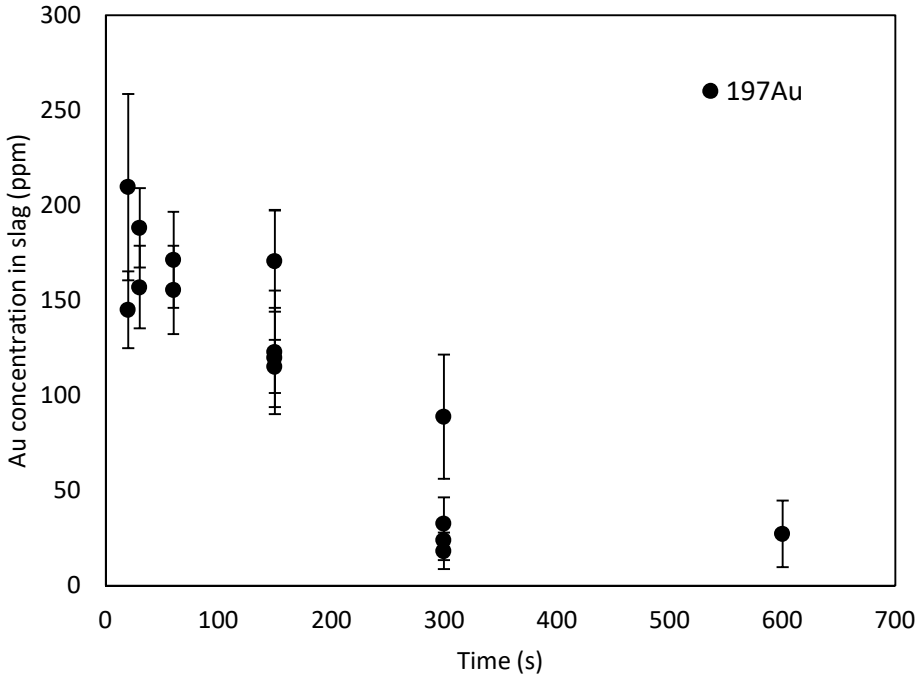


Figure 31. Concentration of gold in slag as function of contact time in air atmosphere.

### 9.1.4 Distributions

In Figures 32-35 the logarithmic distribution coefficients palladium, platinum, silver and gold between matte and slag are shown in comparison with results from equilibration studies between matte and iron-silicate slag. (Shishin, Hidayat et al. 2019, Avarmaa, O'Brien et al. 2015, Henao, Yamaguchi et al. 2006) The equilibration time in referenced studies were 24 h, 3 h and 24 h, respectively. The reference values for the equilibrium distribution coefficients were selected from results where the temperature and matte grade were closest to those in this work.

The distribution of palladium (Figure 32), platinum (Figure 33) and gold (Figure 35) follow a similar increasing trend. In the case of silver (Figure 34), the distribution coefficient shows a slight decrease at first, but starts to increase with contact times longer than 150 s.

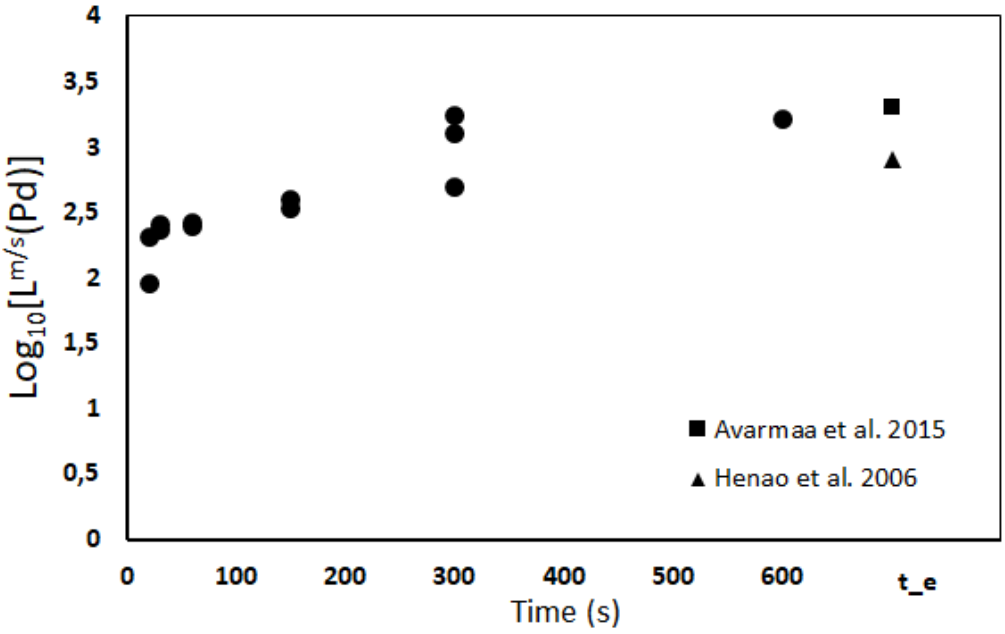


Figure 32. Logarithmic distribution coefficient of palladium as a function of contact time. t_e refers to equilibration time in references.

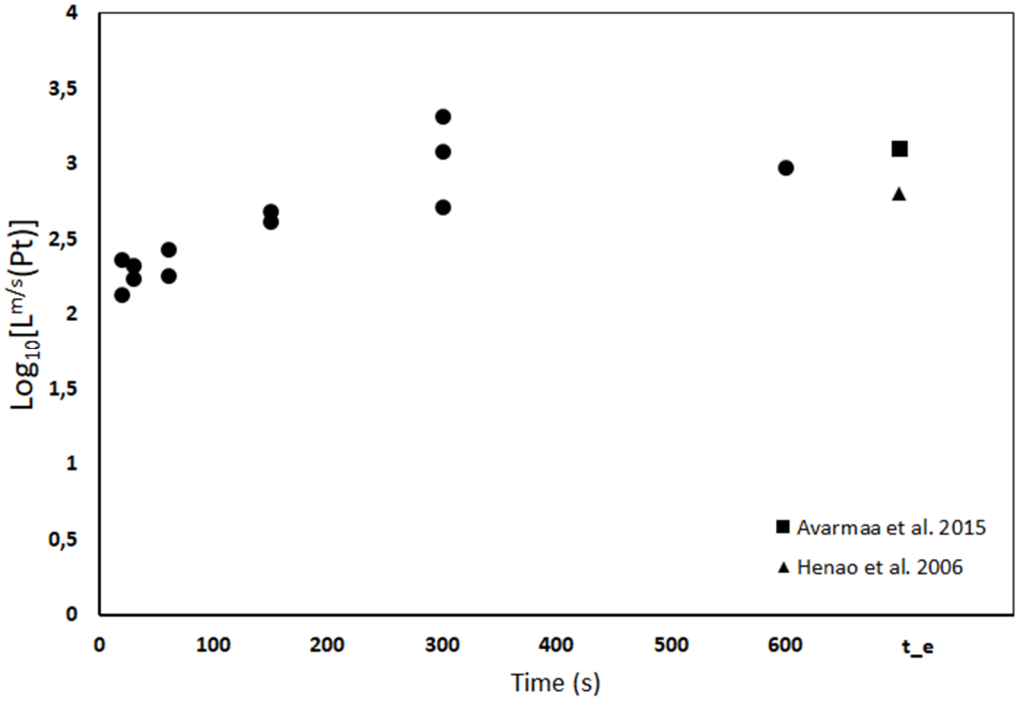


Figure 33. Logarithmic distribution coefficient of platinum as a function of contact time. t_e refers to equilibration time in references.

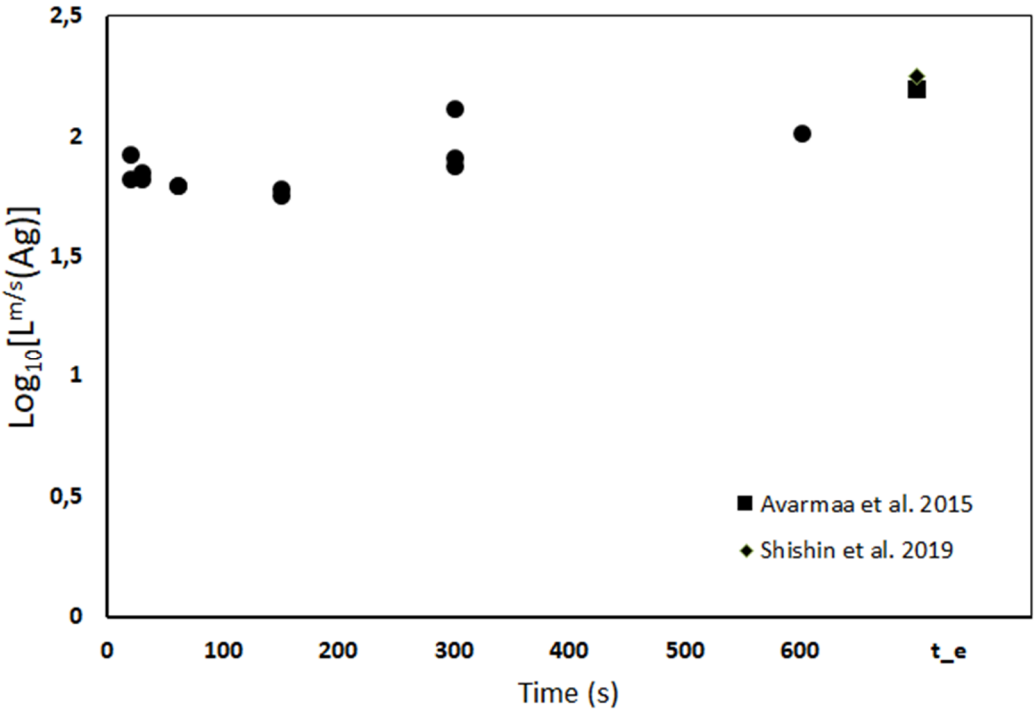


Figure 34. Logarithmic distribution coefficient of silver as a function of contact time. t_e refers to equilibration time in references.

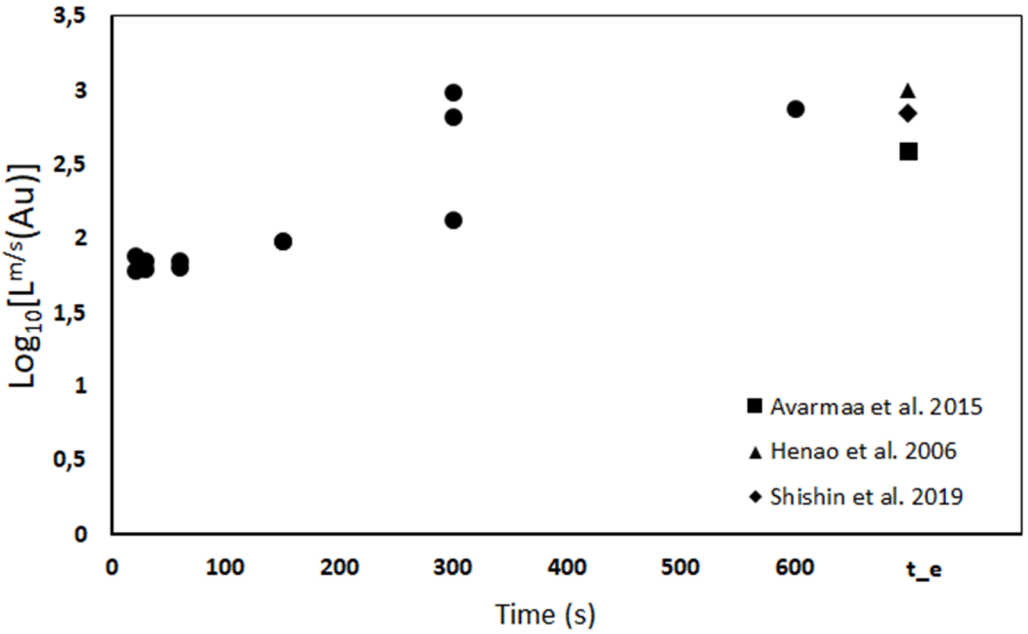


Figure 35. Logarithmic distribution coefficient of gold as a function of contact time. t_e refers to equilibration time in references.

## 9.2 Argon atmosphere

### 9.2.1 SEM-EDS results

After 5 minutes contact time in argon atmosphere the matte and slag phases had clearly separated. However, no settling was observed as the matte and slag were rather unevenly distributed. In Figure 36, a sample with 5 min contact time is shown. Matte and slag phases have formed as pointed by C and B. Clusters of precious metals have formed in the matte (D). Silica crucible is reacting with the liquid slag (A). In Figures 37-39 the samples with 10, 20 and 40 min contact times are shown. It can be seen from these images that there is very little change in the structure of the samples with increasing contact time. With longer contact times, the precious metals have more time migrate and form droplets. In 40 min contact time the precious metal-rich droplets seem to be mostly found near the slag-matte interface.

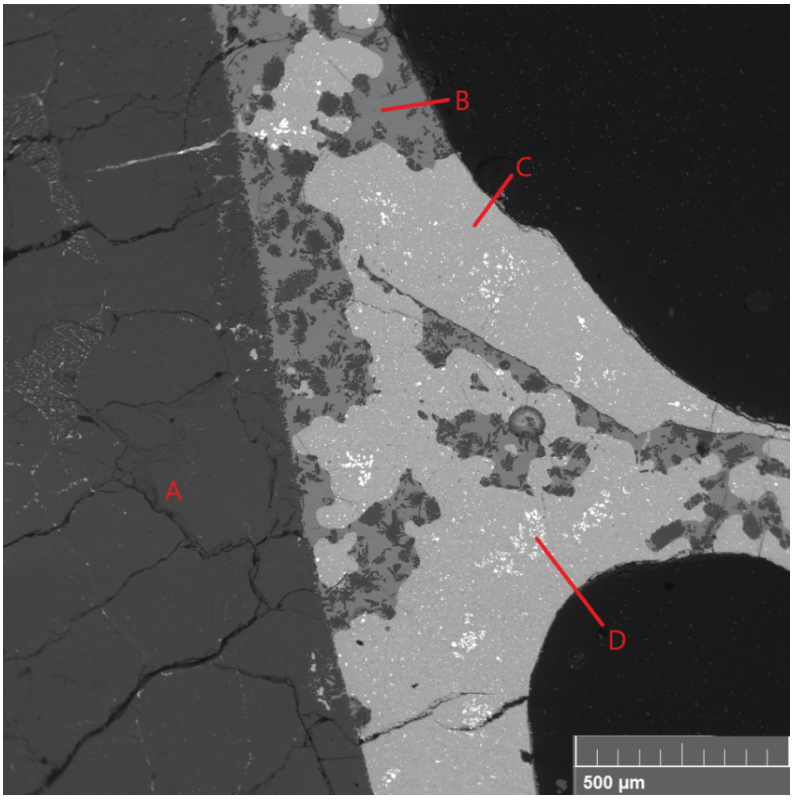


Figure 36. A sample after 5 min contact time in argon atmosphere.

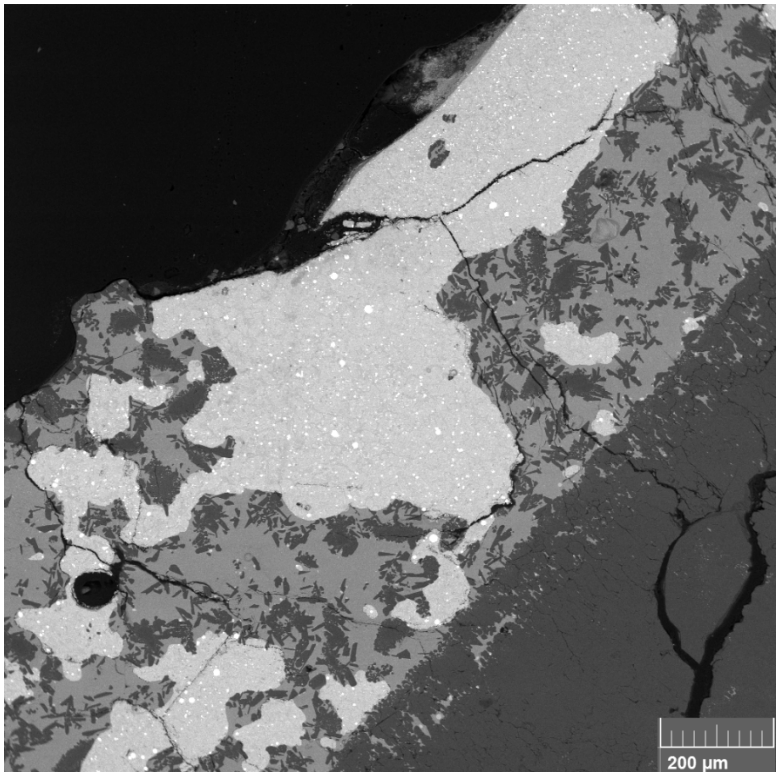


Figure 37. A sample after 10 min contact time in argon atmosphere

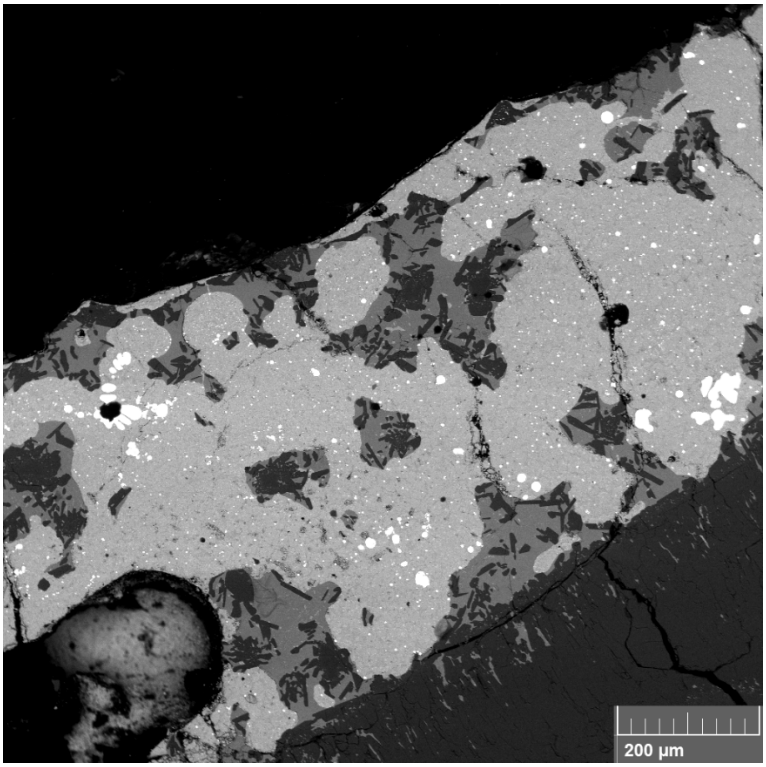


Figure 38. A sample after 20 min contact time in argon atmosphere.

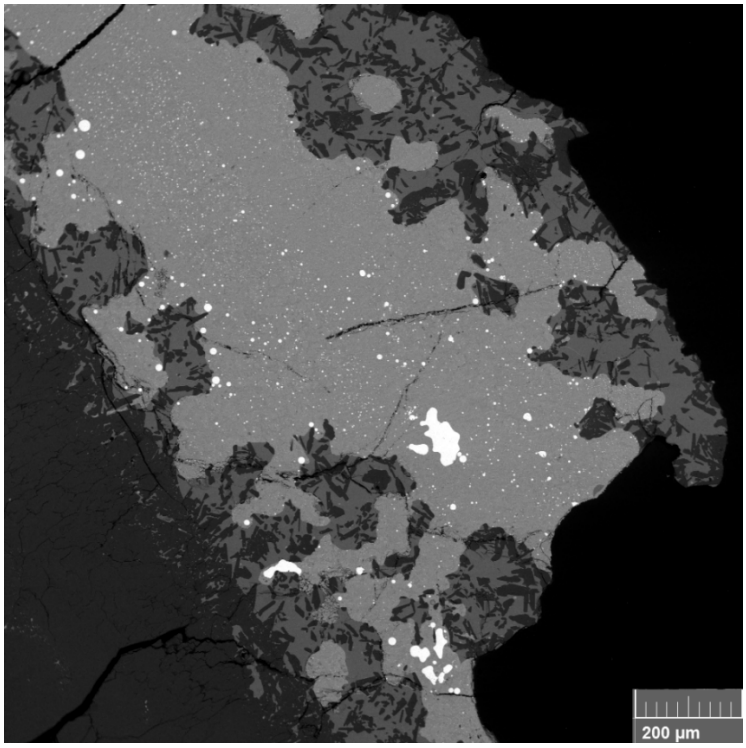


Figure 39. Sample after 40 min contact time in argon atmosphere.

The EDS results for silicon and iron concentration in slag are shown in Figure 40. The silica content of the slag remains relatively stable with increasing contact time. The iron concentration shows a slight increase until 10 min contact and remains stable from thereon.

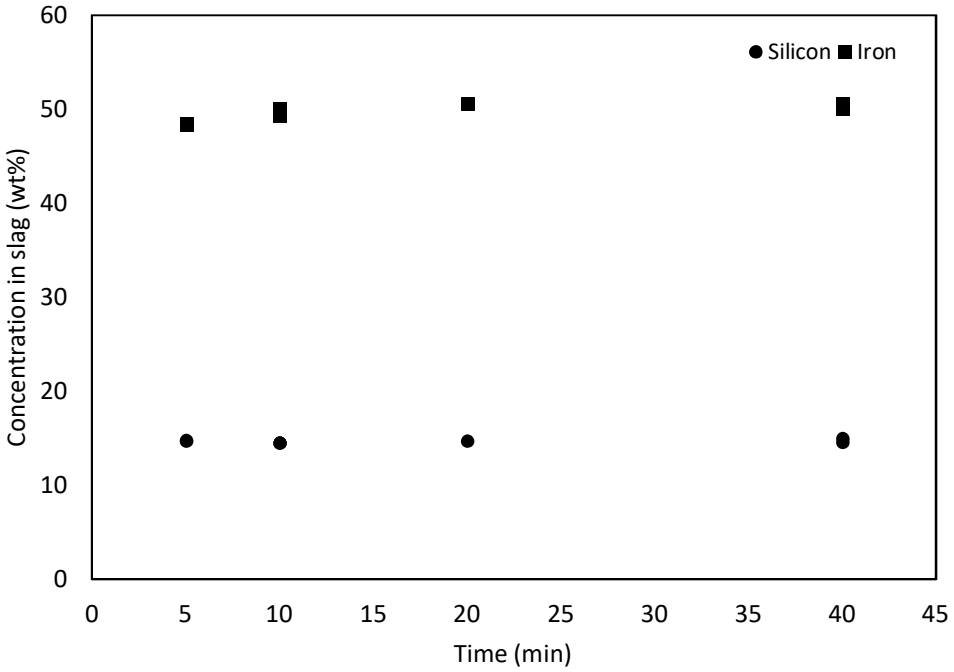


Figure 40. Concentrations of iron and silicon in slag as a function of contact time in argon atmosphere.

### 9.2.2 EPMA results

The EPMA results for the experiments conducted in argon atmosphere are shown in Figures 41-47. One of the experiments in 20 min contact time had a very different microstructure compared to the other samples, and showed deviating results as its precious metals concentrations in matte were very low, and conversely, very high in slag phase. These results are marked with squares in Figures 41-47.

In argon atmosphere the copper concentration in the matte phase increased until 20 min contact time and decreased after that. The iron concentration of matte decreased until 20 min contact time and started to increase in 40 min contact time. The sulphur concentration of matte remained relatively stable throughout the experiments.

The palladium content increased slightly until 20 min time, but decreased with 40 min time. The silver content decreased until 20 min contact time and showed a slight increase with 40 min contact time. The platinum content showed no clear trends as function of time. The gold content in matte increased slightly with longer contact times. The deviations in concentration seem to be broadest for platinum and gold.

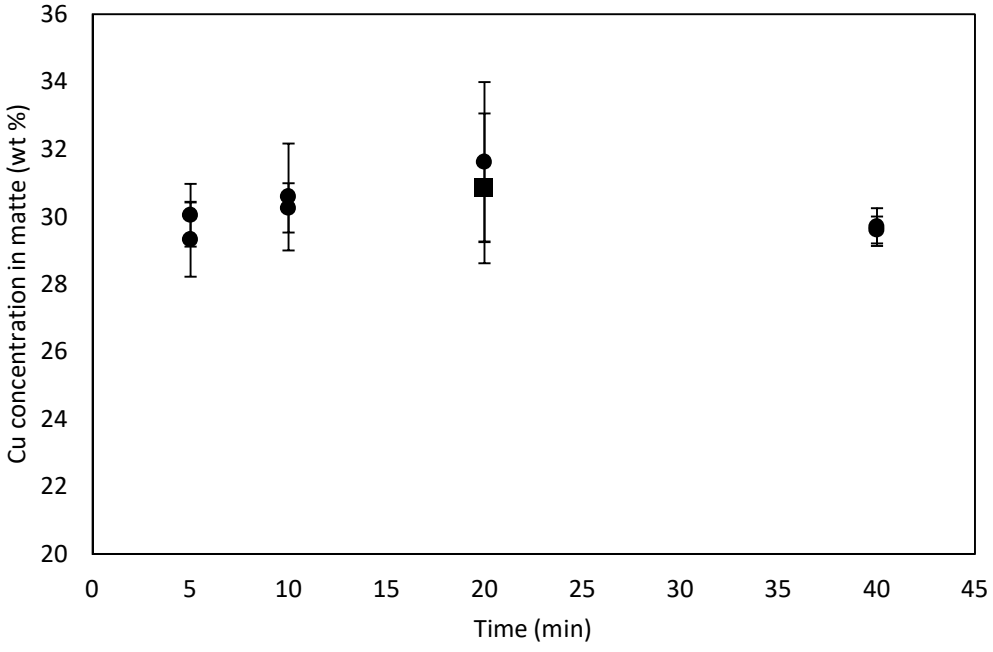


Figure 41. Concentration of copper in matte as a function of contact time in argon atmosphere.

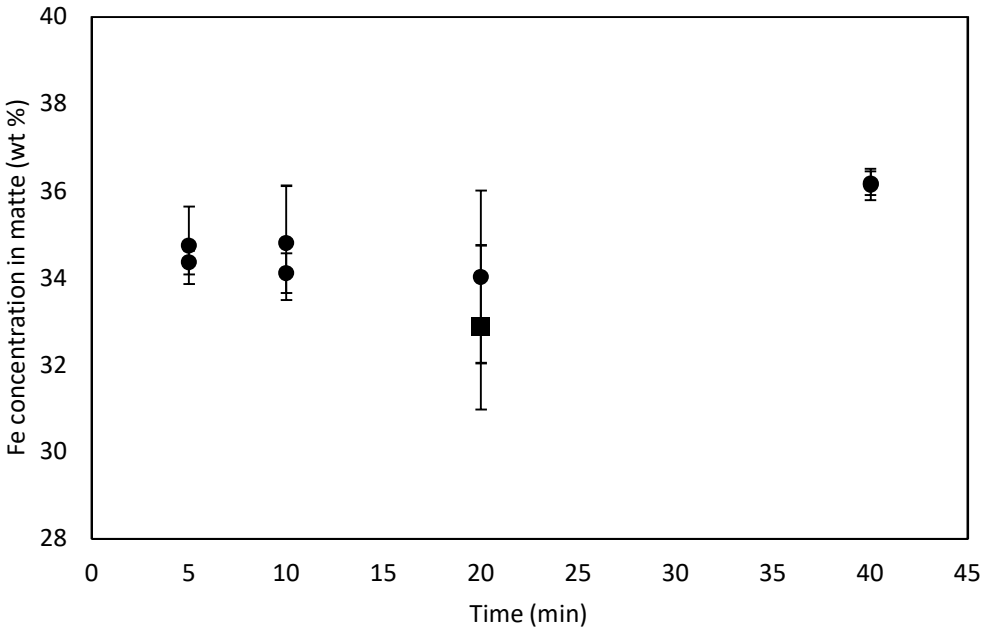


Figure 42. Concentration of iron in matte as a function of contact time in argon atmosphere.

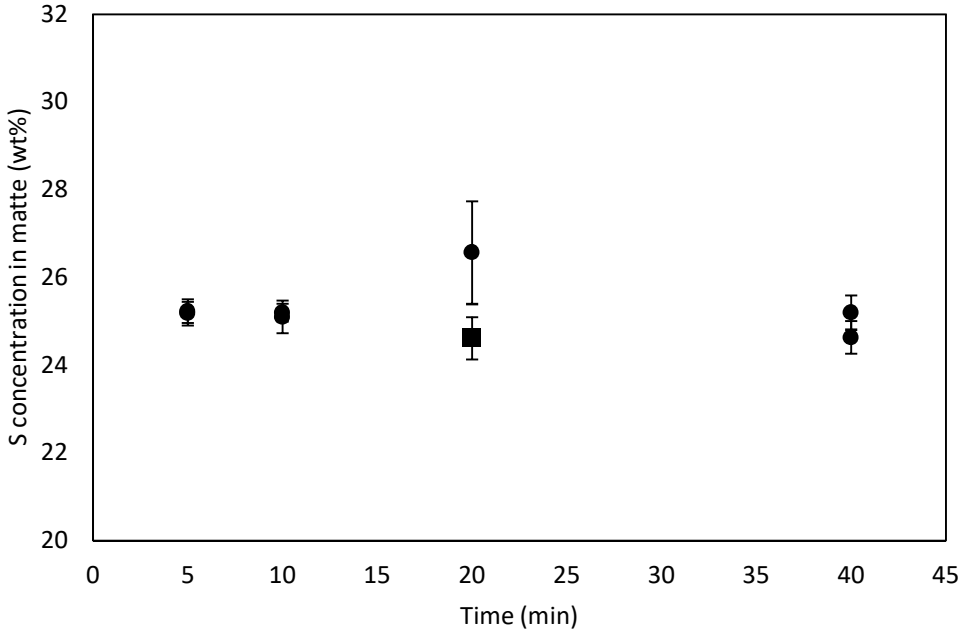


Figure 43. Concentration of sulphur in matte as a function of contact time in argon atmosphere.

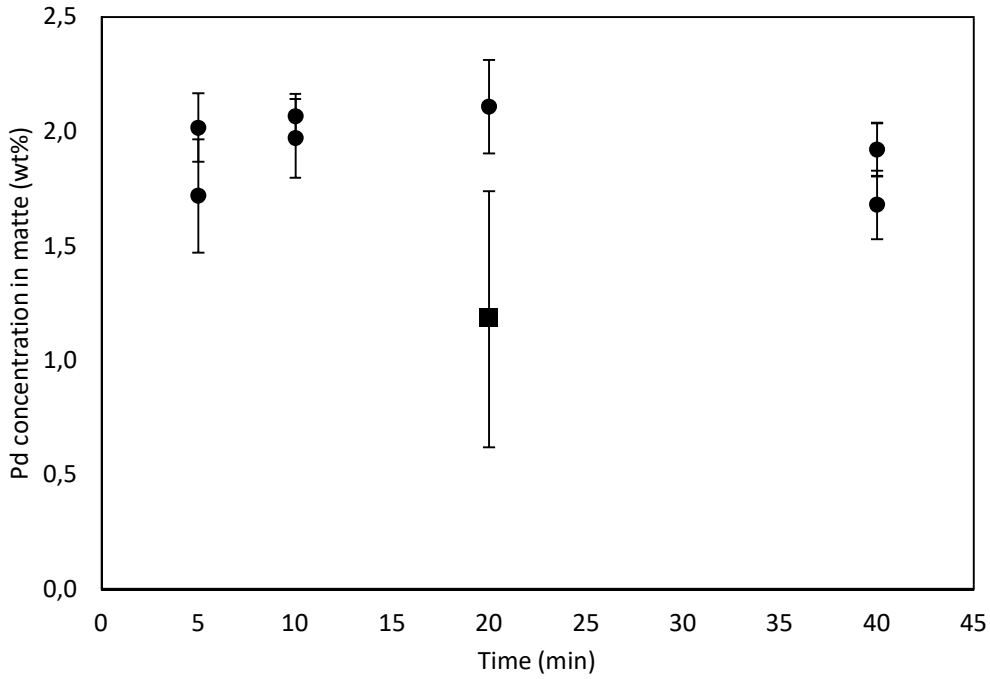


Figure 44. Concentration of palladium in matte as a function of contact time in argon atmosphere.

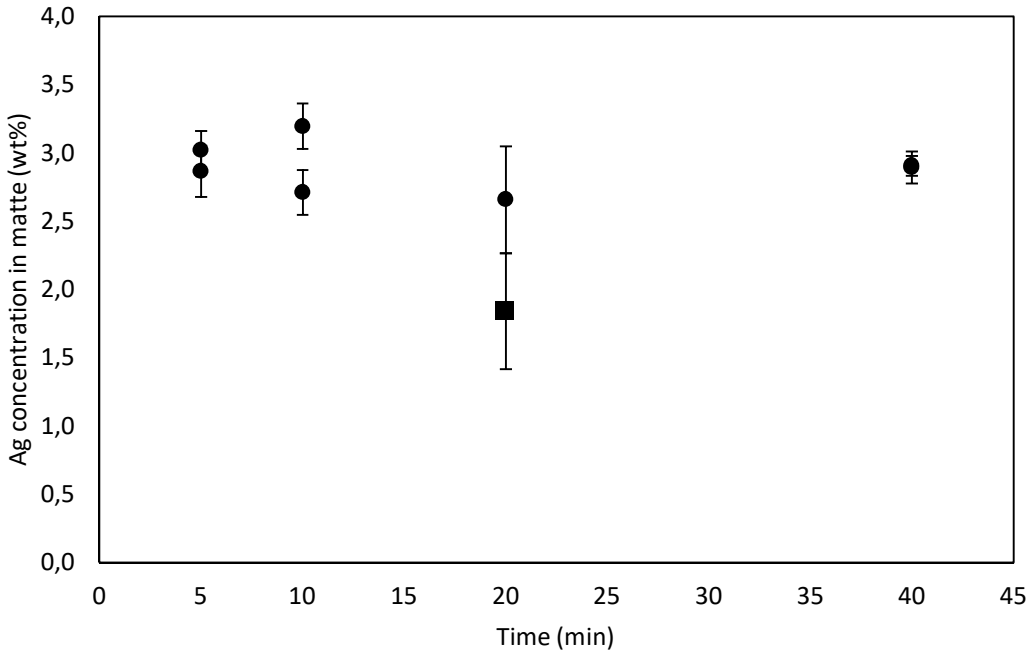


Figure 45. Concentration of silver in matte as a function of contact time in argon atmosphere.

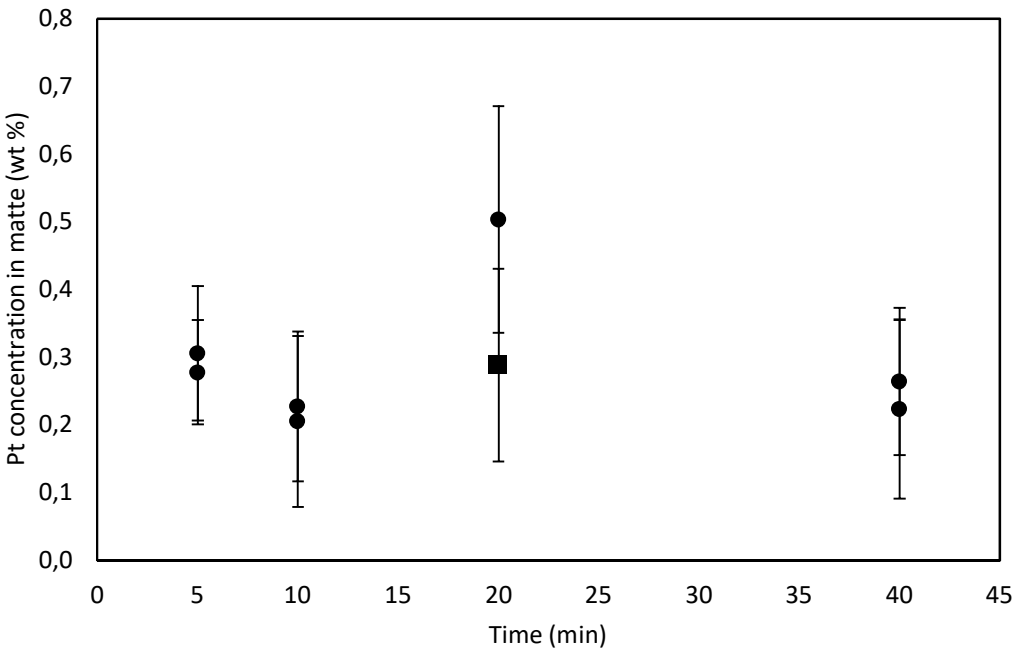


Figure 46. Concentration of platinum in matte as a function of contact time in argon atmosphere.

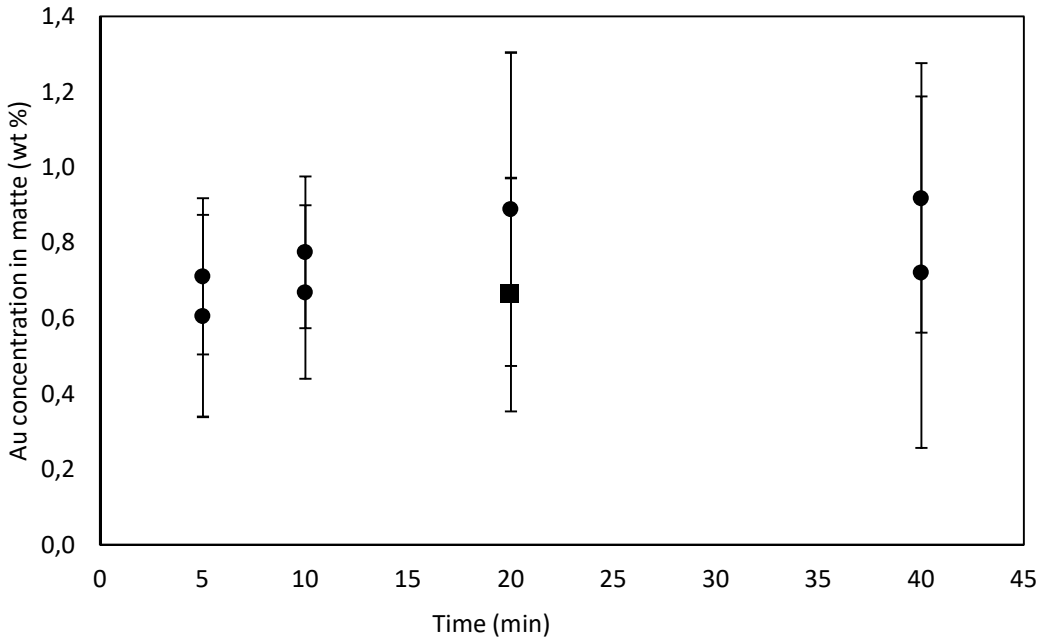


Figure 47. Concentration of gold in matte as a function of contact time in argon atmosphere.

### 9.2.3 LA-ICP-MS results

The LA-ICP-MS results for the slag in argon atmosphere are presented in Figures 48-51. The graphs only show one analysis at contact time of 20 min, as the precious metals concentrations in slag in the other sample at this time point was unusually high and the structure of the sample differed significantly from other samples.

In argon atmosphere all precious metals had a similar kind of downward trend in their concentrations in the slag. Silver and gold concentrations were higher compared to palladium and platinum. The results for palladium and silver at 20 minutes contact time showed significant deviation between different analysis sites. In the case of platinum the broadest range of deviation was found at 5 minutes contact time, which is expected after such a short contact time.

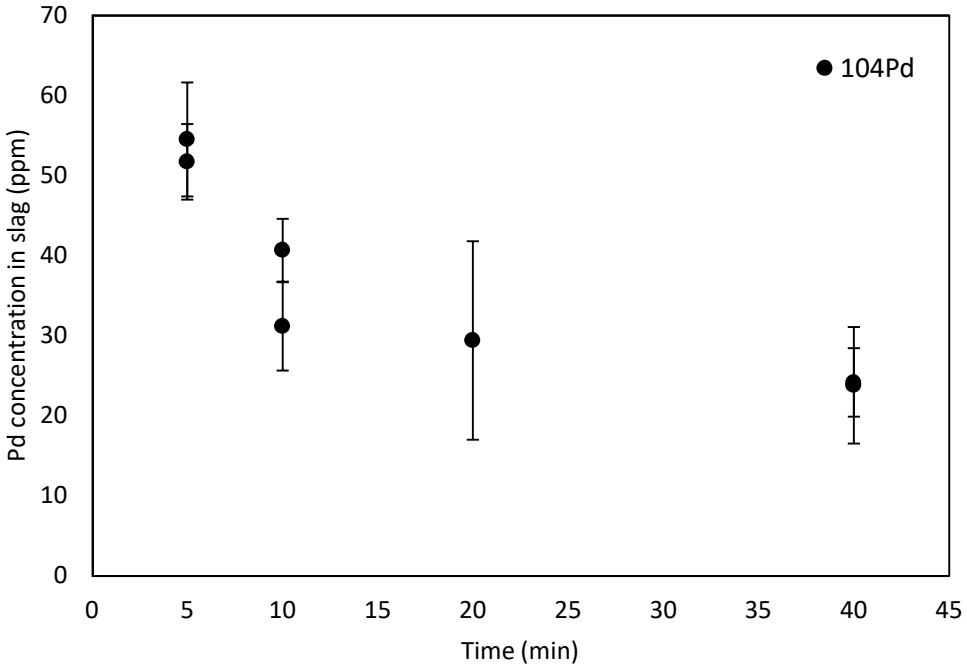


Figure 48. Concentration of palladium in slag as a function of contact time in argon atmosphere.

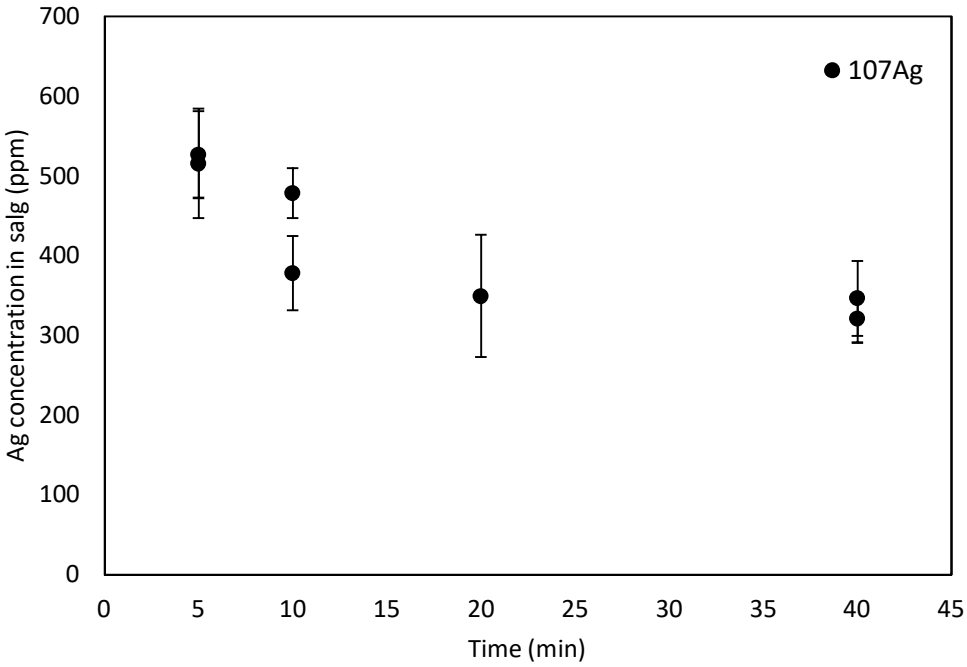


Figure 49. Concentration of silver in slag as a function of contact time in argon atmosphere.

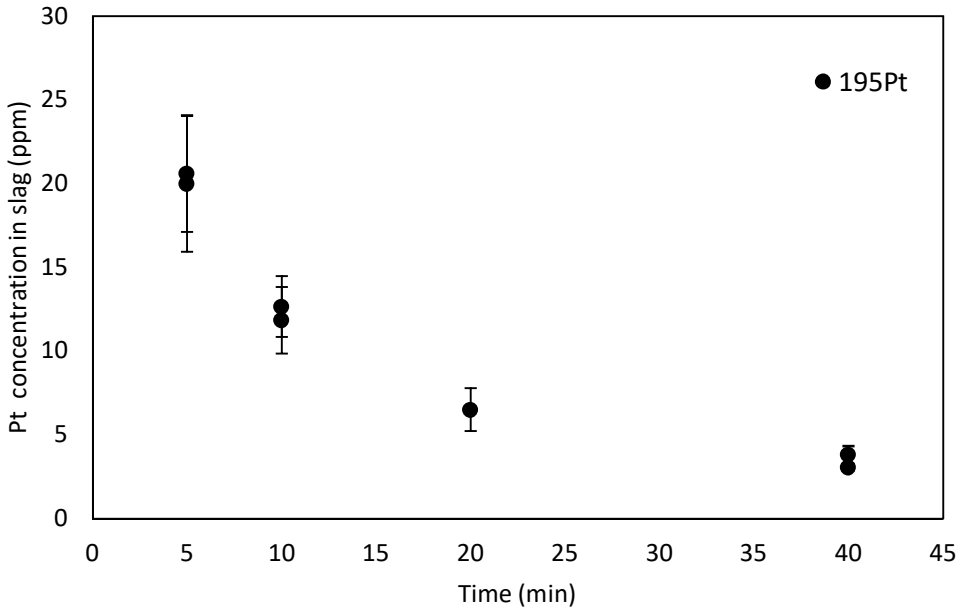


Figure 50. Concentration of platinum in slag as a function of contact time in argon atmosphere.

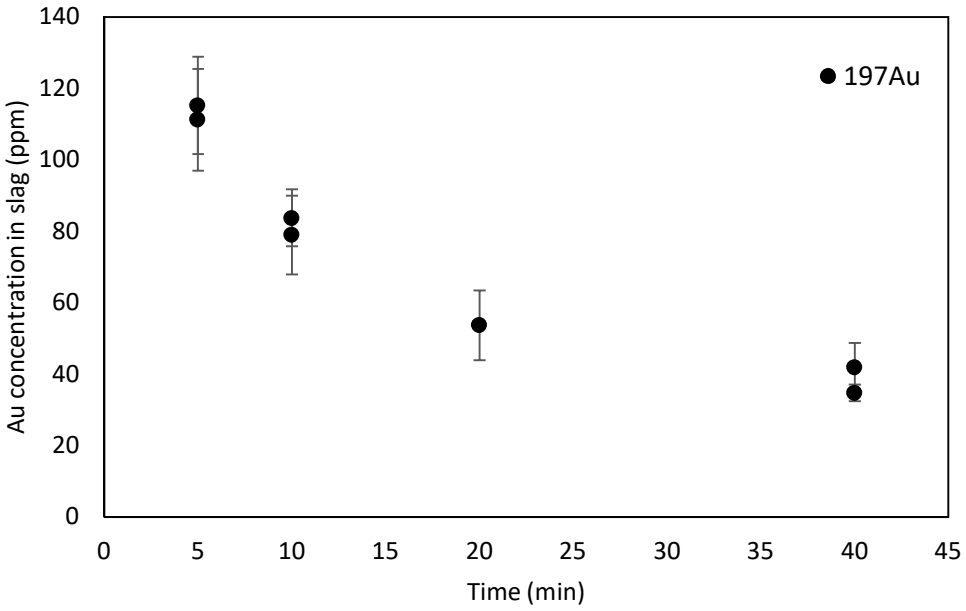


Figure 51. Concentration of gold in slag as a function of contact time in argon atmosphere.

### 9.2.4 Distributions

The logarithmic distribution coefficients of precious metals in argon atmosphere are presented in Figure 52. The change in distribution coefficient follows a same kind of trend with all precious metals. The distribution coefficients are similar to those determined in air atmosphere.

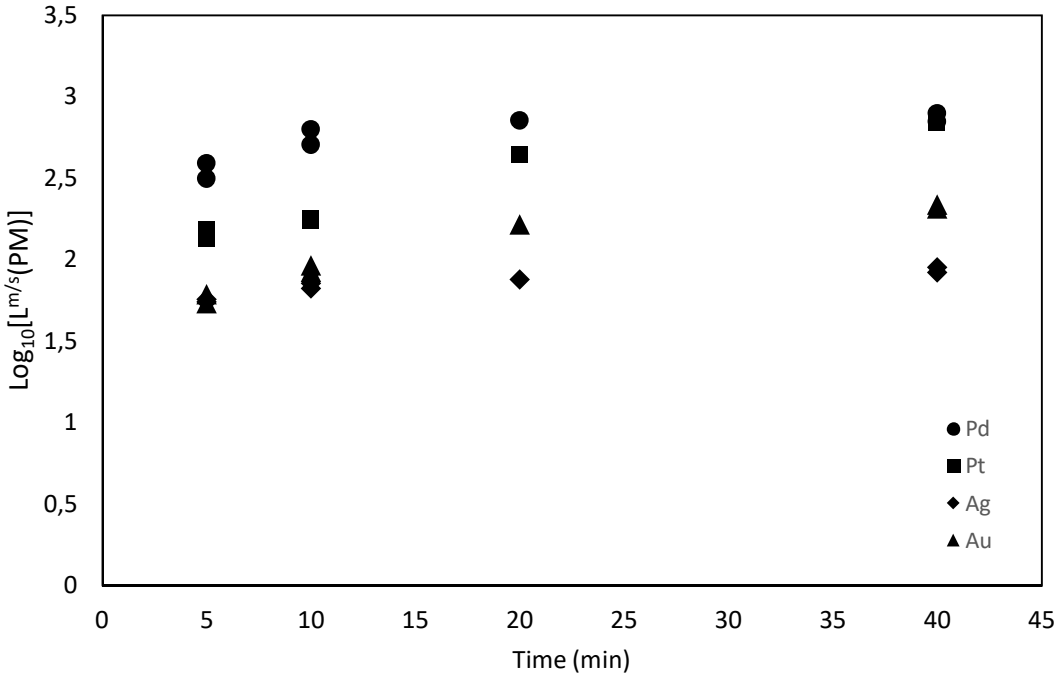


Figure 52. Logarithmic distribution coefficients of precious metals between matte and slag in argon atmosphere as a function of contact time.

# 10 Discussion

The copper concentration of the matte increased as a function of increasing contact time, but it remained relatively low compared to earlier studies. In a study performed by (Guntoro, Jokilaakso et al. 2018) copper content of matte reached 70% in 150s contact time, whereas in this study the highest copper content achieved was approximately 57 % in 300 s contact time. $Cu_2S$ could be oxidised to cuprous oxide in air, but in these experiments this phenomenon was not observed, as the copper content of the slag remained negligible according to EDS results. This indicates that in all samples the copper is found only in the matte phase. Some small matte droplets remained in the slag phase, due to mechanical entrainment. In one experiment at 300 s contact time matte phase was not found in the SEM analysis, but this is likely to be due to issues in the sample preparation and not due to the absence of matte, as no copper was found in the slag phase.

It has been suggested by (Avarmaa, Johto et al. 2016) that the precious metals replace copper and iron the structure of the molten matte. This phenomenon was explained by the fact that copper in mattes with precious metals starts to dissolve in slag at lower matte grades compared to mattes with no precious metals. They also suggested that the precious metals behave as sulphides in the matte. Therefore, as the total precious metals content in this experiment was 10 wt-% of the mass of copper concentrate, this may have an effect on copper concentration of the matte.

Due to the large deviation in the results at 300 s contact time in air atmosphere two extra experiments were performed at 150 s and 300 s contact times. The experiments with 300 s contact time showed no clear trend on copper content in the matte. It was observed after repeated experiments with contact time of 150 s in air atmosphere that the iron content of the matte was very similar in all samples, approximately 30 wt% with relatively small deviation compared to other samples.

This phenomenon and its repeatability suggest the existence of some rate-limiting factor, as the de-ironisation of matte is not progressing at this time point. This is also

contradictory with former experiments performed in similar conditions. (Guntoro, Jokilaakso et al. 2018) studied the reaction sequences in matte smelting conditions in 1300 °C in air atmosphere and they reported that the iron content in the matte rapidly decreased and was less than 10 wt% after 150 s contact time. Even though the de-ironisation of matte does not progress as rapidly as was expected, the physical separation between matte and slag phases proceeds quickly and the matte and slag phases are almost fully separated at 60 s contact time.

As the de-ironisation of matte occurs seemingly slower in this work compared to earlier results, it can be assumed that it is somehow hindered by the presence of precious metals, which increases the number of phases in the system and causes interactions between liquid and solid phases. The total concentration of precious metals is also high, 10 wt% of the mass of the concentrate used in sample preparation. This can give rise to mass transport limitations, thereby slowing down the reactions. It is suspected that the slag formation is limited by some factor, but it is also seen from the EDS results of the slag in Figure 20 that the iron content of the slag stabilises quickly and shows very little change in longer contact times, even though the iron content of the matte decreases. As the change in iron concentration of matte causes little change in iron concentration of slag, it can be assumed that the iron is collected by precious metals and copper. (Lynch, Akagi et al. 1991) has proposed that the excess metal species interact with iron and copper modifying their behaviour. However, this phenomenon was suggested to occur in sulphur-depleted mattes in Lynch's report. In this work the minimum sulphur level in matte was approximately 20%. It should also be noted that the furnace used in this work was only open at the bottom and there was no draft through it. This may cause some local oxygen deficiency in the furnace, which may affect the rate at which the oxidation reactions take place.

It was observed that the precious metals gathered to clusters very quickly and already at 10 s contact time these clusters were found. As it is assumed that the structure of the starting material powder mixture was homogenous, it can be seen that the

separation of precious metals, especially platinum, occurs very fast as the sample reaches high temperature. In the case of platinum, the concentration in both matte and slag decreases at 30 s contact time, indicating that it is separating to another phase. With longer contact times its concentration in matte increases with increasing copper content, as can be predicted by earlier results from distribution studies. No reaction mechanisms for precious metals dispersion were observed in the results, as their clustering to droplets begins very quickly. The EPMA results indicate that precious metals are soluble in matte and it has been suggested by (Avarmaa, Johto et al. 2016) that precious metals behave as sulphides in matte. However, it is not possible to deduce the chemical structure of the precious metals from these data. The peaks in the laser signals from the LA-ICP-MS results for slag in air atmosphere (Figures 10 and 11) indicate that both chemical solubility and mechanical entrainment occur in slag.

Silver is known to be the most volatile of the precious metals studied in this work. It has been suggested by (Takeda, Roghani 1993) that with lower matte grades silver is dissolved in the slag as silver sulphide, and as the matte grade increases and sulphur content of matte decreases, sulphidic solubility of silver to matte gradually decreases. In this work, the silver content increased in both matte and slag within contact time 150 s. After that the silver content in matte increased and decreased in slag. It has been reported by (Roghani, Hino et al. 1997) that with high oxygen partial pressure metallic silver is oxidised and it dissolves in slag as monovalent silver oxide. The behaviour observed in this work could be explained by the oxidation phenomena. It can be assumed that the silver content of the slag increases as the oxidised silver moves to the slag phase, and with longer contact time the un-oxidised metallic silver moves to the matte phase. Silver may also vaporise with longer contact times.

The logarithmic distribution coefficients of the precious metals were calculated as a function of contact time. It was observed that the distribution coefficients of all the precious metals increased with longer contact time and approached their reported equilibrium values already at 300 s contact time. The distributions coefficients were

similar in both air and argon atmospheres, indicating that oxidic solubility of precious metals in slag is very low. It has been formerly suggested by (Avarmaa, O'Brien et al. 2015) that the increase in in the distribution coefficient is not due to the properties of the slag, but due to the decreasing sulphur and iron concentration of matte as well as decreasing sulphur-to-metal ratio. In this work the precious metals, except for gold, showed increase in their concentration in matte in 150 s contact time even though the iron content of the matte remained relatively constant in this time period. On the other hand, the sulphur content and thereby the sulphur-to-metal ratio was decreasing. The equilibrium distribution coefficient of palladium has been formerly reported to decrease with increasing matte grade. (Yamaguchi 2011) However, in this work the palladium distribution coefficient increased with increasing copper content in matte, similarly to Avarmaa's study. The distribution coefficients calculated in this work are in agreement with results from former studies.

It was observed that at 150 s and 300 s contact times a significantly larger droplet of precious metals formed with copper and iron. As this phenomenon was observed, it can be assumed that the precious metals form these droplets under right circumstances. As the precious metal droplets form, they may act as collector metals for copper and iron. This can deprive the matte of copper and thereby cause a lower matte grade in areas where the precious metal droplets are not found, resulting in large variation in matte grade between different samples. However, the copper concentration in the proximity of these large droplets was not specifically high compared to other samples with the same contact time. This suggests that the variation in copper concentration of matte may not be explained by droplet formation.

In argon atmosphere, the matte grade increased until 20 min contact time and showed a slight decrease after that. On the other hand, the iron content of matte showed decrease during 20 min contact time and increased from thereon with 40 min contact time. This has been explained by the behaviour of fayalite in very low

oxygen partial pressure. (Iduozee 2018) In this kind of atmosphere fayalite is likely to decompose according to reaction (16):

$$2\,\mathrm{Fe} - \mathrm{SiO_4(l)} \rightarrow 2\,\mathrm{FeO(s)} + \mathrm{SiO_2(s)} \qquad (16)$$

This may be observed through visual inspection from the SEM-images, as the amount of solid silica in the slag phase increased with longer contact times. The behaviour of copper, on the other hand, has been previously explained by the shifting partial pressures by (Iduozee 2018). In his work it was suggested that the progression of oxygen and sulphur partial pressures in an inert atmosphere causes the system to move to a point on the oxygen-sulphur potential diagram, where liquid Fe, Cu, matte and slag are present. However, it was also mentioned that for such point the matte grade would be 55-60 % Cu, which is not the case in this work, as the maximum copper content in the matte phase was approximately 32 %. However, the trends observed in this work in the behaviour of copper, iron and sulphur as a function of contact time were similar compared to Iduozee's work. The decreasing copper content was explained by the EDS analysis method in the work of (Iduozee 2018), but the same phenomenon is also observed in this work, where the matte composition is analysed with EPMA.

The behaviour of silver was studied in an inert $N_2$ atmosphere by (Louey, Swinbourne et al. 1999) and they reported that the distribution coefficient between copper matte (50% Cu) and iron silicate slag to be 120 ±40, which is close the distribution coefficient value calculated in this work.

(Wang, Peng et al. 2018) have studied the formation mechanism of fayalite in nitrogen atmosphere and reported that there are $Si^{4+}$ ions present in the formation steps. Palladium and platinum have a high affinity for silicon in reducing environments (Irani, Cahn 1972), but in an inert atmosphere no compound formation was observable between palladium/platinum and silicon, when the precious metal droplets and their surroundings were studied with SEM-EDS.

The precious metal droplets were found near (or attached to) the matte-slag interface with 40 min contact time. No large clusters of precious metals were found like in an oxidising atmosphere, but the droplets were rather uniform and smaller in size. This sticking behaviour has been formerly studied by (De Wilde, Bellemans et al. 2016) with copper in spinel solids, and they suggested that this behaviour may be due to chemical reactions between the particles or due to the wetting behaviour of the spinel solids. The sticking of precious metal droplets in the slag interface can also be due to differences in surface energy.

# 11 Conclusions

The time-dependent behaviour of gold, silver, platinum and palladium in copper matte-slag system has been studied experimentally in simulated copper concentrate flash smelting conditions. The experiments were conducted in air and inert argon atmospheres at 1300 °C. The contact times in air atmosphere were 10-600 seconds and 5-40 minutes in argon atmosphere. The samples were prepared for analysis through metallographic sample preparation methods. The samples were analysed with SEM-EDS for visual and compositional inspection, and with EPMA and LA-ICP-MS for more accurate compositional data.

The thermodynamic behaviour of precious metals in copper matte – slag system was discussed. Reported results on the kinetics of precious metals in copper matte-slag system have not been found, so the literature survey is to a large extent based on equilibration studies. The dissolution behaviour of the precious metals, their possible reactions and equilibrium distributions are discussed.

The experimental results of this work indicated that the precious metals prefer the matte phase over the slag phase and that they migrate to copper and iron-bearing phase almost instantly, when they reach high temperatures. The precious metals approached their reported equilibrium distribution already after 300 s contact time in air atmosphere. The precious metal content in matte increases with increasing matte grade. The precious metals concentrations in slag were very low, 408 ppm (Ag), 27 ppm (Au), 17 ppm (Pd) and 9 ppm (Pt) in air atmosphere, and 346 ppm (Ag), 42 ppm (Au), 24 ppm (Pd) and 3 ppm (Pt) in argon atmosphere. Because the chemical solubility of precious metals in the slag is low, the main reason for precious metal losses in industrial operations can be assumed to be due to mechanical entrainment. In air atmosphere the precious metals formed larger clusters with copper and iron. In an inert atmosphere no such clusters were found and the precious metals formed small droplets that attached to slag-matte interface after longer contact times.

The matte grade was observed to increase throughout the experiments in air atmosphere, but there was significant scatter in the data at 300 s contact time. The de-ironisation of the matte did not progress as expected and the iron content in matte was approximately 30 % in repeated experiments at 150 s contact time. This suggest the existence of some rate-limiting factor. It is suspected that the addition of significant amount of precious metals to the matte-slag system creates mass transfer limitations, thus hindering the de-ironisation of matte. It is also possible that the precious metals replace copper and iron in the structure of the matte, thereby modifying their behaviour.

As there was significant scatter in the data at 300 s contact time, it is suggested for future work that the contact times in the proximity of 300 s are studied in more detail. The same kind of scatter was also observed at 20 min contact time in argon atmosphere, suggesting that this time period is a turning point in the reactions between matte, slag and precious metals in an inert atmosphere. The chemical dissolution behaviour of precious metals would require more analysis, as it is unclear whether the precious metals exist in matte as sulphides. Also, explaining the sticking behaviour of the precious metal droplets would require more data on possible chemical reactions occurring between matte, slag and trace elements.

As the analysis of the samples was based on investigating a random cross section, it is likely that more accurate data on sample composition could be obtained, if more cross sections of the samples were studied. For example, the existence and formation of large precious metal droplets would require more detailed analysis of samples.

# 12 References


ANINDYA, A., 2012. *Minor elements distribution during the smelting of WEEE with copper scrap*, RMIT University.

ANINDYA, A., SWINBOURNE, D.R., REUTER, M.A. and MATUSEWICZ, R.W., 2013. Distribution of elements between copper and FeO x –CaO–SiO 2 slags during pyrometallurgical processing of WEEE: Part 1 – Tin. *Mineral Processing and Extractive Metallurgy,* **122**(3), pp. 165-173.

AVARMAA, K., JOHTO, H. and TASKINEN, P., 2016. Distribution of Precious Metals (Ag, Au, Pd, Pt, and Rh) Between Copper Matte and Iron Silicate Slag. *Metallurgical and Materials Transactions B,* **47**(1), pp. 244-255.

AVARMAA, K., O'BRIEN, H., JOHTO, H. and TASKINEN, P., 2015. Equilibrium Distribution of Precious Metals Between Slag and Copper Matte at 1250–1350 °C. *Journal of Sustainable Metallurgy,* **1**(3), pp. 216-228.

AVARMAA, K., O'BRIEN, H. and TASKINEN, P., 2016. Equilibria of gold and silver between molten copper and FeOX-SiO2-Al2O3 slag in WEEE smelting at 1300 °C. *Advances in Molten Slags, Fluxes, and Salts: Proceedings of The 10th International Conference on Molten Slags, Fluxes and Salts (MOLTEN16),* , pp. 193-202.

BALDÉ, C.P., FORTI, V., GRAY, V., KUEHR, R. and STEGMANN, P., 2017. *The Global E-waste Monitor – 2017.* Bonn/Geneva/Vienna: United Nations University (UNU), International Telecommunication Union (ITU) & International Solid Waste Association (ISWA).

BELL, T., 2 November, 2018-last update, The Properties and Applications of Platinum. Available: https://www.thebalance.com/metal-profile-platinum-2340149 [18 March, 2019].

CAYUMIL, R., KHANNA, R., RAJARAO, R., MUKHERJEE, P.S. and SAHAJWALLA, V., 2016. Concentration of precious metals during their recovery from electronic waste. *Waste Management,* **57**, pp. 121-130.

CHANCEREL, P., MESKERS, C., HAGELUKEN, C. and ROTTER, V., 2009. Assessment of Precious Metal Flows During Preprocessing of Waste Electrical and Electronic Equipment. *Journal of Industrial Ecology,* **13**(5), pp. 791-810.

CHARLES, R., DOUGLAS, P., HALLIN, I., MATTHEWS, I. and LIVERSAGE, G., 2017. An investigation of trends in precious metal and copper content of RAM modules in WEEE: Implications for long term recycling potential. *Waste Management,* **60**, pp. 505-520.

CHOU, E., 4 July, 2018-last update, Gold Investor July 2018. Available: https://www.gold.org/goldhub/research/gold-investor/gold-investor-july-2018/gold-and-the-electronics-sector [9 January, 2019].

CUI, J. and ZHANG, L., 2008. Metallurgical recovery of metals from electronic waste: A review. *Journal of hazardous materials,* **158**(2), pp. 228-256.

DE WILDE, E., BELLEMANS, I., ZHENG, L., CAPMFORTS, M., GUO, M., BLANPAIN, E., MOELANS, N. and VERBEKEN, K., 2016. Origin and sedimentation of Cu-droplets sticking to spinel solids in pyrometallurgical slags. *Materials Science and Technology,* **32**(18), pp. 1911-1924.

EUROSTAT, 2016-last update, Waste electrical and electronic equipment. Available: https://ec.europa.eu/eurostat/web/waste/key-waste-streams/weee [23 March, 2019].

GHOSH, B., GHOSH, M.K., PARHI, P., MUKHERJEE, P.S. and MISHRA, B.K., 2015. Waste Printed Circuit Boards recycling: an extensive assessment of current status. *Journal of Cleaner Production,* **94**, pp. 5-19.

GLAESER, W., 2012. Technique summaries - Energy Dispersive X-ray Spectroscopy (EDS). *Characterization of Tribological Materials, Second Edition.* Momentum Press, pp. 160.

GOODGE, J., 2017-last update, Electron probe micro-analyzer (EPMA). Available: https://serc.carleton.edu/research_education/geochemsheets/techniques/EPMA.html [23 January, 2019].

GUNN, G., 2013. 12. Platinum-group metals. *Critical metals handbook.* John Wiley & Sons, pp. 284-311.

GUNTORO, P.I., JOKILAAKSO, A., HELLSTEN, N. and TASKINEN, P., 2018. Copper matte-slag reaction sequences and separation processes in matte smelting. *Journal of Mining and Metallurgy, Section B: Metallurgy,* **54**(3), pp. 301-311.

HABIB AL RAZI, K. and KHADANKAR, M.D., 2016. Resourceful recycling process of waste desktop computers: A review study. *Resources, Conservation and Recycling,* **110**, pp. 30-47.

HAGELUKEN, C., 2012. Recycling the Platinum Group Metals: A European Perspective Effective recycling systems for pgm-containing materials will ensure sustainable supply. *Platinum Metals Review,* **56**(1), pp. 29-35.

HAGELÜKEN, C., 2010. Recycling of gold from electronics: Cost-effective use through 'Design for Recycling'. *Gold Bulletin,* **43**(3), pp. 209-220.

HELLSTÉN, N., KLEMETTINEN, L., SUKHOMLINOV, D., O'BRIEN, H., TASKINEN, P., JOKILAAKSO, A. and SALMINEN, J., 2019. Slag Cleaning Equilibria in Iron Silicate Slag-Copper Systems. Manuscript under review in Journal of Sustainable Metallurgy.

HENAO, H., YAMAGUCHI, K. and UEDA, S., 2006. Distribution of precious metals (Au, Pt, Pd, Rh and Ru) between copper matte and iron-silicate slag at 1573 K.

IDUOZEE, I., 2018. *Kinetics of WEEE scrap elements' reactions in slag-matte system*, Aalto University School of Chemical Engineering.

IRANI, R.S. and CAHN, R.W., 1972. Copper-platinum alloys. *Platinum Metals Review,* **16**(2), pp. 48-49.

JOCHUM, K.P., WEISS, U., STOLL, B., KUZMIN, D., YANF, Q., RACZEK, I., JACOB, D.E., STRACKE, A., BIRBAUM, K., FRICK, D.A., G, ÜNTHER, D. and ENZWEILER, J., 2011. Determination of Reference Values for NIST SRM 610–617 Glasses Following ISO Guidelines. *Geostandards and Geoanalytical Research,* **35**(4), pp. 397-429.

JOCHUM, K.P., WILLBOLD, M., RACZEK, I., STOLL, B. and HERWIG, K., 2005. Chemical Characterisation of the USGS Reference Glasses GSA-1G, GSC-1G, GSD-1G, GSE-1G, BCR-2G, BHVO-2G and BIR-1G Using EPMA, ID-TIMS, ID-ICP-MS and LA-ICP-MS. *Geostandards and Geoanalytical Research,* **29**(3), pp. 285-302.

JOKILAAKSO, A., SUOMINEN, R., TASKINEN, P. and LILIUS, K., 1991. Oxidation of chalcopyrite in simulated suspension smelting. *Transactions of the Institute of Mining and Metallurgy Section C-Mineral,* **100**, pp. C90.

KAYA, M., 2016. Recovery of metals and nonmetals from electronic waste by physical and chemical recycling processes. *Waste Management,* **57**, pp. 64-90.

KHALIQ, A., RHAMDHANI, M.A., BROOKS, G. and MASOOD, S., 2014. Metal Extraction Processes for Electronic Waste and Existing Industrial Routes: A Review and Australian Perspective. *Resources,* **3**(1), pp. 152-179.

KLEMETTINEN, L., 2017. *Experimental determination of trace element concentrations in copper-slag equilibria with laser ablation technique*, Aalto University School of Chemical Engineering.

LIMBECK, A., GALLER, P., BONTA, M., BAUER, G., NISCHKAUER, W. and VANHAECKE, F., 2015. Recent advances in quantitative LA-ICP-MS analysis: challenges and

solutions in the life sciences and environmental chemistry. *Analytical and Bioanalytical Chemistry,* **407**(22), pp. 6593–6617.

LOESCHE, D., 19 December, 2017-last update, Mining gold from e-waste. Available: https://www.statista.com/chart/12332/value-and-volume-of-raw-materials-in-e-waste-worldwide/ [23 January, 2019].

LOUEY, R., SWINBOURNE, D. and LEHNER, T., 1999. Silver and tin distribution between copper matte and fayalite slag. *AusIMM Proceedings,* **304**(2), pp. 31-36.

LYNCH, D.C., AKAGI, S. and DAVENPORT, W.G., 1991. Thermochemical nature of minor elements in copper smelting mattes. *Metallurgical Transactions B,* **22B**, pp. 677-688.

MESKERS, C.E.M., HAGELTIKENI, C. and VAN DAMME, G., 2009. Green recycling of EEE:Special and precious metal recovery from EEE. *EPD Congress,* .

MULLER, J. and FRIMMEL, H.E., 2010. Numerical Analysis of Historic Gold Production Cycles and Implications for Future Sub-Cycles. *The Open Geology Journal,* **4**(1), pp. 29-34.

NAGAMORI, M. and MACKEY, P.J., 1978. Thermodynamics of copper matte converting: part II. *Metall. Trans. B,* **9**, pp. 567-579.

NAKAMURA, S.I., K., MORITA, K. and SANO, N., 1998. The influence of basicity on the solubility of platinum in oxide melts. *Metallurgical and materials transactions B,* **29B**, pp. 411-414.

NEUFELD, L., 2004. *Introduction to Laser Ablation ICP-MS for the Analysis of Forensic Samples.* Agilent Technologies.

NORGATE, T. and HAQUE, N., 2012. Using life cycle assessment to evaluate some environmental impacts of gold production. *Journal of Cleaner Production,* **29-30**, pp. 53-63.

PARK, J. and MIN, D., 1999. Quantitative analysis of the relative basicity of CaO and BaO by silver solubility in slags. *Metallurgical and Materials Transactions B,* **30**(4), pp. 689-694.

RAO, S., 2006. Chapter 7 - Metal Recycling. *Waste Management Series.* Elsevier, pp. 167-268.

RECK, B. and GRAEDEL, T., 2012. Challenges in Metal Recycling. *Science,* **337**(6095), pp. 690-695.

REUTER, M.A., BOIN, U.M.J., VAN SCHAIK, A., VERHOEF, E., HEISKANEN, K., YANG, Y. and GEORGALLI, G., 2005. *The Metrics of Material and Metal Ecology: Harmonizing the Resource, Technology and Environmental Cycles.* Elsevier.

ROGHANI, G., HINO, M. and ITAGAKI, K., 1997. Phase equilibrium and minor element distribution between SiO2-CaO-FeOx-MgO slag and copper matte under high partial pressures of SO2  *Material Transactions,* **38**, pp. 707-713.

SCHLESINGER, M., KING, M., SOLE, K. and DAVENPORT, W., 2011. Chemical Metallurgy of Copper Recycling. *Extractive Metallurgy of Copper.* pp. 389-396.

SCHLITT, W. and RICHARDS, K., 1975. The distribution of silver, gold, platinum and palladium in metal-matte systems. *Metallurgical Transactions B,* **6**(2), pp. 237-243.

SHISHIN, D., HIDAYAT, T., CHENG, J., HAYES, P.C. and JAK, E., 2019. Experimental investigation and thermodynamic modeling of the distributions of Ag and Au between slag, matte and metal in the Cu-Fe-O-S-Si system. *Journal of Sustainable Metallurgy,* .

SHUVA, M., 2017. *Analysis of Thermodynamic Behaviour of Valuable Elements and Slag Structure during E-Waste Processing through Copper Smelting*, Swinburne University of Technology.

SHUVA, M., RHAMDHANI, M., BROOKS, G., MASOOD, S. and REUTER, M., 2017. Thermodynamics of Palladium (Pd) and Tantalum (Ta) Relevant to Secondary Copper Smelting. *Metallurgical and Materials Transactions B,* **48**(1), pp. 317-327.

STATISTA, 2019a-last update, Forecast of electronic waste generated worldwide from 2010 to 2018 (in million metric tons). Available: https://www.statista.com/statistics/499891/projection-ewaste-generation-worldwide/ [3 June, 2019].

STATISTA, 2019b-last update, Global recycled platinum by former use 2010-2018. Available: https://www.statista.com/statistics/593072/platinum-recycled-worldwide-by-former-use/ [3 March, 2019].

STATISTA, 2018a-last update, Global silver demand in 2017. Available: https://www.statista.com/statistics/253345/global-silver-demand-by-purpose/ [14 February, 2019].

STATISTA, 2018b-last update, Statista dossier on platinum. Available: https://www.statista.com/study/37300/platinum-statista-dossier/ [15 April, 2019].

STATISTA, 2011-last update, Areas of application for palladium worldwide 2010 (in percent)*. Available: https://www.statista.com/statistics/270795/areas-of-application-for-palladium-2010/ [15 April, 2019].

SUKHOMLINOV, D., KLEMETTINEN, L., AVARMAA, K., O'BRIEN, H., TASKINEN, P. and JOKILAAKSO, A., 2019. Distribution of Ni, Co, precious and platinum group metals in copper making process. *Metallurgical and materials transactions,* , pp. 1-14.

SWINBOURNE, D.R., YAN, S. and SALIM, S., 2005. The solubility of gold in metallurgical slags. *Mineral Processing and Extractive Metallurgy,* **114**(1), pp. 23-29.

TAKEDA, Y. and ROGHANI, G., 1993Distribution equilibrium of silver in copper smelting system. 1993, pp. 357–360.

TAVERA, F. and DAVENPORT, W., 1979. Equilibrations of Copper Matte and Fayalite Under Controlled Partial Pressures of S02. *Metallurgical Transactions B,* **10B**, pp. 237-241.

TESFAYE, F., LINDBERG, D., HAMUYUNI, J., TASKINEN, P. and HUPA, L., 2017. Improving urban mining practices for optimal recovery of resources from e-waste. *Minerals Engineering,* **111**, pp. 209-221.

THE ROYAL SOCIETY OF CHEMISTRY, 2019a-last update, Gold. Available: http://www.rsc.org/periodic-table/element/79/gold [18 March, 2019].

THE ROYAL SOCIETY OF CHEMISTRY, 2019b-last update, Palladium. Available: http://www.rsc.org/periodic-table/element/46/Palladium [18.3., 2019].

THE SILVER INSTITUTE, 2018-last update, Global silver demand in 2017, by purpose (in million ounces). Available: https://www.statista.com/statistics/253345/global-silver-demand-by-purpose/ [January 14, 2019].

UNEP, 2011. *Recycling rate of metals, A status report.*

VAN ACHTERBERG, E., RYAN, C., JACKSON, S. and GRIFFIN, W., 2001. Chemical Characterisation of the USGS Reference Glasses GSA-1G, GSC-1G, GSD-1G, GSE-1G, BCR-2G, BHVO-2G and BIR-1G Using EPMA, ID-TIMS, ID-ICP-MS and LA-ICP-MS. *Mineralogical Association of Canada short course series St John, Newfoundland,* **29**, pp. 239-243.

WAN, X., JOKILAAKSO, A., IDUOZE, I., H, ÜRMAN, E. and LATOSTENMAA, P., 2019. Experimental research on the behavior of WEEE scrap in flash smelting settler with copper con-centrate and synthetic slag. *Proceedings of EMC 2019,* .

WANG, Z., PENG, B., ZHANG, L., ZHAO, Z., LIU, D., PENG, N., WANG, D., HE, Y., LIANG, Y. and LIU, H., 2018. Study on Formation Mechanism of Fayalite (Fe2SiO4) by Solid State Reaction in Sintering Process. *JOM,* **70**(4), pp. 539-546.

YAMAGUCHI, K., 2011. Distribution of platinum and palladium in iron oxide slags equilibrated with molten copper at 1573 K. *Proceedings of European Metallurgical Conference EMC,* **1**, pp. 171-179.

YAZAWA, A., 1974. Thermodynamic considerations of copper smelting. *Canadian Metallurgical Quarterly,* **13**(3), pp. 443-453.

# 13 Appendices

Table 8. EPMA results for matte in air atmosphere (in wt-%).

| | Norm Weight% | | | | | | | | | | |
|---|---|---|---|---|---|---|---|---|---|---|---|
| **Sample** | **O** | **Mg** | **S** | **Fe** | **Cu** | **Zn** | **Pd** | **Ag** | **Pt** | **Pb** | **Au** |
| **20/2_1** | 5,85 | 0,01 | 24,30 | 31,60 | 29,45 | 1,48 | 2,17 | 3,31 | 0,77 | 0,03 | 1,04 |
| 20/2_2 | 4,77 | 0,00 | 25,09 | 31,57 | 29,59 | 1,60 | 2,16 | 3,34 | 0,94 | 0,04 | 0,91 |
| 20/2_2 | 3,80 | 0,01 | 25,50 | 30,57 | 30,47 | 1,59 | 2,62 | 3,65 | 0,83 | 0,11 | 0,83 |
| 20/2_3 | 3,66 | 0,00 | 25,45 | 30,73 | 30,04 | 1,53 | 2,47 | 3,52 | 1,26 | 0,11 | 1,23 |
| 20/2_4 | 3,87 | 0,00 | 25,84 | 31,76 | 29,43 | 1,59 | 2,32 | 3,45 | 0,84 | 0,03 | 0,86 |
| 20/2_4 | 4,48 | 0,01 | 25,21 | 31,98 | 28,99 | 1,62 | 2,14 | 3,29 | 1,23 | 0,12 | 0,95 |
| 20/2_5 | 4,72 | 0,00 | 24,62 | 32,24 | 28,90 | 1,56 | 2,16 | 3,27 | 1,31 | 0,08 | 1,13 |
| 20/2_5 | 4,82 | 0,00 | 24,47 | 32,22 | 28,80 | 1,53 | 2,22 | 3,23 | 1,38 | 0,09 | 1,24 |
| 20/2_6 | 4,12 | 0,00 | 24,43 | 32,44 | 28,01 | 1,54 | 2,46 | 3,60 | 1,83 | 0,02 | 1,56 |
| 20/2_6 | 4,06 | 0,00 | 24,46 | 32,40 | 28,17 | 1,57 | 2,39 | 3,49 | 1,82 | 0,09 | 1,54 |
| **20/3_1** | 6,48 | 0,00 | 24,05 | 33,30 | 26,99 | 1,67 | 2,06 | 2,57 | 1,47 | 0,07 | 1,34 |
| 20/3_1 | 6,55 | 0,00 | 23,90 | 33,35 | 26,99 | 1,70 | 2,08 | 2,55 | 1,48 | 0,08 | 1,32 |
| 20/3_2 | 4,52 | 0,01 | 25,12 | 30,75 | 30,13 | 1,81 | 2,29 | 2,02 | 1,68 | 0,09 | 1,57 |
| 20/3_3 | 5,01 | 0,01 | 24,98 | 32,32 | 28,27 | 1,78 | 2,34 | 1,79 | 1,83 | 0,06 | 1,59 |
| 20/3_4 | 4,64 | 0,01 | 24,75 | 31,10 | 29,12 | 1,85 | 2,35 | 3,03 | 1,60 | 0,10 | 1,45 |
| 20/3_5 | 4,99 | 0,00 | 25,58 | 34,81 | 25,18 | 1,99 | 2,11 | 2,61 | 1,35 | 0,15 | 1,24 |
| 20/3_5 | 4,91 | 0,01 | 25,55 | 34,91 | 25,34 | 2,01 | 2,13 | 2,65 | 1,25 | 0,08 | 1,18 |
| 20/3_6 | 5,79 | 0,00 | 25,28 | 32,99 | 27,04 | 2,51 | 2,03 | 2,57 | 0,77 | 0,09 | 0,93 |
| 20/3_6 | 5,37 | 0,00 | 25,34 | 32,73 | 27,65 | 2,46 | 2,01 | 2,56 | 0,85 | 0,09 | 0,94 |
| **30/2_1** | 2,98 | 0,01 | 25,64 | 28,93 | 32,79 | 1,39 | 2,70 | 3,62 | 0,68 | 0,11 | 1,15 |
| 30/2_1 | 3,38 | 0,00 | 25,64 | 29,28 | 33,11 | 1,34 | 2,42 | 3,31 | 0,52 | 0,00 | 0,98 |
| 30/2_2 | 4,01 | 0,01 | 25,08 | 29,57 | 32,23 | 1,40 | 2,54 | 3,11 | 0,88 | 0,08 | 1,11 |
| 30/2_3 | 4,79 | 0,01 | 25,00 | 29,94 | 31,93 | 1,37 | 2,33 | 2,96 | 0,63 | 0,05 | 0,99 |
| 30/2_4 | 3,21 | 0,01 | 26,05 | 28,88 | 33,27 | 1,40 | 2,16 | 3,16 | 1,08 | 0,05 | 0,74 |
| 30/2_5 | 2,80 | 0,01 | 26,18 | 28,85 | 33,52 | 1,37 | 2,20 | 3,13 | 1,06 | 0,02 | 0,88 |
| 30/2_6 | 4,52 | 0,00 | 24,37 | 29,40 | 33,16 | 1,31 | 2,15 | 2,88 | 1,01 | 0,09 | 1,11 |
| **30/3_1** | 3,93 | 0,01 | 25,07 | 30,43 | 31,94 | 1,43 | 2,28 | 2,89 | 0,87 | 0,04 | 1,12 |
| 30/3_1 | 4,07 | 0,00 | 24,92 | 30,15 | 31,74 | 1,43 | 2,38 | 2,90 | 0,98 | 0,11 | 1,32 |
| 30/3_2 | 4,51 | 0,01 | 24,66 | 29,87 | 32,52 | 1,34 | 2,08 | 2,81 | 0,95 | 0,13 | 1,13 |
| 30/3_3 | 2,94 | 0,00 | 25,47 | 29,32 | 32,69 | 1,40 | 2,46 | 2,93 | 1,20 | 0,08 | 1,50 |
| 30/3_3 | 2,98 | 0,00 | 25,37 | 29,18 | 32,62 | 1,39 | 2,47 | 3,03 | 1,31 | 0,08 | 1,56 |
| 30/3_4 | 4,62 | 0,01 | 24,27 | 30,50 | 31,08 | 1,38 | 2,43 | 2,88 | 1,29 | 0,04 | 1,49 |
| 30/3_5 | 3,55 | 0,01 | 25,15 | 30,15 | 31,64 | 1,40 | 2,64 | 2,92 | 0,96 | 0,10 | 1,49 |
| 30/3_5 | 3,91 | 0,01 | 24,83 | 30,54 | 31,74 | 1,38 | 2,55 | 2,93 | 0,83 | 0,00 | 1,29 |
| 30/3_5 | 4,28 | 0,00 | 24,70 | 30,54 | 31,62 | 1,40 | 2,55 | 2,88 | 0,79 | 0,10 | 1,13 |
| 30/3_6 | 4,67 | 0,01 | 24,23 | 30,67 | 30,98 | 1,40 | 2,39 | 2,84 | 1,37 | 0,08 | 1,37 |
| 30/3_6 | 4,96 | 0,00 | 23,78 | 30,83 | 31,22 | 1,37 | 2,25 | 2,70 | 1,35 | 0,10 | 1,43 |

| | | | | | | | | | | | |
|---|---|---|---|---|---|---|---|---|---|---|---|
| 30/3_6 | 4,93 | 0,01 | 23,89 | 30,72 | 31,33 | 1,39 | 2,31 | 2,69 | 1,35 | 0,00 | 1,36 |
| 30/3_6 | 5,01 | 0,00 | 23,58 | 30,60 | 31,33 | 1,35 | 2,33 | 2,71 | 1,54 | 0,05 | 1,51 |
| **60/2_1** | 4,64 | 0,01 | 24,06 | 31,25 | 30,26 | 1,33 | 2,40 | 2,84 | 1,65 | 0,17 | 1,40 |
| 60/2_2 | 4,34 | 0,01 | 24,17 | 31,48 | 30,85 | 1,28 | 2,36 | 2,94 | 1,36 | 0,07 | 1,13 |
| 60/2_3 | 4,36 | 0,00 | 23,72 | 30,96 | 31,46 | 1,30 | 2,34 | 2,62 | 1,76 | 0,06 | 1,43 |
| 60/2_4 | 4,62 | 0,01 | 24,37 | 31,22 | 31,89 | 1,31 | 1,85 | 2,58 | 1,06 | 0,12 | 0,97 |
| 60/2_5 | 4,74 | 0,01 | 24,37 | 31,40 | 32,30 | 1,27 | 1,85 | 2,69 | 0,62 | 0,06 | 0,67 |
| 60/2_6 | 3,81 | 0,00 | 24,74 | 30,58 | 32,71 | 1,30 | 2,10 | 2,74 | 0,84 | 0,06 | 1,10 |
| **60/3-1** | 3,81 | 0,00 | 25,26 | 31,06 | 30,62 | 1,35 | 2,56 | 3,29 | 0,72 | 0,04 | 1,28 |
| 60/3-2 | 4,41 | 0,01 | 24,96 | 31,37 | 30,01 | 1,36 | 2,50 | 3,22 | 0,75 | 0,08 | 1,33 |
| 60/3-3 | 5,65 | 0,01 | 24,46 | 31,62 | 30,09 | 1,29 | 2,13 | 3,17 | 0,59 | 0,07 | 0,93 |
| 60/3-4 | 4,18 | 0,00 | 24,48 | 31,18 | 30,25 | 1,24 | 2,21 | 3,14 | 1,85 | 0,08 | 1,39 |
| 60/3-5 | 2,97 | 0,01 | 26,10 | 30,54 | 31,31 | 1,32 | 2,50 | 3,39 | 0,65 | 0,17 | 1,02 |
| 60/3-6 | 6,08 | 0,00 | 25,18 | 32,44 | 28,76 | 1,38 | 2,02 | 3,03 | 0,33 | 0,03 | 0,75 |
| **150/1_1** | 4,67 | 0,01 | 23,60 | 29,68 | 32,97 | 1,07 | 1,98 | 3,07 | 1,74 | 0,09 | 1,12 |
| 150/1_1 | 4,54 | 0,00 | 23,68 | 29,97 | 33,17 | 1,12 | 1,92 | 3,02 | 1,48 | 0,03 | 1,08 |
| 150/1_2 | 4,83 | 0,00 | 23,33 | 30,00 | 32,93 | 1,10 | 2,15 | 3,05 | 1,45 | 0,04 | 1,12 |
| 150/1_2 | 4,69 | 0,01 | 23,44 | 29,78 | 33,53 | 1,07 | 2,05 | 2,96 | 1,44 | 0,05 | 0,99 |
| 150/1_2 | 4,64 | 0,01 | 23,56 | 29,63 | 33,80 | 1,06 | 1,90 | 2,99 | 1,36 | 0,03 | 1,01 |
| 150/1_3 | 4,56 | 0,01 | 24,16 | 30,44 | 33,16 | 1,11 | 1,78 | 2,83 | 0,96 | 0,07 | 0,92 |
| 150/1_4 | 4,41 | 0,01 | 23,25 | 29,84 | 32,77 | 1,07 | 2,13 | 2,84 | 2,02 | 0,07 | 1,59 |
| 150/1_4 | 4,51 | 0,01 | 23,38 | 29,82 | 33,17 | 1,07 | 1,95 | 2,76 | 1,86 | 0,05 | 1,41 |
| 150/1_4 | 4,23 | 0,00 | 23,73 | 30,14 | 32,67 | 1,08 | 2,11 | 2,77 | 1,79 | 0,00 | 1,47 |
| 150/1_4 | 4,46 | 0,01 | 23,57 | 30,15 | 32,76 | 1,06 | 2,06 | 2,79 | 1,70 | 0,01 | 1,43 |
| 150/1_5 | 4,44 | 0,00 | 23,88 | 30,11 | 32,69 | 1,11 | 2,13 | 3,27 | 1,28 | 0,02 | 1,05 |
| 150/1_5 | 4,27 | 0,01 | 23,96 | 30,14 | 32,58 | 1,08 | 2,16 | 3,33 | 1,30 | 0,06 | 1,12 |
| 150/1_5 | 4,43 | 0,01 | 23,70 | 30,04 | 32,81 | 1,08 | 2,09 | 3,27 | 1,38 | 0,03 | 1,17 |
| 150/1_5 | 4,57 | 0,02 | 23,90 | 29,96 | 32,92 | 1,10 | 2,04 | 3,30 | 1,21 | 0,00 | 0,99 |
| 150/1_5 | 4,33 | 0,00 | 23,81 | 30,17 | 32,64 | 1,12 | 2,18 | 3,36 | 1,24 | 0,07 | 1,08 |
| 150/1_6 | 5,06 | 0,00 | 23,01 | 29,69 | 31,84 | 1,09 | 2,46 | 3,16 | 2,00 | 0,10 | 1,59 |
| 150/1_6 | 4,49 | 0,00 | 23,66 | 29,70 | 33,32 | 1,07 | 1,82 | 2,86 | 1,74 | 0,11 | 1,23 |
| 150/1_6 | 4,51 | 0,00 | 23,66 | 29,73 | 33,49 | 1,07 | 1,77 | 2,88 | 1,72 | 0,01 | 1,17 |
| **150/2_1** | 4,54 | 0,01 | 23,77 | 30,40 | 31,99 | 1,12 | 2,16 | 4,03 | 0,94 | 0,07 | 0,99 |
| 150/2_2 | 4,18 | 0,00 | 23,48 | 30,12 | 31,42 | 1,12 | 2,51 | 3,86 | 1,94 | 0,08 | 1,29 |
| 150/2_2 | 4,41 | 0,01 | 23,71 | 30,30 | 31,40 | 1,16 | 2,30 | 3,88 | 1,50 | 0,05 | 1,28 |
| 150/2_3 | 4,40 | 0,01 | 24,16 | 30,19 | 31,41 | 1,11 | 2,56 | 4,42 | 0,85 | 0,08 | 0,81 |
| 150/2_4 | 5,32 | 0,00 | 23,11 | 29,49 | 30,02 | 1,11 | 2,20 | 3,69 | 3,44 | 0,06 | 1,55 |
| 150/2_4 | 4,75 | 0,00 | 24,03 | 30,18 | 30,97 | 1,09 | 2,38 | 4,10 | 1,48 | 0,06 | 0,98 |
| 150/2_5 | 5,45 | 0,01 | 23,17 | 30,23 | 31,48 | 1,09 | 2,22 | 3,84 | 1,26 | 0,10 | 1,15 |
| 150/2_6 | 4,14 | 0,01 | 23,60 | 30,54 | 30,22 | 1,14 | 2,40 | 3,92 | 2,79 | 0,05 | 1,20 |
| **300/1_1** | 5,24 | 0,00 | 23,24 | 28,22 | 34,70 | 0,93 | 2,28 | 3,19 | 1,10 | 0,00 | 1,09 |
| 300/1_2 | 6,44 | 0,00 | 22,31 | 29,20 | 33,05 | 0,87 | 2,22 | 2,86 | 1,74 | 0,09 | 1,22 |
| 300/1_2 | 3,72 | 0,01 | 23,72 | 27,02 | 34,65 | 0,97 | 3,28 | 3,41 | 1,61 | 0,04 | 1,58 |
| 300/1_2 | 5,59 | 0,01 | 22,95 | 28,40 | 33,90 | 0,87 | 2,33 | 3,13 | 1,45 | 0,05 | 1,32 |
| 300/1_3 | 3,59 | 0,00 | 24,88 | 27,99 | 35,62 | 0,97 | 2,25 | 3,31 | 0,55 | 0,05 | 0,79 |

| | | | | | | | | | | | |
|---|---|---|---|---|---|---|---|---|---|---|---|
| 300/1_4 | 5,18 | 0,00 | 23,10 | 28,32 | 34,37 | 0,90 | 2,29 | 3,15 | 1,40 | 0,07 | 1,21 |
| 300/1_5 | 3,62 | 0,01 | 23,99 | 27,94 | 34,77 | 0,95 | 2,39 | 3,23 | 1,75 | 0,03 | 1,32 |
| 300/1_5 | 4,13 | 0,01 | 23,62 | 28,73 | 34,34 | 0,93 | 2,22 | 3,17 | 1,64 | 0,01 | 1,21 |
| 300/1_5 | 4,08 | 0,01 | 23,62 | 28,54 | 34,55 | 0,94 | 2,25 | 3,19 | 1,61 | 0,05 | 1,15 |
| 300/1_6 | 3,81 | 0,00 | 23,85 | 27,27 | 35,03 | 0,91 | 2,51 | 3,28 | 1,91 | 0,00 | 1,42 |
| 300/1_6 | 4,03 | 0,00 | 24,01 | 28,96 | 33,88 | 0,96 | 2,43 | 3,36 | 1,40 | 0,00 | 0,97 |
| **300/2_1** | 0,65 | 0,01 | 19,90 | 6,25 | 57,51 | 0,33 | 3,82 | 5,62 | 2,39 | 0,07 | 3,44 |
| 300/2_1 | 0,84 | 0,00 | 19,99 | 6,37 | 57,69 | 0,33 | 4,04 | 5,76 | 1,71 | 0,12 | 3,15 |
| 300/2_2 | 0,80 | 0,00 | 19,95 | 6,38 | 57,02 | 0,32 | 4,29 | 5,88 | 1,77 | 0,10 | 3,50 |
| 300/2_3 | 0,86 | 0,00 | 20,25 | 6,40 | 57,13 | 0,32 | 4,34 | 5,62 | 1,91 | 0,00 | 3,18 |
| 300/2_4 | 0,85 | 0,00 | 20,06 | 6,28 | 57,29 | 0,35 | 3,98 | 5,69 | 2,04 | 0,08 | 3,39 |
| 300/2_5 | 0,98 | 0,00 | 20,07 | 6,58 | 57,26 | 0,35 | 4,10 | 5,51 | 1,87 | 0,06 | 3,22 |
| 300/2_6 | 1,07 | 0,01 | 20,38 | 6,49 | 59,06 | 0,35 | 2,79 | 4,47 | 2,49 | 0,07 | 2,83 |
| **300/3_1** | 2,18 | 0,01 | 21,95 | 15,48 | 47,54 | 0,42 | 4,18 | 5,55 | 0,92 | 0,11 | 1,67 |
| 300/3_2 | 1,95 | 0,01 | 22,28 | 15,66 | 49,90 | 0,41 | 3,06 | 4,64 | 0,71 | 0,07 | 1,32 |
| 300/3_3 | 2,08 | 0,01 | 22,67 | 17,36 | 47,96 | 0,40 | 2,74 | 4,02 | 1,05 | 0,02 | 1,69 |
| 300/3_4 | 2,15 | 0,01 | 22,49 | 17,79 | 47,24 | 0,42 | 2,88 | 4,18 | 1,10 | 0,03 | 1,72 |
| 300/3_4 | 2,30 | 0,01 | 22,71 | 18,54 | 46,28 | 0,46 | 2,70 | 3,99 | 1,24 | 0,03 | 1,73 |
| 300/3_5 | 2,08 | 0,01 | 22,94 | 16,83 | 47,89 | 0,42 | 3,12 | 4,81 | 0,64 | 0,03 | 1,23 |
| 300/3_6 | 2,17 | 0,01 | 22,91 | 17,42 | 48,04 | 0,43 | 2,42 | 3,99 | 1,12 | 0,00 | 1,49 |
| 300/3_6 | 2,21 | 0,01 | 22,76 | 17,48 | 47,40 | 0,46 | 2,65 | 4,23 | 1,11 | 0,00 | 1,70 |
| 300/3_6 | 2,00 | 0,00 | 22,85 | 17,71 | 47,29 | 0,46 | 2,73 | 3,98 | 1,18 | 0,03 | 1,76 |
| 300/3_6 | 2,14 | 0,01 | 22,62 | 17,63 | 46,37 | 0,47 | 3,20 | 4,57 | 1,10 | 0,08 | 1,82 |
| **600/1_1** | 1,53 | 0,00 | 21,92 | 13,54 | 50,39 | 0,47 | 3,22 | 4,46 | 1,79 | 0,11 | 2,56 |
| 600/1_2 | 1,97 | 0,00 | 21,65 | 14,02 | 50,55 | 0,49 | 3,30 | 4,65 | 1,04 | 0,02 | 2,30 |
| 600/1_2 | 1,54 | 0,00 | 21,68 | 13,78 | 50,37 | 0,47 | 3,32 | 4,73 | 1,62 | 0,01 | 2,49 |
| 600/1_3 | 1,63 | 0,01 | 22,63 | 13,88 | 52,30 | 0,46 | 2,64 | 3,99 | 0,53 | 0,04 | 1,89 |
| 600/1_3 | 1,76 | 0,00 | 22,58 | 14,17 | 52,73 | 0,49 | 2,39 | 3,67 | 0,57 | 0,05 | 1,61 |
| 600/1_3 | 2,80 | 0,01 | 21,96 | 14,90 | 51,30 | 0,47 | 2,34 | 3,58 | 0,73 | 0,00 | 1,92 |
| 600/1_4 | 1,76 | 0,00 | 22,08 | 13,78 | 51,59 | 0,44 | 2,70 | 3,95 | 0,93 | 0,08 | 2,68 |
| 600/1_4 | 1,84 | 0,00 | 21,98 | 13,89 | 51,59 | 0,47 | 2,69 | 4,00 | 0,96 | 0,03 | 2,55 |
| 600/1_5 | 2,77 | 0,01 | 21,75 | 14,73 | 50,25 | 0,47 | 3,12 | 4,53 | 0,50 | 0,01 | 1,86 |
| 600/1_5 | 1,45 | 0,01 | 22,11 | 13,67 | 51,07 | 0,46 | 3,17 | 4,58 | 1,05 | 0,03 | 2,40 |
| 600/1_6 | 1,69 | 0,00 | 22,46 | 13,66 | 52,03 | 0,46 | 2,95 | 4,32 | 0,51 | 0,00 | 1,92 |
| 600/1_6 | 1,66 | 0,01 | 22,73 | 14,08 | 52,15 | 0,45 | 2,83 | 4,24 | 0,37 | 0,04 | 1,45 |
| 600/1_6 | 1,73 | 0,01 | 22,49 | 13,98 | 51,51 | 0,46 | 3,15 | 4,63 | 0,59 | 0,04 | 1,42 |

Table 9. EPMA results for matte in argon atmosphere (in wt-%). The values marked with red are below detection limit.

| | Norm Weight% | | | | | | | | | | |
|---|---|---|---|---|---|---|---|---|---|---|---|
| **Sample** | **O** | **Mg** | **S** | **Fe** | **Cu** | **Zn** | **Pd** | **Ag** | **Pt** | **Pb** | **Au** |
| **Ar5_1_matte1** | 3,85 | 0,01 | 25,47 | 34,74 | 28,95 | 1,20 | 2,06 | 3,02 | 0,00 | 0,10 | 0,61 |
| Ar5_1_matte1 | 3,37 | 0,00 | 25,43 | 34,38 | 29,50 | 1,14 | 1,80 | 3,01 | 0,30 | 0,00 | 1,07 |
| Ar5_1_matte2 | 3,68 | 0,00 | 25,13 | 34,79 | 28,89 | 1,22 | 2,16 | 3,29 | 0,00 | 0,07 | 0,77 |
| Ar5_1_matte2 | 3,78 | 0,01 | 25,32 | 34,65 | 29,19 | 1,15 | 1,98 | 2,85 | 0,07 | 0,10 | 0,91 |
| Ar5_1_matte3 | 4,02 | 0,01 | 25,42 | 35,16 | 28,48 | 1,25 | 1,95 | 3,01 | 0,00 | 0,07 | 0,63 |
| Ar5_1_matte3 | 3,81 | 0,01 | 24,70 | 33,25 | 30,97 | 1,15 | 1,94 | 2,91 | 0,24 | 0,09 | 0,94 |
| Ar5_1_matte4 | 3,40 | 0,00 | 25,62 | 37,79 | 25,78 | 1,01 | 2,44 | 3,45 | 0,00 | 0,07 | 0,44 |
| Ar5_1_matte4 | 3,52 | 0,00 | 25,09 | 34,74 | 29,22 | 1,22 | 1,93 | 2,99 | 0,43 | 0,05 | 0,81 |
| Ar5_1_matte4 | 3,60 | 0,00 | 25,20 | 34,91 | 29,09 | 1,19 | 1,93 | 3,02 | 0,26 | 0,03 | 0,76 |
| Ar5_1_matte4 | 3,81 | 0,01 | 25,48 | 35,46 | 29,04 | 1,13 | 1,77 | 2,94 | 0,00 | 0,09 | 0,28 |
| Ar5_1_matte5 | 3,44 | 0,01 | 25,11 | 34,86 | 28,92 | 1,16 | 2,25 | 3,00 | 0,18 | 0,01 | 1,06 |
| Ar5_1_matte5 | 3,52 | 0,00 | 25,32 | 34,70 | 29,69 | 1,14 | 2,00 | 2,97 | 0,00 | 0,09 | 0,57 |
| Ar5_1_matte5 | 3,72 | 0,00 | 25,13 | 34,53 | 29,58 | 1,20 | 1,97 | 3,14 | 0,00 | 0,04 | 0,68 |
| Ar5_1_matte5 | 3,87 | 0,00 | 24,93 | 34,47 | 29,81 | 1,15 | 1,95 | 2,95 | 0,04 | 0,03 | 0,78 |
| Ar5_1_matte5 | 3,85 | 0,01 | 25,04 | 34,44 | 29,81 | 1,14 | 2,05 | 2,93 | 0,00 | 0,01 | 0,71 |
| Ar5_1_matte6 | 3,68 | 0,00 | 25,23 | 34,49 | 30,00 | 1,11 | 2,02 | 2,87 | 0,00 | 0,06 | 0,56 |
| Ar5_1_matte6 | 3,25 | 0,00 | 25,73 | 34,61 | 29,72 | 1,10 | 2,10 | 3,03 | 0,00 | 0,03 | 0,42 |
| Ar5_1_matte6 | 3,36 | 0,00 | 24,76 | 33,44 | 31,30 | 1,11 | 1,97 | 2,98 | 0,26 | 0,03 | 0,79 |
| **Ar5_2_matte1** | 3,80 | 0,01 | 25,13 | 34,09 | 30,53 | 1,20 | 1,68 | 2,89 | 0,00 | 0,10 | 0,59 |
| Ar5_2_matte1 | 3,54 | 0,00 | 25,37 | 33,82 | 31,42 | 1,20 | 1,48 | 2,70 | 0,00 | 0,05 | 0,42 |
| Ar5_2_matte1 | 3,61 | 0,00 | 25,22 | 34,70 | 29,88 | 1,20 | 1,63 | 3,03 | 0,05 | 0,04 | 0,65 |
| Ar5_2_matte1 | 3,62 | 0,00 | 25,38 | 34,16 | 30,61 | 1,18 | 1,45 | 2,82 | 0,06 | 0,07 | 0,64 |
| Ar5_2_matte2 | 4,00 | 0,01 | 25,15 | 34,79 | 29,59 | 1,17 | 1,80 | 2,91 | 0,00 | 0,05 | 0,55 |
| Ar5_2_matte2 | 3,97 | 0,00 | 25,17 | 34,49 | 29,59 | 1,14 | 1,97 | 2,96 | 0,00 | 0,05 | 0,66 |
| Ar5_2_matte2 | 4,01 | 0,00 | 25,05 | 34,65 | 29,71 | 1,12 | 1,88 | 3,03 | 0,00 | 0,00 | 0,56 |
| Ar5_2_matte3 | 4,46 | 0,00 | 25,36 | 33,67 | 31,47 | 1,20 | 1,24 | 2,45 | 0,00 | 0,03 | 0,12 |
| Ar5_2_matte3 | 4,44 | 0,01 | 25,35 | 33,49 | 31,39 | 1,16 | 1,35 | 2,52 | 0,00 | 0,09 | 0,22 |
| Ar5_2_matte4 | 3,93 | 0,00 | 25,53 | 34,44 | 29,70 | 1,19 | 1,78 | 3,06 | 0,00 | 0,10 | 0,28 |
| Ar5_2_matte4 | 4,58 | 0,01 | 25,07 | 34,62 | 29,20 | 1,13 | 1,79 | 3,16 | 0,00 | 0,04 | 0,39 |
| Ar5_2_matte4 | 4,49 | 0,00 | 25,08 | 35,25 | 28,26 | 1,11 | 1,77 | 2,65 | 0,38 | 0,05 | 0,95 |
| Ar5_2_matte5 | 3,63 | 0,00 | 24,68 | 33,87 | 30,58 | 1,17 | 1,85 | 2,99 | 0,17 | 0,03 | 1,05 |
| Ar5_2_matte5 | 3,81 | 0,00 | 24,50 | 33,58 | 31,00 | 1,14 | 1,90 | 2,84 | 0,26 | 0,02 | 0,95 |
| Ar5_2_matte5 | 3,47 | 0,01 | 25,58 | 35,25 | 28,67 | 1,20 | 1,96 | 2,84 | 0,07 | 0,00 | 0,96 |
| Ar5_2_matte6 | 3,79 | 0,01 | 24,98 | 34,47 | 29,18 | 1,07 | 2,23 | 2,99 | 0,42 | 0,00 | 0,86 |
| Ar5_2_matte6 | 4,01 | 0,01 | 25,33 | 34,69 | 29,90 | 1,16 | 1,45 | 2,86 | 0,07 | 0,04 | 0,48 |
| **Ar10_1_matte1** | 3,97 | 0,01 | 24,78 | 34,37 | 30,48 | 0,34 | 2,03 | 2,75 | 0,19 | 0,05 | 1,03 |
| Ar10_1_matte1 | 3,81 | 0,00 | 24,88 | 33,35 | 32,15 | 0,34 | 1,72 | 2,70 | 0,17 | 0,00 | 0,89 |
| Ar10_1_matte1 | 3,60 | 0,01 | 24,95 | 34,41 | 30,67 | 0,34 | 1,98 | 2,76 | 0,27 | 0,06 | 0,97 |
| Ar10_1_matte2 | 3,51 | 0,01 | 25,15 | 34,23 | 31,28 | 0,32 | 1,96 | 2,85 | 0,12 | 0,05 | 0,54 |

| | | | | | | | | | | | |
|---|---|---|---|---|---|---|---|---|---|---|---|
| Ar10_1_matte2 | 3,62 | 0,00 | 24,94 | 33,31 | 31,89 | 0,34 | 1,78 | 2,84 | 0,53 | 0,00 | 0,75 |
| Ar10_1_matte2 | 3,45 | 0,00 | 25,48 | 35,36 | 30,46 | 0,35 | 1,94 | 2,75 | 0,00 | 0,04 | 0,15 |
| Ar10_1_matte3 | 3,62 | 0,00 | 25,22 | 34,94 | 30,89 | 0,35 | 2,15 | 2,69 | 0,00 | 0,03 | 0,11 |
| Ar10_1_matte3 | 3,39 | 0,01 | 25,06 | 34,12 | 31,97 | 0,33 | 2,17 | 2,48 | 0,06 | 0,04 | 0,38 |
| Ar10_1_matte4 | 3,39 | 0,00 | 25,66 | 36,22 | 29,16 | 0,33 | 1,88 | 2,45 | 0,09 | 0,11 | 0,70 |
| Ar10_1_matte4 | 3,44 | 0,00 | 25,89 | 37,75 | 27,15 | 0,34 | 2,09 | 2,40 | 0,08 | 0,07 | 0,80 |
| Ar10_1_matte5 | 3,88 | 0,01 | 24,33 | 33,10 | 32,62 | 0,39 | 1,94 | 2,90 | 0,14 | 0,07 | 0,62 |
| Ar10_1_matte5 | 3,79 | 0,00 | 24,96 | 35,04 | 30,00 | 0,34 | 1,94 | 2,84 | 0,28 | 0,04 | 0,77 |
| Ar10_1_matte5 | 3,43 | 0,00 | 25,35 | 37,15 | 27,30 | 0,36 | 2,39 | 2,99 | 0,34 | 0,00 | 0,70 |
| Ar10_1_matte6 | 4,00 | 0,00 | 25,04 | 34,87 | 30,86 | 0,29 | 1,79 | 2,63 | 0,09 | 0,03 | 0,41 |
| Ar10_1_matte6 | 3,89 | 0,00 | 24,77 | 33,80 | 31,93 | 0,29 | 1,77 | 2,66 | 0,18 | 0,03 | 0,67 |
| **Ar10_2_matte1** | 3,55 | 0,01 | 25,45 | 34,36 | 30,07 | 0,30 | 2,24 | 3,35 | 0,12 | 0,01 | 0,54 |
| Ar10_2_matte2 | 3,45 | 0,01 | 25,28 | 33,39 | 31,65 | 0,30 | 2,04 | 3,25 | 0,11 | 0,03 | 0,49 |
| Ar10_2_matte2 | 3,61 | 0,00 | 25,27 | 33,27 | 31,42 | 0,30 | 1,90 | 3,41 | 0,18 | 0,08 | 0,56 |
| Ar10_2_matte3 | 3,39 | 0,00 | 25,47 | 34,19 | 30,26 | 0,32 | 2,11 | 3,35 | 0,17 | 0,00 | 0,74 |
| Ar10_2_matte3 | 3,37 | 0,01 | 25,38 | 33,90 | 30,32 | 0,37 | 2,15 | 3,38 | 0,22 | 0,11 | 0,79 |
| Ar10_2_matte4 | 3,83 | 0,01 | 25,11 | 34,18 | 30,15 | 0,45 | 2,01 | 3,06 | 0,27 | 0,06 | 0,86 |
| Ar10_2_matte4 | 3,79 | 0,00 | 25,16 | 34,05 | 30,13 | 0,45 | 2,09 | 3,22 | 0,29 | 0,01 | 0,79 |
| Ar10_2_matte5 | 3,99 | 0,01 | 25,00 | 33,96 | 30,46 | 0,47 | 2,12 | 3,18 | 0,09 | 0,04 | 0,69 |
| Ar10_2_matte5 | 4,07 | 0,00 | 24,75 | 33,90 | 30,66 | 0,46 | 2,10 | 3,23 | 0,12 | 0,05 | 0,65 |
| Ar10_2_matte6 | 3,95 | 0,01 | 25,35 | 34,62 | 29,41 | 0,46 | 1,94 | 2,91 | 0,33 | 0,00 | 1,03 |
| Ar10_2_matte6 | 3,86 | 0,00 | 25,17 | 34,56 | 29,68 | 0,46 | 1,92 | 2,92 | 0,38 | 0,05 | 1,01 |
| Ar10_2_matte6 | 3,88 | 0,00 | 24,95 | 34,91 | 28,93 | 0,48 | 2,15 | 3,07 | 0,45 | 0,02 | 1,16 |
| **Ar 20_1_matte1** | 4,22 | 0,01 | 26,21 | 32,92 | 29,32 | 1,68 | 2,29 | 2,48 | 0,02 | 0,13 | 0,73 |
| Ar 20_1_matte1 | 4,19 | 0,00 | 26,72 | 32,63 | 30,81 | 1,73 | 1,05 | 2,07 | 0,02 | 0,06 | 0,72 |
| Ar 20_1_matte2 | 3,78 | 0,00 | 27,02 | 32,46 | 30,47 | 1,73 | 1,38 | 1,90 | 0,34 | 0,06 | 0,87 |
| Ar 20_1_matte2 | 6,26 | 0,01 | 25,51 | 34,60 | 29,06 | 1,59 | 1,06 | 1,84 | 0,00 | 0,00 | 0,08 |
| Ar 20_1_matte3 | 2,43 | 0,01 | 27,74 | 28,97 | 36,90 | 1,32 | 0,90 | 1,59 | 0,00 | 0,09 | 0,07 |
| Ar 20_1_matte3 | 2,68 | 0,00 | 28,48 | 33,90 | 30,67 | 1,99 | 0,77 | 1,19 | 0,00 | 0,00 | 0,30 |
| Ar 20_1_matte3 | 2,53 | 0,01 | 28,32 | 31,27 | 34,21 | 1,55 | 0,68 | 1,26 | 0,00 | 0,02 | 0,15 |
| Ar 20_1_matte4 | 6,52 | 0,01 | 25,05 | 34,32 | 29,20 | 1,63 | 1,04 | 1,56 | 0,05 | 0,00 | 0,62 |
| Ar 20_1_matte4 | 6,28 | 0,00 | 25,26 | 34,03 | 29,67 | 1,54 | 1,03 | 1,67 | 0,00 | 0,05 | 0,46 |
| Ar 20_1_matte5 | 4,67 | 0,00 | 26,67 | 33,06 | 31,30 | 1,61 | 0,66 | 1,97 | 0,00 | 0,00 | 0,06 |
| Ar 20_1_matte5 | 4,99 | 0,00 | 26,52 | 33,59 | 30,73 | 1,58 | 0,69 | 1,84 | 0,00 | 0,04 | 0,03 |
| Ar 20_1_matte6 | 3,50 | 0,00 | 27,15 | 32,48 | 30,20 | 1,66 | 1,31 | 1,76 | 0,67 | 0,05 | 1,23 |
| Ar 20_1_matte6 | 6,07 | 0,01 | 24,62 | 32,94 | 28,42 | 1,64 | 2,48 | 2,81 | 0,03 | 0,09 | 0,89 |
| **Ar 20_2_matte1** | 3,78 | 0,00 | 24,35 | 35,03 | 30,81 | 0,03 | 1,98 | 2,77 | 0,30 | 0,00 | 0,95 |
| Ar 20_2_matte1 | 3,68 | 0,00 | 24,67 | 35,78 | 29,56 | 0,03 | 2,09 | 2,91 | 0,33 | 0,04 | 0,92 |
| Ar 20_2_matte2 | 3,81 | 0,01 | 24,56 | 34,33 | 30,79 | 0,06 | 1,99 | 2,83 | 0,40 | 0,05 | 1,17 |
| Ar 20_2_matte2 | 3,82 | 0,01 | 24,99 | 35,37 | 29,85 | 0,05 | 2,06 | 2,90 | 0,28 | 0,00 | 0,68 |
| Ar 20_2_matte3 | 4,15 | 0,01 | 24,50 | 34,51 | 30,85 | 0,06 | 1,97 | 2,93 | 0,21 | 0,11 | 0,72 |
| Ar 20_2_matte3 | 3,95 | 0,00 | 24,48 | 34,46 | 30,93 | 0,05 | 2,12 | 2,91 | 0,22 | 0,02 | 0,85 |
| Ar 20_2_matte4 | 3,88 | 0,01 | 25,25 | 35,42 | 30,25 | 0,06 | 1,86 | 2,88 | 0,10 | 0,00 | 0,29 |
| Ar 20_2_matte4 | 4,00 | 0,00 | 25,36 | 35,55 | 29,69 | 0,05 | 1,98 | 2,88 | 0,07 | 0,05 | 0,36 |
| Ar 20_2_matte4 | 3,81 | 0,00 | 25,23 | 35,75 | 29,83 | 0,06 | 1,92 | 2,93 | 0,12 | 0,00 | 0,35 |

| | | | | | | | | | | | |
|---|---|---|---|---|---|---|---|---|---|---|---|
| Ar 20_2_matte6 | 3,42 | 0,01 | 23,91 | 30,62 | 35,82 | 0,00 | 2,42 | 1,96 | 0,45 | 0,00 | 1,38 |
| Ar 20_2_matte6 | 3,27 | 0,01 | 23,99 | 30,77 | 35,45 | 0,02 | 2,47 | 2,00 | 0,49 | 0,00 | 1,54 |
| Ar 20_2_matte6 | 3,24 | 0,00 | 24,05 | 30,67 | 35,66 | 0,00 | 2,43 | 1,99 | 0,49 | 0,00 | 1,46 |
| **Ar 40_1_matte1** | 3,37 | 0,00 | 24,46 | 35,60 | 30,45 | 0,00 | 2,00 | 2,91 | 0,27 | 0,00 | 0,94 |
| Ar 40_1_matte1 | 3,59 | 0,01 | 24,47 | 35,85 | 30,05 | 0,00 | 1,98 | 2,99 | 0,21 | 0,00 | 0,85 |
| Ar 40_1_matte2 | 3,68 | 0,00 | 24,99 | 36,38 | 29,54 | 0,00 | 1,82 | 2,85 | 0,15 | 0,07 | 0,53 |
| Ar 40_1_matte2 | 3,59 | 0,00 | 24,62 | 35,99 | 29,63 | 0,00 | 1,98 | 3,05 | 0,25 | 0,02 | 0,88 |
| Ar 40_1_matte3 | 3,64 | 0,01 | 24,87 | 36,93 | 28,85 | 0,00 | 1,81 | 2,97 | 0,22 | 0,00 | 0,72 |
| Ar 40_1_matte3 | 3,39 | 0,01 | 25,04 | 36,44 | 29,41 | 0,00 | 1,77 | 2,61 | 0,28 | 0,05 | 1,01 |
| Ar 40_1_matte4 | 3,56 | 0,00 | 25,27 | 36,61 | 29,24 | 0,00 | 1,86 | 2,97 | 0,12 | 0,01 | 0,36 |
| Ar 40_1_matte4 | 3,38 | 0,00 | 25,10 | 36,15 | 30,06 | 0,00 | 1,85 | 2,98 | 0,07 | 0,06 | 0,34 |
| Ar 40_1_matte5 | 3,74 | 0,00 | 24,35 | 35,82 | 29,44 | 0,00 | 1,95 | 2,87 | 0,40 | 0,03 | 1,38 |
| Ar 40_1_matte5 | 3,83 | 0,00 | 24,32 | 35,88 | 29,32 | 0,00 | 1,98 | 2,93 | 0,41 | 0,01 | 1,32 |
| Ar 40_1_matte6 | 3,71 | 0,00 | 24,49 | 36,37 | 29,82 | 0,00 | 1,76 | 2,68 | 0,25 | 0,03 | 0,90 |
| Ar 40_1_matte6 | 3,61 | 0,00 | 24,16 | 35,97 | 29,70 | 0,00 | 2,04 | 2,91 | 0,37 | 0,00 | 1,23 |
| Ar 40_1_matte6 | 3,64 | 0,01 | 24,02 | 35,91 | 29,37 | 0,02 | 2,17 | 2,90 | 0,42 | 0,04 | 1,50 |
| **Ar 40_2_matte1** | 3,49 | 0,01 | 25,08 | 36,21 | 30,25 | 0,00 | 1,70 | 2,79 | 0,11 | 0,00 | 0,35 |
| Ar 40_2_matte1 | 3,53 | 0,01 | 25,06 | 36,20 | 30,02 | 0,02 | 1,71 | 2,83 | 0,16 | 0,02 | 0,45 |
| Ar 40_2_matte2 | 3,58 | 0,01 | 24,57 | 35,84 | 29,54 | 0,00 | 1,95 | 2,87 | 0,40 | 0,00 | 1,24 |
| Ar 40_2_matte2 | 3,58 | 0,00 | 24,61 | 35,90 | 29,50 | 0,00 | 1,85 | 2,90 | 0,39 | 0,03 | 1,25 |
| Ar 40_2_matte3 | 3,60 | 0,01 | 24,84 | 36,38 | 28,63 | 0,00 | 1,85 | 2,87 | 0,37 | 0,08 | 1,36 |
| Ar 40_2_matte3 | 3,53 | 0,01 | 24,90 | 36,41 | 28,70 | 0,00 | 1,81 | 2,97 | 0,36 | 0,00 | 1,30 |
| Ar 40_2_matte4 | 3,54 | 0,00 | 25,41 | 36,17 | 29,83 | 0,00 | 1,49 | 3,01 | 0,16 | 0,00 | 0,38 |
| Ar 40_2_matte4 | 3,61 | 0,00 | 25,42 | 36,61 | 29,79 | 0,00 | 1,48 | 2,82 | 0,03 | 0,00 | 0,25 |
| Ar 40_2_matte5 | 3,53 | 0,01 | 25,56 | 36,28 | 29,75 | 0,00 | 1,51 | 2,96 | 0,09 | 0,00 | 0,31 |
| Ar 40_2_matte5 | 3,62 | 0,00 | 25,49 | 36,50 | 29,48 | 0,02 | 1,58 | 2,86 | 0,11 | 0,01 | 0,32 |
| Ar 40_2_matte6 | 3,45 | 0,01 | 25,70 | 35,67 | 30,48 | 0,00 | 1,57 | 2,97 | 0,04 | 0,01 | 0,09 |
| Ar 40_2_matte6 | 3,20 | 0,01 | 25,73 | 35,92 | 30,37 | 0,00 | 1,63 | 3,01 | 0,08 | 0,00 | 0,05 |

Table 10. LA-ICP-MS data for slags in air atmosphere (in ppm) The concentration values not included in the calculation of average values and standard deviations are marked with A and/or red colour.

| | | | | | | | | | | |
|---|---|---|---|---|---|---|---|---|---|---|
| 20//2 | | | | | | | | | | |
| Si29 | 130088,38 | 130088,38 | 130088,38 | 130088,38 | 130088,38 | 130088,38 | 130088,38 | 130088,38 | 130088,38 | 130088,38 |
| Pd104 | 76,47 | 81,21 | 121,39 | 63,23 | A60.59 | 141,38 | 187,84 | 133,21 | 85,47 | 516,83 |
| Pd105 | 75,72 | 84,31 | 128,08 | 64,53 | A60.91 | 147,21 | 205,5 | 142,76 | 90,57 | 589,38 |
| Pd106 | 8,82 | 9,52 | 14,27 | 7,24 | A6.75 | 16,23 | 22,44 | 15,38 | 10,07 | 70,46 |
| Ag107 | 407,39 | 432,58 | 550,32 | 387,12 | 320,05 | 381,08 | 1323,64 | 435,24 | 385,94 | 632,2 |
| Pd108 | 11,14 | 12,8 | 18,88 | 9,54 | A8.99 | 21,49 | 30,02 | 20,82 | 13,43 | 87,94 |
| Ag109 | 423,72 | 423,18 | 548,17 | 385,54 | 339,25 | 393,12 | 1285,39 | 434,92 | 382,98 | 726,99 |
| Pd110 | 0,501 | 0,543 | 0,762 | 0,404 | 0,368 | 0,873 | 1,13 | 0,814 | 0,542 | 3,31 |
| Pt194 | 40,12 | 42,93 | 53,31 | 32,47 | A26.42 | 73,45 | 71,72 | 64,66 | 46,19 | 214,65 |
| Pt195 | 41,41 | 43,09 | 53,68 | 32,6 | A25.99 | 72,13 | 70,14 | 63,42 | 45,3 | 212,61 |
| Pt196 | 42,36 | 44,19 | 54,43 | 32,58 | A25.74 | 71,34 | 70,6 | 62,63 | 45,16 | 215,78 |
| Au197 | 140,19 | 125,97 | 150,16 | 108,35 | A92.26 | 159,04 | 179,83 | 154,24 | 143,38 | 361,3 |
| Pb208 | 189,98 | 197,49 | 218,54 | 197,52 | 173,19 | 175,58 | 174,96 | 165,71 | 164,17 | 172,18 |
| 20//3 | | | | | | | | | | |
| Si29 | 116252,19 | 116252,19 | 116252,19 | 116252,19 | 116252,17 | 116252,18 | 116252,18 | 116252,18 | 116252,18 | 116252,18 |
| Pd104 | 273,47 | 217,02 | A490.63 | 366,75 | 88,89 | 334,44 | 222,62 | 161,56 | 3354,43 | 756,59 |
| Pd105 | 244,82 | 190,83 | A444.58 | 320,15 | 76,68 | 298,75 | 194,44 | 137,13 | 2994,07 | 669,82 |
| Pd106 | 27,91 | 21,18 | A48.47 | 35,75 | 8,52 | 32,9 | 20,91 | 15 | 355,67 | 70,36 |
| Ag107 | 327,04 | 439,37 | 437,04 | 240,6 | 330,55 | 327,38 | 86,73 | 164,86 | 3166,3 | 465,11 |
| Pd108 | 38,06 | 28,19 | A51.21 | 47,24 | 11,61 | 43,08 | 28,01 | 19,64 | 419,01 | 93,65 |
| Ag109 | 322,61 | 382,02 | 392,76 | 238,27 | 342,73 | 330,93 | 87,66 | 166,43 | 3301,03 | 468,7 |
| Pd110 | 1,46 | 1,09 | 2,39 | 1,82 | 0,46 | 1,69 | 1,09 | 0,78 | 9,4 | 3,62 |
| Pt194 | 88,19 | 93,89 | 134,1 | 132,96 | A38.19 | 122,64 | 50,78 | 50,63 | 1555,13 | 220,41 |
| Pt195 | 96,63 | 96,56 | 138,22 | 135,55 | A40 | 129,81 | 53,41 | 52,93 | 1656,66 | 227,33 |
| Pt196 | 98,42 | 98,17 | 138,81 | 138,04 | A41.12 | 131,74 | 54,64 | 53,96 | 1596 | 233,12 |
| Au197 | 202,43 | 167,27 | 293,42 | 251,83 | A90.87 | 236,4 | 167,11 | 149,27 | 1675,06 | 534,37 |
| Pb208 | 128,13 | 134,59 | 146,08 | 128,57 | 119,74 | 126,32 | 146,15 | 138,43 | 260,26 | 453,24 |
| 30//2 | | | | | | | | | | |
| Si29 | 131817,91 | 131817,91 | 131817,91 | 131817,91 | 131817,91 | 131817,91 | 131817,91 | 131817,91 | 131817,91 | 131817,91 |
| Pd104 | 103,9 | 93,7 | 83,73 | 85,7 | 63,28 | 111,98 | 90,57 | 80,37 | 90,3 | 113,57 |
| Pd105 | 107,91 | 95,05 | 84,9 | 86,18 | 62,92 | 114,28 | 92,02 | 80,6 | 90,85 | 115,08 |
| Pd106 | 12,06 | 10,93 | 9,51 | 9,66 | 7,17 | 12,77 | 10,38 | 9,18 | 10,21 | 12,68 |
| Ag107 | 510,54 | 465,45 | 434,58 | 419,3 | 446,13 | 496,95 | 447,65 | 401 | 376,67 | 457,4 |
| Pd108 | 16,29 | 14,59 | 12,87 | 13,25 | 9,9 | 17,48 | 14,07 | 12,55 | 13,6 | 17,5 |
| Ag109 | 505,41 | 476,93 | 441,56 | 417 | 452,51 | 484,92 | 467,23 | 410,97 | 358,17 | 454,62 |
| Pd110 | 0,657 | 0,615 | 0,522 | 0,537 | 0,409 | 0,727 | 0,591 | 0,515 | 0,555 | 0,695 |
| Pt194 | 67,56 | 54,73 | 36,11 | 30,99 | A19.84 | 55,99 | 49,73 | 37,82 | 44,14 | 52,84 |
| Pt195 | 68,18 | 55,11 | 36,29 | 31,04 | A21.18 | 57,2 | 50,76 | 38,05 | 45,09 | 53,79 |
| Pt196 | 67,26 | 54,71 | 35,99 | 31,3 | A21.62 | 57,06 | 50,63 | 38,04 | 43,72 | 53,19 |
| Au197 | 179,78 | 162,31 | 127,39 | 121,25 | A104.24 | 184,93 | 166,94 | 146,97 | 146,33 | 177,29 |
| Pb208 | 224,36 | 225,78 | 229,68 | 223,09 | 254,68 | 238,47 | 245,23 | 215,4 | 183,17 | 210,77 |
| 30//3 | | | | | | | | | | |
| Si29 | 129761,16 | 129761,17 | 129761,17 | 129761,18 | 129761,18 | 129761,18 | 129761,18 | 129761,17 | 129761,16 | 129761,18 |
| Pd104 | 81,24 | 87,48 | 82,93 | 110,46 | 104 | 84,04 | 135,33 | 110,14 | 109,76 | 118,07 |
| Pd105 | 78,03 | 86,82 | 82,18 | 106,65 | 103,23 | 79,63 | 131,64 | 107,44 | 105,71 | 115,15 |
| Pd106 | 40,14 | 44,46 | 43,05 | 54,74 | 52,17 | 41,23 | 66,92 | 54,78 | 54,02 | 57,47 |
| Ag107 | 362,76 | 371,93 | 385,38 | 412,64 | 496,07 | 426,83 | 565,8 | 433,98 | 412,36 | 423,11 |
| Pd108 | 47,83 | 52,85 | 49,23 | 63,89 | 61,42 | 48,4 | 77,5 | 64,69 | 61,55 | 65,94 |
| Ag109 | 379,41 | 402,96 | 400,85 | 448,02 | 461,41 | 435,22 | 466,27 | 426,37 | 378,54 | 391,94 |
| Pd110 | 3,99 | 4,35 | 4,2 | 5,17 | 5,09 | 4,1 | 6,27 | 5,17 | 4,89 | 5,17 |
| Pt194 | 37,89 | 44,44 | 41,44 | 53,92 | 64,73 | 47,34 | A82.07 | 59,58 | 63,31 | 66,55 |
| Pt195 | 38,54 | 45,13 | 41,24 | 54,97 | 66,14 | 47,99 | A82.87 | 61,03 | 63,12 | 67,04 |
| Pt196 | 39,81 | 46,35 | 42,44 | 57,06 | 67,5 | 49,62 | A84.31 | 62,6 | 63,79 | 67,19 |
| Au197 | 161,39 | 168,12 | 165,05 | 197,87 | 212,91 | 168,99 | A225.58 | 198,25 | 205,57 | 215,4 |
| Pb208 | 199,49 | 205,93 | 215,01 | 216,75 | 236,25 | 220,42 | 227,39 | 220,66 | 246,27 | 232,09 |
| 60/2 | | | | | | | | | | |
| Si29 | 142382,05 | 142382,05 | 142382,03 | 142382,05 | 142382,03 | 142382,05 | 142382,05 | 142382,05 | 142382,05 | 142382,05 |
| Pd104 | 108,54 | 86,47 | 79,52 | 69,77 | 72,14 | 67 | 77,13 | 97,79 | 83,63 | 101,19 |

| | | | | | | | | | | |
|---|---|---|---|---|---|---|---|---|---|---|
| Pd105 | 102,49 | 81,27 | 74,41 | 64,83 | 65,31 | 64,95 | 72,85 | 94,78 | 79,57 | 97,85 |
| Pd106 | 53,78 | 42,94 | 38,02 | 33,48 | 34,47 | 35,51 | 38,16 | 49,28 | 40,46 | 50,45 |
| Ag107 | 626,81 | 527,48 | 399,17 | 330,98 | 385,81 | 359,74 | 421,2 | 434,47 | 408,95 | 448,31 |
| Pd108 | 62,78 | 49,86 | 44,66 | 38,96 | 39,86 | 40,41 | 44,46 | 57,07 | 48,31 | 60,54 |
| Ag109 | 613,52 | 521,4 | 392,69 | 338,24 | 380,87 | 365,18 | 408,72 | 426,14 | 387,34 | 441,87 |
| Pd110 | 4,88 | 3,9 | 3,41 | 2,99 | 3,03 | 3,15 | 3,46 | 4,36 | 3,69 | 4,6 |
| Pt194 | 78,47 | 59,19 | 37,4 | 28,74 | 32,69 | 40,65 | 34,27 | 42,04 | 38,88 | 48,03 |
| Pt195 | 79,82 | 60,09 | 37,42 | 29,46 | 32,8 | 40,46 | 34,3 | 42,48 | 38,59 | 48,57 |
| Pt196 | 78,92 | 59,79 | 37,53 | 29,31 | 32,81 | 41,12 | 34,77 | 42,81 | 39,1 | 48,98 |
| Au197 | 207,66 | 172,78 | 142,16 | 123,4 | 128,55 | 143,23 | 150,96 | 166,85 | 153,78 | 165,85 |
| Pb208 | 256,81 | 247,52 | 227,31 | 189,1 | 225,24 | 195,6 | 209,2 | 206,51 | 205,94 | 205,16 |
| 60/3 | | | | | | | | | | |
| Si29 | 144158,3 | 144158,3 | 144158,3 | 144158,3 | 144158,3 | 144158,3 | 144158,3 | 144158,3 | 144158,3 | 144158,3 |
| Pd104 | 100,35 | 94,73 | 54,81 | 102,97 | 103,58 | 80,29 | 77,22 | 102,7 | 79,12 | 57,48 |
| Pd105 | 108,98 | 100,52 | 53,57 | 113,21 | 111,42 | 88,16 | 80,02 | 110,87 | 84,89 | 58,87 |
| Pd106 | 12,02 | 11,12 | 6,09 | 12,11 | 12,29 | 9,31 | 9,07 | 12,21 | 9,38 | 6,73 |
| Ag107 | 532,98 | 583,22 | 486,45 | 545,88 | 558,17 | 509,98 | 450,82 | 525,76 | 496,04 | 435,56 |
| Pd108 | 15,79 | 15 | 8,19 | 16,51 | 16,96 | 12,51 | 11,94 | 16,35 | 12,88 | 9 |
| Ag109 | 545,21 | 583,39 | 498,13 | 572,26 | 575,91 | 512,44 | 463,12 | 521,63 | 459 | 428,73 |
| Pd110 | 0,643 | 0,605 | 0,362 | 0,676 | 0,695 | 0,51 | 0,507 | 0,668 | 0,497 | 0,367 |
| Pt194 | 53,83 | 59,5 | 40,77 | 53,39 | 53,96 | 42,16 | 35,91 | 51,04 | 36,7 | 25,06 |
| Pt195 | 52,56 | 59 | 40,47 | 53,66 | 55,43 | 41,57 | 36,28 | 50,46 | 36,78 | 25,7 |
| Pt196 | 53,52 | 59,25 | 41,27 | 54,17 | 57,75 | 43,44 | 36,56 | 51,38 | 38,38 | 26,59 |
| Au197 | 194,95 | 186,6 | 133,99 | 197,78 | 201,77 | 163,34 | 168,22 | 185,72 | 154,89 | 126,25 |
| Pb208 | 222,06 | 241,14 | 250,24 | 221,66 | 246,83 | 233,16 | 235,99 | 221,34 | 211,42 | 212,21 |
| 150/1 | | | | | | | | | | |
| Si29 | 145794,36 | 145794,36 | 145794,36 | 145794,36 | 145794,36 | 145794,36 | 145794,36 | 145794,36 | 145794,36 | 145794,36 |
| Pd104 | 44,5 | 45,99 | 40,64 | 96,73 | 58,92 | 47,32 | 78,46 | 56,88 | 60,55 | 66,89 |
| Pd105 | 40,21 | 41,06 | 36,58 | 93,73 | 54,63 | 41,76 | 76,38 | 52,25 | 57,39 | 62,61 |
| Pd106 | 21,11 | 21,88 | 19 | 46,84 | 28,47 | 21,73 | 38,34 | 26,54 | 29,15 | 32,25 |
| Ag107 | 461,58 | 426,86 | 456,51 | 688,86 | 528,72 | 444,08 | 672,29 | 502,45 | 582,2 | 536,44 |
| Pd108 | 24,45 | 25,04 | 22,71 | 57,28 | 33,62 | 25,58 | 45,45 | 31,29 | 34,44 | 37,88 |
| Ag109 | 450,42 | 433,81 | 448,76 | 707,45 | 526,54 | 454,5 | 687,94 | 513,85 | 576,34 | 528,58 |
| Pd110 | 1,78 | 1,81 | 1,64 | 4,14 | 2,42 | 1,88 | 3,24 | 2,31 | 2,53 | 2,77 |
| Pt194 | 23,96 | 20,14 | 18,26 | 68,39 | 35,68 | 27,9 | 52,98 | 37,34 | 40,03 | 41,82 |
| Pt195 | 24,29 | 20,12 | 18,39 | 68,74 | 36,24 | 27,84 | 54,06 | 37,87 | 40,71 | 42,7 |
| Pt196 | 24,55 | 20,89 | 18,81 | 69,73 | 36,65 | 29,04 | 55,01 | 38,11 | 41,87 | 43,19 |
| Au197 | 89,7 | 88,53 | 80,78 | 184,6 | 119,8 | 99,92 | 162,89 | 122,86 | 136,21 | 141,89 |
| Pb208 | 190,81 | 182,95 | 190,26 | 197,95 | 181,09 | 186,33 | 179,51 | 179,84 | 180,44 | 185,5 |
| 150/2 | | | | | | | | | | |
| Si29 | 146074,81 | 146074,81 | 146074,81 | 146074,81 | 146074,8 | 146074,81 | 146074,81 | 146074,81 | 146074,81 | 146074,81 |
| Pd104 | 51,34 | 55,46 | 54,34 | 58,13 | 52,23 | 72,67 | 70,9 | 68,88 | 64,35 | 32,37 |
| Pd105 | 46,36 | 51,15 | 49,48 | 53,4 | 48,29 | 67,25 | 67,51 | 64,34 | 60,87 | 27,79 |
| Pd106 | 24,24 | 26,67 | 25,55 | 27,89 | 24,66 | 33,89 | 34,29 | 32,73 | 31,23 | 14,4 |
| Ag107 | 546,7 | 615,76 | 519,06 | 617,65 | 556,96 | 795,8 | 791,99 | 767,1 | 745,54 | 550,63 |
| Pd108 | 28,45 | 30,55 | 30,29 | 31,88 | 28,48 | 39,99 | 39,85 | 38,32 | 36,63 | 17,53 |
| Ag109 | 547,92 | 610,33 | 532,66 | 620,46 | 543,52 | 790,76 | 794,33 | 762,65 | 774,32 | 565,09 |
| Pd110 | 2,05 | 2,21 | 2,15 | 2,25 | 2,05 | 2,88 | 2,88 | 2,7 | 2,67 | 1,265 |
| Pt194 | 28,63 | 32,19 | 25,49 | 36,03 | 26,41 | 50,4 | 50,85 | 47,83 | 44,94 | 15,84 |
| Pt195 | 28,92 | 32,57 | 25,71 | 36,17 | 26,57 | 51,09 | 51,28 | 48,86 | 45,27 | 16,15 |
| Pt196 | 29,67 | 32,44 | 26,23 | 36,71 | 26,86 | 51,52 | 51,78 | 49,57 | 46,75 | 16,67 |
| Au197 | 100,96 | 111,63 | 102,52 | 117,47 | 98,86 | 153,76 | 151,39 | 147,67 | 142,34 | 73,46 |
| Pb208 | 204,67 | 208,43 | 204,86 | 209,96 | 199,95 | 201,05 | 205,49 | 200,54 | 189,24 | 165,44 |
| 150/4 | | | | | | | | | | |
| Si29 | 157901,02 | 157901,02 | 157901,02 | 157901,02 | 157901,02 | 157901 | 157901 | 157901 | 157901 | 157901 |
| Zn67 | 30148,96 | 31169,66 | 27582,38 | 29368,11 | 27694,42 | 27956,58 | 27875,47 | 27661,93 | 27197,29 | 27496,76 |
| Zn70 | 521,16 | 529,82 | 475,2 | 500,33 | 482,67 | 483,04 | 479,11 | 476,43 | 466,6 | 479,52 |
| Pd104 | 62,81 | 42,37 | 62,92 | 49,13 | 60,51 | 49,35 | 52,08 | 55,51 | 43,68 | 48,44 |
| Pd105 | 51,04 | 31,9 | 51,6 | 38,14 | 48,55 | 38,16 | 41,63 | 44,4 | 34,22 | 37,71 |
| Pd106 | 6,53 | 4,18 | 6,65 | 4,99 | 6,29 | 4,95 | 5,38 | 5,8 | 4,44 | 4,94 |
| Ag107 | 573,24 | 419,42 | 507,3 | 473,32 | 580,57 | 510,7 | 513,66 | 494,52 | 484,65 | 512,26 |
| Pd108 | 8,62 | 5,38 | 8,69 | 6,42 | 8,2 | 6,35 | 7,09 | 7,44 | 5,7 | 6,46 |
| Ag109 | 583,79 | 411,76 | 489,62 | 435,3 | 555,58 | 494,36 | 505,35 | 485,6 | 444,73 | 499,07 |

| | | | | | | | | | | |
|---|---|---|---|---|---|---|---|---|---|---|
| Pd110 | 0,311 | 0,201 | 0,319 | 0,233 | 0,296 | 0,239 | 0,258 | 0,283 | 0,212 | 0,233 |
| Pt194 | 47,17 | 23,9 | 39,8 | 28,48 | 39,76 | 28,24 | 27,35 | 35,96 | 22,15 | 29,31 |
| Pt195 | 46,9 | 23,73 | 39,95 | 28,28 | 40,32 | 28,59 | 28,07 | 36,1 | 22,35 | 29,8 |
| Pt196 | 46,1 | 23,01 | 39,13 | 27,59 | 39,28 | 27,79 | 27,25 | 34,91 | 21,94 | 29,23 |
| Au197 | 140,99 | 101,2 | 135,56 | 108,02 | 122,83 | 106,26 | 112,54 | 121,34 | 94,72 | 108,74 |
| Pb208 | 182,09 | 199,76 | 199,59 | 171,91 | 194,07 | 181,54 | 170,95 | 171,95 | 188,91 | 185,93 |
| 150/5 | | | | | | | | | | |
| Si29 | 148739,23 | 148739,23 | 148739,22 | 148739,23 | 148739,23 | 148739,23 | 148739,23 | 148739,23 | 148739,23 | 148739,22 |
| Zn67 | 31574,23 | 30007,42 | 30227,41 | 30447,95 | 30249,02 | 31360,29 | 30882,17 | 31875,31 | 36406,02 | 36461,9 |
| Zn70 | 547,94 | 516,65 | 521,69 | 523,86 | 523,04 | 544,57 | 533,15 | 554,17 | 626,69 | 622,72 |
| Pd104 | 63,53 | 55,8 | 63,33 | 49,82 | 59,88 | 71,89 | 66,63 | 75,38 | 20,68 | 12,29 |
| Pd105 | 55,4 | 47,32 | 56,46 | 42,68 | 52,9 | 62,76 | 57,88 | 66,25 | 12,47 | 5,11 |
| Pd106 | 7,15 | 6,16 | 7,3 | 5,47 | 6,71 | 8,08 | 7,63 | 8,66 | 1,57 | 0,546 |
| Ag107 | 698,16 | 625,72 | 679,55 | 571,12 | 658,45 | 740,48 | 677,18 | 755,96 | A1015.6 | A1225.53 |
| Pd108 | 9,44 | 8,14 | 9,43 | 7,31 | 8,92 | 10,71 | 9,94 | 11,3 | 1,96 | 0,616 |
| Ag109 | 680,96 | 611,39 | 676,99 | 581,69 | 657,45 | 743,06 | 695,1 | 770,81 | A1019.87 | A1263.23 |
| Pd110 | 0,348 | 0,299 | 0,355 | 0,271 | 0,334 | 0,402 | 0,375 | 0,432 | 0,0779 | 0,0274 |
| Pt194 | 45,02 | 39,19 | 45,72 | 35,2 | 41,29 | 50,55 | 46,67 | 53,7 | 6,78 | 0,689 |
| Pt195 | 45,39 | 39,63 | 46,31 | 35,12 | 41,88 | 51,38 | 46,94 | 54,39 | 6,86 | 0,649 |
| Pt196 | 44,74 | 39,37 | 45,47 | 34,5 | 41,23 | 50,3 | 46,41 | 53,78 | 6,85 | 0,682 |
| Au197 | 166,5 | 146,03 | 162,49 | 130,13 | 154,36 | 206,55 | 191,92 | 207,73 | 23,8 | 2,77 |
| Pb208 | 186,35 | 183,59 | 182,65 | 185,73 | 182,83 | 188,52 | 181,39 | 193,97 | 969,63 | 1060,48 |
| 300/1 | | | | | | | | | | |
| Si29 | 149674,08 | 149674,09 | 149674,09 | 149674,08 | 149674,09 | 149674,09 | 149674,09 | 149674,09 | 149674,09 | 149674,09 |
| Pd104 | A23.3 | 40,36 | 35,34 | 36,56 | 51,14 | 68,77 | 29,99 | 87,84 | 46,85 | 30,9 |
| Pd105 | A15.78 | 31,43 | 27,01 | 29,08 | 42,86 | 58,95 | 21,67 | 72,13 | 35,07 | 21,38 |
| Pd106 | A1.95 | 3,85 | 3,27 | 3,42 | 5,14 | 6,88 | 2,57 | 8,23 | 3,97 | 2,51 |
| Ag107 | A266.23 | 470,83 | 487,79 | 357,98 | 429,81 | 519,24 | 379,06 | 565,42 | 321,47 | 264,67 |
| Pd108 | A2.61 | 5,02 | 4,4 | 4,74 | 6,84 | 9,41 | 3,34 | 10,97 | 5,09 | 3,14 |
| Ag109 | 264,81 | 442,68 | 500,37 | 356,14 | 404,99 | 527,58 | 351,92 | 446,13 | 288,32 | 247,4 |
| Pd110 | 0,0882 | 0,18 | 0,161 | 0,165 | 0,255 | 0,344 | 0,118 | 0,394 | 0,178 | 0,113 |
| Pt194 | A9.19 | 25,13 | 17,56 | 19,41 | 31,58 | 47,25 | 13,3 | 60,98 | 25,1 | 13,6 |
| Pt195 | A9.29 | 24,98 | 17,44 | 19,54 | 31,74 | 48,16 | 13,67 | 60,75 | 25,27 | 13,73 |
| Pt196 | A8.95 | 24,85 | 17,59 | 19,38 | 31,53 | 47,61 | 13,43 | 59,62 | 24,92 | 13,51 |
| Au197 | A40.43 | 81,75 | 70,2 | 65,81 | 95,33 | 126,4 | 57,67 | 160,67 | 87,04 | 54,84 |
| Pb208 | 240,7 | 207,02 | 412,8 | 204,89 | 189,19 | 183,75 | 222,66 | 227,23 | 233,85 | 282,78 |
| 300/2 | | | | | | | | | | |
| Si29 | 148739,2 | 148739,2 | 148739,2 | 148739,2 | 148739,2 | 148739,2 | 148739,2 | 148739,2 | 148739,2 | 148739,2 |
| Zn67 | 27199,03 | 26717,92 | 26551,47 | 25797 | 26632,33 | 26851,79 | 26984,54 | 27420,25 | 26078,96 | 26249,52 |
| Zn70 | 465,01 | 453,54 | 449,13 | 445,74 | 456,6 | 458,58 | 453,37 | 461,61 | 446,2 | 437,97 |
| Pd104 | 22,04 | 13,19 | 29,39 | 18,51 | 36,52 | 18,74 | 28,88 | 21,15 | 20,54 | 7,94 |
| Pd105 | 18,01 | 8,05 | 27,1 | 13,7 | 33,78 | 13,96 | 26,07 | 17,31 | 16,63 | 2,03 |
| Pd106 | 2,22 | 1,061 | 3,17 | 1,728 | 3,93 | 1,72 | 3,23 | 2,075 | 2,04 | 0,4 |
| Ag107 | 543 | 416,87 | A841.49 | 484,06 | 673,39 | 534,88 | 638,02 | 566,86 | 466,07 | 159,63 |
| Pd108 | 2,89 | 1,303 | 4,22 | 2,226 | 5,22 | 2,213 | 4,12 | 2,62 | 2,64 | 0,408 |
| Ag109 | 555,08 | 411,94 | A847.72 | 483,15 | 671,41 | 527,51 | 648,31 | 555,99 | 475,44 | 158 |
| Pd110 | 0,1016 | 0,044 | 0,1522 | 0,0771 | 0,1883 | 0,075 | 0,1548 | 0,0929 | 0,0955 | 0,01007 |
| Pt194 | 7,74 | 1,358 | 8,66 | 6,13 | 20,33 | 4,97 | 11,82 | 6,9 | 8,15 | 0,852 |
| Pt195 | 7,52 | 1,374 | 8,56 | 5,85 | 20,21 | 4,9 | 11,84 | 6,73 | 7,9 | 0,87 |
| Pt196 | 7,52 | 1,336 | 8,32 | 6,06 | 20,13 | 4,78 | 11,93 | 6,66 | 7,73 | 0,884 |
| Au197 | 22,95 | 8,28 | 27,79 | 19,03 | 46,49 | 15,13 | 32,48 | 20,19 | 21,87 | 3,55 |
| Pb208 | 442,12 | 418,54 | 420,73 | 413,05 | 423,71 | 439,29 | 431,53 | 425,75 | 420,87 | 391,3 |
| 300/3 | | | | | | | | | | |
| Si29 | 157012,95 | 157012,94 | 157012,94 | 157012,94 | 157012,94 | 157012,94 | 157012,94 | 157012,94 | 157012,92 | 157012,92 |
| Zn67 | 20840,04 | 21423,04 | 24387,7 | 23572,48 | 19811 | 20233,33 | 23152,58 | 22355,28 | 21433,96 | 23059,34 |
| Zn70 | 356,03 | 363,38 | 419,9 | 400,14 | 336,04 | 345,73 | 390,62 | 386,1 | 373,53 | 395,56 |
| Pd104 | 14,83 | 13,23 | 24,33 | 24,45 | 24,31 | 26,83 | 11,91 | 28,85 | 25,07 | 28,42 |
| Pd105 | 10,54 | 9,62 | 18,63 | 20,22 | 20,32 | 22,8 | 6,99 | 23,9 | 20,73 | 23,6 |
| Pd106 | 1,38 | 1,223 | 2,49 | 2,63 | 2,61 | 2,94 | 0,938 | 3,04 | 2,72 | 3,11 |
| Ag107 | 364,26 | 407,56 | 408,44 | 419,79 | 468,38 | 486,26 | 339,86 | 543,27 | 427,47 | 374,39 |
| Pd108 | 1,79 | 1,493 | 3,17 | 3,31 | 3,37 | 3,73 | 1,153 | 3,93 | 3,55 | 3,99 |
| Ag109 | 369,99 | 419,75 | 415,87 | 413 | 452,66 | 475 | 346,84 | 552,74 | 422,76 | 376,62 |
| Pd110 | 0,0629 | 0,0558 | 0,1187 | 0,1247 | 0,1182 | 0,1403 | 0,0409 | 0,1466 | 0,13 | 0,1438 |

| | | | | | | | | | | |
|---|---|---|---|---|---|---|---|---|---|---|
| Pt194 | 3,55 | 2,1 | 8,59 | 9,39 | 13,25 | 15,4 | 4,24 | 14,25 | 12,15 | 14,69 |
| Pt195 | 3,55 | 2,13 | 8,73 | 9,46 | 13,34 | 15,72 | 4,26 | 14,11 | 12,36 | 14,57 |
| Pt196 | 3,51 | 2,08 | 8,65 | 9,34 | 13,27 | 15,51 | 4,19 | 14,03 | 12,31 | 14,31 |
| Au197 | 15,47 | 10,69 | 28,62 | 29,9 | 44,9 | 48,52 | 17,7 | 43,64 | 40,79 | 47,81 |
| Pb208 | 330,87 | 386,76 | 536,06 | 452,07 | 154,3 | 168,5 | 253,01 | 329,84 | 309,97 | 306,21 |
| 300/4 | | | | | | | | | | |
| Si29 | 151123,17 | 151123,17 | 151123,17 | 151123,17 | 151123,17 | 151123,17 | 151123,17 | 151123,17 | 151123,16 | 151123,16 |
| Zn67 | 25599,3 | 25933,36 | 26137,32 | 26325,25 | 26954,37 | 26898,09 | 27281,64 | 25892,05 | 25810,88 | 23167,15 |
| Zn70 | 443,27 | 447,06 | 450,19 | 456,32 | 461,19 | 464,33 | 472,04 | 454,99 | 443,58 | 390,61 |
| Pd104 | 16,8 | 26,35 | 28,81 | 23,67 | 10,36 | 19,07 | 21,11 | 10,19 | 12,57 | 14,14 |
| Pd105 | 9,8 | 19,36 | 21,63 | 16,18 | 3,52 | 12,19 | 13,02 | 3,33 | 5,63 | 9,12 |
| Pd106 | 1,314 | 2,5 | 2,74 | 2,12 | 0,602 | 1,65 | 1,81 | 0,565 | 0,856 | 1,253 |
| Ag107 | 453,81 | 458,93 | 555,79 | 530,16 | 137,13 | 443,98 | 395,78 | 183,69 | 121,18 | 273,29 |
| Pd108 | 1,67 | 3,27 | 3,65 | 2,76 | 0,726 | 2,09 | 2,36 | 0,653 | 0,998 | 1,53 |
| Ag109 | 456,57 | 453,55 | 566,34 | 513,51 | 136,52 | 443,64 | 393,47 | 183,85 | 121,12 | 280,55 |
| Pd110 | 0,058 | 0,1176 | 0,1345 | 0,0973 | 0,0239 | 0,0764 | 0,0807 | 0,0209 | 0,0366 | 0,0518 |
| Pt194 | 1,42 | 9,91 | 9,24 | 4,82 | 1,9 | 5,6 | 6,22 | 2,13 | 3,98 | 2,75 |
| Pt195 | 1,4 | 9,81 | 9,25 | 4,94 | 1,9 | 5,52 | 6,04 | 2,09 | 3,9 | 2,64 |
| Pt196 | 1,31 | 9,79 | 9,1 | 4,73 | 1,92 | 5,47 | 6,02 | 2,17 | 3,83 | 2,67 |
| Au197 | 9,6 | 31,01 | 35,47 | 20,02 | 6,08 | 22,7 | 25,48 | 7,87 | 13,2 | 11,58 |
| Pb208 | 418,11 | 425,73 | 438,51 | 470,66 | 416,24 | 431,6 | 441,53 | 411,04 | 422,42 | 391,8 |

Table 11. LA-ICP-MS data for slag in argon atmosphere (in ppm).

| Ar5/1 | | | | | | | | | | | |
|---|---|---|---|---|---|---|---|---|---|---|---|
| Si29 | 154348,47 | 154348,47 | 154348,47 | 154348,48 | 154348,47 | 154348,47 | 154348,47 | 154348,47 | 154348,47 | 154348,47 | 154348,45 |
| Zn67 | 26639,01 | 27868,53 | 31133,35 | 30516,55 | 27204,13 | 18423,1 | 29250,19 | 30023,3 | 27449,74 | 27376,07 | 28748,73 |
| Zn70 | 424,07 | 446,57 | 508,55 | 511,45 | 440,45 | 303,19 | 495 | 505,5 | 455,84 | 435,8 | 456,68 |
| Pd104 | 54,36 | 51,07 | 49,12 | 56,27 | 45,61 | 41,28 | 52,79 | 54,24 | 52,92 | 52,02 | 59,27 |
| Pd105 | 47,75 | 44,42 | 39,84 | 48,88 | 38,42 | 35,96 | 44,85 | 45,62 | 46,27 | 43,18 | 50,24 |
| Pd106 | 6,67 | 6,39 | 5,71 | 6,77 | 5,62 | 5,2 | 6,56 | 6,67 | 6,56 | 6,35 | 7,3 |
| Ag107 | 535,23 | 533,71 | 480,54 | 567,35 | 519,63 | 380,36 | 564,05 | 586,77 | 559,91 | 511,77 | 555,35 |
| Pd108 | 8,71 | 8,86 | 7,18 | 9,12 | 7,33 | 6,79 | 8,39 | 8,74 | 8,6 | 7,87 | 9,42 |
| Ag109 | 522,35 | 525,94 | 476,75 | 556,47 | 501,38 | 367,22 | 552,52 | 587,84 | 549,18 | 507,97 | 551,16 |
| Pd110 | 0,308 | 0,307 | 0,2812 | 0,339 | 0,2633 | 0,2587 | 0,316 | 0,308 | 0,311 | 0,299 | 0,35 |
| Pt194 | 21,14 | 21,24 | 11,24 | 16,33 | 20,1 | 21,46 | 22,23 | 22,36 | 24,15 | 21,47 | 23,17 |
| Pt195 | 20,87 | 21,38 | 11,48 | 16,52 | 20,07 | 21,12 | 22,46 | 22,55 | 24,26 | 22,26 | 23,37 |
| Pt196 | 20,76 | 21,33 | 11,52 | 16,41 | 20,1 | 21,26 | 22,28 | 22,41 | 24,07 | 21,97 | 23,06 |
| Au197 | 119,09 | 119,53 | 99,11 | 122,62 | 105,51 | 83,71 | 123,27 | 127,4 | 125,81 | 109,56 | 131,52 |
| Pb208 | 103,45 | 103,75 | 138,84 | 137,97 | 105,85 | 82,57 | 128,18 | 139,14 | 122,79 | 123,04 | 129,31 |
| Ar5/2 | | | | | | | | | | | |
| Si29 | 154722,42 | 154722,42 | 154722,42 | 154722,42 | 154722,42 | 154722,42 | 154722,42 | 154722,42 | 154722,41 | 154722,42 | 154722,42 |
| Zn67 | 27902,63 | 29368,03 | 30304,18 | 37062,73 | 29664,39 | 29240,77 | 29016,66 | 25895,65 | 30378,57 | 25912,73 | 15721,15 |
| Zn70 | 471,44 | 498,14 | 523,5 | 625,01 | 506,48 | 473,94 | 490,26 | 438,88 | 490,85 | 419,89 | 256,97 |
| Pd104 | 60,36 | 60,57 | 61,23 | 57,84 | 51,24 | 58,08 | 58,22 | 44,17 | 41,83 | 60,85 | 45,23 |
| Pd105 | 47,92 | 48,41 | 47,73 | 43,42 | 38,51 | 46,87 | 45,34 | 32,76 | 29,94 | 47,33 | 35,79 |
| Pd106 | 6,3 | 6,54 | 6,7 | 6,11 | 5,34 | 6,24 | 6,07 | 4,53 | 4,12 | 6,15 | 4,99 |
| Ag107 | 562,67 | 574,32 | 590,04 | 537,07 | 446,98 | 564,71 | 558,71 | 391,35 | 454,39 | 570,21 | 421,79 |
| Pd108 | 8,3 | 8,43 | 8,62 | 7,85 | 6,95 | 8,35 | 8 | 6,04 | 5,33 | 8,26 | 6,58 |
| Ag109 | 559,95 | 570,31 | 596,61 | 540,6 | 454,23 | 571,43 | 557,62 | 396,01 | 468,24 | 582,52 | 429,3 |
| Pd110 | 0,296 | 0,306 | 0,316 | 0,318 | 0,246 | 0,292 | 0,297 | 0,221 | 0,188 | 0,291 | 0,238 |
| Pt194 | 21,73 | 21,93 | 21,56 | 30,75 | 18,77 | 21,5 | 21,28 | 15,85 | 14,54 | 20,57 | 16,64 |
| Pt195 | 20,86 | 21,73 | 21,14 | 30,16 | 18,39 | 20,97 | 20,56 | 15,12 | 14,36 | 20,43 | 16,16 |
| Pt196 | 21,26 | 21,89 | 21,27 | 30,12 | 18,53 | 21,6 | 21,21 | 15,73 | 14,63 | 20,47 | 16,59 |
| Au197 | 118,23 | 122,01 | 125,24 | 123,31 | 99,44 | 119,23 | 118,73 | 89,91 | 89,97 | 125,22 | 91,99 |
| Pb208 | 112,48 | 118,85 | 122,77 | 185,98 | 131,5 | 126,05 | 124,24 | 99,86 | 119,4 | 106,54 | 67,91 |
| Ar10/1 | | | | | | | | | | | |
| Si29 | 151123,13 | 151123,11 | 151123,11 | 151123,13 | 151123,11 | 151123,13 | 151123,11 | 151123,14 | 151123,14 | 151123,14 | 151123,14 |
| Zn67 | 7904,15 | 7152,98 | 7146,6 | 7473,76 | 6472,77 | 10456,63 | 11024,11 | 10006,29 | 9508,62 | 9817,47 | 7750,79 |
| Zn70 | 127,29 | 115,51 | 114,17 | 120,24 | 106,16 | 170,13 | 178,38 | 161,21 | 153,51 | 159,24 | 125,5 |
| Pd104 | 25,82 | 29,97 | 32,34 | 37,33 | 34,8 | 21,51 | A17.19 | 38,1 | 26,93 | 26,93 | 37,87 |
| Pd105 | 25,53 | 30,83 | 32,32 | 38,53 | 35,59 | 20,77 | A15.66 | 37,85 | 26,47 | 25,77 | 38,48 |
| Pd106 | 3,46 | 4,24 | 4,42 | 5,29 | 4,68 | 2,81 | A2.2 | 5,29 | 3,72 | 3,69 | 5,38 |
| Ag107 | 327,73 | 377,81 | 387,08 | 411,92 | 395,64 | 284,72 | A244.03 | 457,09 | 350,16 | 370,05 | 419,74 |
| Pd108 | 4,57 | 5,51 | 5,81 | 6,92 | 6,38 | 3,73 | A2.83 | 6,58 | 4,92 | 4,68 | 6,79 |
| Ag109 | 329,25 | 369,7 | 381,93 | 413,96 | 383,82 | 278,36 | A243.4 | 453,27 | 345,76 | 369,09 | 417,62 |
| Pd110 | 0,1629 | 0,1973 | 0,2059 | 0,2532 | 0,2294 | 0,132 | A0.1044 | 0,2502 | 0,1812 | 0,1748 | 0,25 |
| Pt194 | 9,77 | 11,87 | 12,12 | 13,63 | 12,3 | 8,77 | A6.69 | 15,21 | 10,13 | 9,83 | 13,71 |
| Pt195 | 10,1 | 11,75 | 12,07 | 13,59 | 12,42 | 8,63 | A6.74 | 15,31 | 10,49 | 9,94 | 14,03 |
| Pt196 | 9,58 | 11,49 | 11,74 | 13,46 | 12,21 | 8,52 | A6.52 | 15,17 | 10,13 | 9,88 | 13,92 |
| Au197 | 68,57 | 78,86 | 79,91 | 90,97 | 83,81 | 58,78 | A51.52 | 94,92 | 68,8 | 73,43 | 91,19 |
| Pb208 | 26,85 | 26,97 | 26,46 | 27,2 | 24,39 | 31,7 | 35,29 | 36,27 | 32,54 | 33,94 | 28,79 |

| Ar20/2 | | | | | | | | | | |
|---|---|---|---|---|---|---|---|---|---|---|
| Si29 | 151310,09 | 151310,08 | 151310,09 | 151310,08 | 151310,08 | 151310,08 | 151310,09 | 151310,09 | 151310,08 | 151310,11 |
| Zn67 | 491,86 | 658,4 | 717,8 | 763,22 | 1442,35 | 2193,05 | 1162,76 | 1046,39 | 973,39 | 968,85 |
| Zn70 | 8,02 | 11,16 | 12,05 | 12,7 | 23,56 | 36,85 | 18,97 | 17,75 | 15,83 | 15,97 |
| Pd104 | 27 | 25,82 | 62,46 | 37,19 | 17,18 | 24,02 | 30,41 | 22,42 | 18,05 | 29,63 |
| Pd105 | 25,8 | 23,61 | 58,53 | 36,1 | 15,89 | 22,01 | 29,12 | 20,13 | 16,74 | 26,69 |
| Pd106 | 3,19 | 2,96 | 7,6 | 4,33 | 1,95 | 2,82 | 3,81 | 2,63 | 2,12 | 3,44 |
| Ag107 | 309,6 | 310,75 | 522,56 | 432,48 | 264,72 | 319,77 | 393,68 | 286,77 | 282,56 | 372,2 |
| Pd108 | 4,31 | 4,18 | 9,82 | 6,05 | 2,55 | 3,74 | 5 | 3,44 | 2,97 | 4,49 |
| Ag109 | 310,56 | 309,62 | 507,33 | 432,74 | 263,54 | 322,9 | 393,38 | 284,39 | 279,9 | 379,12 |
| Pd110 | 0,1544 | 0,1458 | 0,344 | 0,216 | 0,0949 | 0,1383 | 0,1781 | 0,1266 | 0,1027 | 0,1697 |
| Pt194 | 6,05 | 6,1 | 8,81 | 8,47 | 5,33 | 5,69 | 8,17 | 6,28 | 4,6 | 6,62 |
| Pt195 | 5,93 | 6,03 | 8,58 | 8,56 | 5,06 | 5,85 | 7,76 | 6,03 | 4,73 | 6,47 |
| Pt196 | 5,74 | 5,68 | 8,74 | 8,32 | 5,2 | 5,69 | 7,71 | 6,03 | 4,4 | 6,46 |
| Au197 | 52,07 | 53,12 | 64,23 | 71,43 | 40,87 | 49,72 | 61,18 | 44,64 | 40,54 | 58,73 |
| Pb208 | 2,85 | 3,82 | 5,56 | 4,86 | 9,8 | 16,67 | 7,84 | 6,58 | 6,12 | 6,22 |
| Ar40/1 | | | | | | | | | | |
| Si29 | 153133,13 | 153133,13 | 153133,13 | 153133,13 | 153133,13 | 153133,13 | 153133,13 | 153133,13 | 153133,11 | 153133,13 |
| Zn67 | 61,36 | 56,63 | 49,23 | 54,45 | 57,8 | 58,07 | 67,3 | 64 | 56,06 | 52,93 |
| Zn70 | 1,116 | 0,894 | 0,8 | 1,019 | 0,953 | 0,986 | 1,155 | 1,085 | 0,903 | 0,846 |
| Pd104 | 29,91 | 20,8 | 23,78 | 27,59 | 29,89 | 25,12 | 16,2 | 21,15 | 20,69 | 26,63 |
| Pd105 | 27,82 | 20,11 | 21,56 | 25,57 | 28,67 | 23,72 | 14,76 | 19,81 | 19,74 | 23,68 |
| Pd106 | 3,92 | 2,83 | 3,21 | 3,76 | 4,1 | 3,31 | 2,06 | 2,69 | 2,76 | 3,59 |
| Ag107 | 377,38 | 298,85 | 283,68 | 374,24 | 419,39 | 392,52 | 292,08 | 365,07 | 293,78 | 367 |
| Pd108 | 5,07 | 3,75 | 4,26 | 4,93 | 5,26 | 4,43 | 2,61 | 3,67 | 3,8 | 4,5 |
| Ag109 | 380,33 | 298,95 | 282,22 | 374,98 | 420,93 | 390,55 | 287,19 | 368,64 | 293,15 | 372,28 |
| Pd110 | 0,1916 | 0,1393 | 0,1552 | 0,1801 | 0,1879 | 0,1524 | 0,0956 | 0,1325 | 0,1346 | 0,1646 |
| Pt194 | 4,52 | 3,28 | 3,98 | 4,24 | 4,75 | 3,82 | 2,83 | 3,25 | 3,14 | 3,77 |
| Pt195 | 4,3 | 3,37 | 3,97 | 4,39 | 4,68 | 3,87 | 2,91 | 3,32 | 3,38 | 3,81 |
| Pt196 | 4,53 | 3,12 | 4,14 | 4,45 | 4,75 | 3,73 | 2,9 | 3,37 | 3,2 | 3,9 |
| Au197 | 50,06 | 37,86 | 36,9 | 48,32 | 52,74 | 45,71 | 31,03 | 37,94 | 35,28 | 43,75 |
| Pb208 | 0,1325 | 0,1138 | 0,1041 | 0,1294 | 0,1792 | 0,218 | 0,221 | 0,231 | 0,259 | 0,1873 |
| Ar40/2 | | | | | | | | | | |
| Si29 | 152245 | 152245,02 | 152245,02 | 152245,02 | | | | | | |
| Zn67 | 73,24 | 70,26 | 69,06 | 47,6 | | | | | | |
| Zn70 | 1,255 | 1,136 | 1,05 | 0,912 | | | | | | |
| Pd104 | 17,39 | 22,57 | 19,28 | 36,05 | | | | | | |
| Pd105 | 15,22 | 18,26 | 17,34 | 30,6 | | | | | | |
| Pd106 | 2,16 | 2,67 | 2,48 | 4,39 | | | | | | |
| Ag107 | 290,94 | 331,78 | 296,09 | 366,42 | | | | | | |
| Pd108 | 2,93 | 3,54 | 3,2 | 5,87 | | | | | | |
| Ag109 | 291,87 | 333,84 | 293,11 | 361,74 | | | | | | |
| Pd110 | 0,108 | 0,1277 | 0,1106 | 0,2165 | | | | | | |
| Pt194 | 2,8 | 3,15 | 2,95 | 3,19 | | | | | | |
| Pt195 | 2,78 | 3,26 | 3,02 | 3,15 | | | | | | |
| Pt196 | 2,64 | 3,19 | 3,24 | 3,1 | | | | | | |
| Au197 | 30,83 | 36,48 | 35,23 | 36,35 | | | | | | |
| Pb208 | 0,0955 | 0,0766 | 0,0751 | 0,0651 | | | | | | |

Table 12. LA-ICP-MS data for slag in sample Ar10/2 in argon atmosphere (in ppm).

| Ar10/2 | | | | | | | | | | | | | | |
|---|---|---|---|---|---|---|---|---|---|---|---|---|---|---|
| Si29 | 153320,1 | 153320,1 | 153320,1 | 153320,1 | 153320,1 | 153320,1 | 153320,1 | 153320,1 | 153320,1 | 153320,1 | 153320,1 | 153320,1 | 153320,1 | 153320,1 |
| Zn67 | 3519,45 | 3900,36 | 3364,84 | 4850,4 | 4450,1 | 5714,17 | 5830,83 | 8915,6 | 9265,17 | 9653,46 | 12871,51 | 12691,26 | 12456,85 | 10670,29 |
| Zn70 | 57,29 | 63,44 | 54,27 | 78,75 | 71,42 | 92,7 | 95,43 | 145,01 | 149,75 | 154,83 | 210,05 | 211,11 | 198,99 | 173,2 |
| Pd104 | 39,35 | 39,4 | 40,26 | 44,22 | 40,76 | 32,69 | 34,93 | 45,22 | 44,8 | 42,97 | 37,35 | 46,65 | 40,39 | A86.74 |
| Pd105 | 37,71 | 37,86 | 38 | 41,41 | 38,23 | 28,82 | 32,5 | 41 | 39,81 | 39,29 | 33,59 | 41,25 | 35,71 | A79.05 |
| Pd106 | 4,61 | 4,74 | 4,72 | 5,12 | 4,65 | 3,67 | 4,07 | 5,1 | 5,06 | 4,93 | 4,23 | 5,08 | 4,32 | A9.96 |
| Ag107 | 447,4 | 487,43 | 482,64 | 495,49 | 465,32 | 438,72 | 416,64 | 524,46 | 513,58 | 513,76 | 449,92 | 509,67 | 493,72 | 462,69 |
| Pd108 | 6,31 | 6,48 | 6,33 | 6,86 | 6,39 | 4,88 | 5,41 | 6,72 | 6,79 | 6,75 | 5,69 | 6,91 | 5,86 | A13.65 |
| Ag109 | 443,52 | 488,96 | 473,61 | 491,92 | 459,47 | 432,81 | 416,22 | 506,28 | 516,05 | 509,09 | 448,34 | 494,56 | 481,66 | 465,26 |
| Pd110 | 0,23 | 0,234 | 0,227 | 0,244 | 0,223 | 0,1837 | 0,1993 | 0,241 | 0,253 | 0,24 | 0,206 | 0,252 | 0,207 | A0.474 |
| Pt194 | 10,57 | 11,29 | 10,79 | 12,97 | 11,72 | 11,72 | 10,71 | 13,51 | 14 | 15,06 | 12,86 | 14,82 | 15 | 9,54 |
| Pt195 | 10,81 | 11,48 | 10,66 | 13,33 | 11,64 | 12,24 | 11,06 | 13,65 | 14,16 | 15,09 | 12,79 | 15,78 | 14,87 | 9,54 |
| Pt196 | 10,51 | 11,25 | 10,48 | 12,99 | 11,67 | 11,75 | 10,86 | 13,56 | 13,95 | 15,24 | 12,78 | 14,83 | 14,51 | 9,53 |
| Au197 | 79,25 | 85,16 | 84,72 | 88,05 | 80,8 | 69,75 | 73,18 | 91 | 92,96 | 91,46 | 82,83 | 95,95 | 86,08 | 70,41 |
| Pb208 | 11,5 | 13,01 | 10,42 | 15,93 | 14,95 | 17,78 | 18,56 | 30,64 | 32,09 | 33,27 | 44,05 | 44,76 | 43,13 | 36,7 |

Table 13. LA-ICP-MS data for slag in sample Ar20/1 in argon atmosphere (in ppm).

| Ar20/1 | | | | | | | | | | | | |
|---|---|---|---|---|---|---|---|---|---|---|---|---|
| Si29 | 134622,5 | 134622,5 | 134622,5 | 134622,5 | 134622,5 | 134622,5 | 134622,5 | 134622,5 | 134622,5 | 134622,5 | 134622,5 | 134622,5 |
| Zn67 | 39497,09 | 39510,51 | 38768,98 | 29794,42 | 49471,86 | 32554,01 | 40412,16 | 40668,12 | 42664,26 | 69385,27 | 36454,4 | 34113,11 |
| Zn70 | 674,49 | 655,67 | 655,87 | 485,51 | 808,34 | 522,75 | 682,58 | 662,9 | 707,7 | 1135,08 | 618,96 | 560,75 |
| Pd104 | 64,16 | 48,15 | 93,54 | 360,02 | 56,87 | 158,21 | 226,79 | 299,75 | 137,24 | 659,53 | 99,98 | 543,32 |
| Pd105 | 50,01 | 33,56 | 76,66 | 327,51 | 41,89 | 131,79 | 198,43 | 269,06 | 116,16 | 577,03 | 79,52 | 429,03 |
| Pd106 | 6,86 | 4,89 | 10,3 | 43,26 | 6,09 | 17,48 | 25,37 | 35,19 | 15,4 | 75,54 | 10,6 | 57,7 |
| Ag107 | 289,32 | 164,94 | 228,55 | 368,44 | 367,37 | 209,83 | 476,8 | 546,68 | 304,94 | 871,75 | 345,96 | 519,55 |
| Pd108 | 9,04 | 6,39 | 13,54 | 56,57 | 7,44 | 22,9 | 35,41 | 49,41 | 20,79 | 104,85 | 14,15 | 76,41 |
| Ag109 | 290,59 | 159,96 | 226,87 | 384,29 | 358,71 | 227,32 | 471 | 542,55 | 311,46 | 766,95 | 350,37 | 484,32 |
| Pd110 | 0,366 | 0,266 | 0,535 | 2,22 | 0,35 | 0,862 | 1,31 | 1,74 | 0,827 | 3,84 | 0,591 | 2,82 |
| Pt194 | 23,28 | 15,6 | 29,25 | 11,71 | 18,11 | 101,32 | 95,32 | 45,92 | 47,39 | 177,28 | 35,63 | 126,87 |
| Pt195 | 24,01 | 16,07 | 28,71 | 11,24 | 18,24 | 106,06 | 94,25 | 45,1 | 47,16 | 173,76 | 34,89 | 123,68 |
| Pt196 | 24,15 | 15,81 | 28,12 | 11,23 | 18,08 | 104,53 | 94,47 | 45,15 | 46,57 | 177,84 | 34,42 | 122,97 |
| Au197 | 111,98 | 58,39 | 76,95 | 52,24 | 108,95 | 145,45 | 177,5 | 131,72 | 150,62 | 336,68 | 146,3 | 176,38 |
| Pb208 | 254,33 | 162,47 | 117,14 | 58,52 | 276,7 | 47,85 | 129,3 | 96,85 | 170,54 | 248,16 | 118,05 | 180,3 |

Table 14. SEM-EDS data for silicon and iron in slag in air atmosphere (in wt-%).

| Si (wt%) | | | | | | | | |
|---|---|---|---|---|---|---|---|---|
| 20--2 | 13,76 | 13,6 | 13,7 | 13,53 | 13,79 | 13,41 | 13,54 | |
| 20--3 | 11,03 | 13,42 | 12,73 | | | | | |
| 30--2 | 13,51 | 13,51 | 14,22 | 13,26 | 13,44 | 13,52 | | |
| 30--3 | 12,97 | 12,84 | 13,22 | 13,5 | 13,62 | 13,32 | 13,56 | 13,33 |
| 60--2 | 15,13 | 14,05 | 14,07 | 14,75 | 14,82 | 14,41 | 14,7 | 14,65 |
| 60--3 | 14,55 | 14,27 | 14,46 | 14,42 | 14,33 | | | |
| 150--1 | 15,5 | 15,42 | 15,05 | 15,12 | 14,48 | 14,7 | 14,37 | 14,77 |
| 150--2 | 14,56 | 14,56 | 14,55 | 14,79 | 15 | 14,74 | 14,72 | 14,99 |
| 150--4 | 15,74 | 15,56 | 15,93 | 15,67 | 16,03 | 15,79 | 15,8 | |
| 150--5 | 15,27 | 15,48 | 14,26 | 15,36 | 12,69 | 15,58 | 15,51 | |
| 300--1 | 15,36 | 15,34 | 15,36 | 15,42 | 15,1 | 14,79 | 15,37 | 16,57 |
| 300--2 | 14,31 | 14,54 | 14,29 | 14,26 | 14,36 | 14,45 | 14,22 | 14,45 |
| 300--3 | 15,03 | 15,02 | 15,99 | 16,03 | 14,91 | 15,06 | 15,1 | 15,03 |
| 300--4 | 15,26 | 15,78 | 15,19 | 15,25 | 15,03 | 15 | 14,6 | 14,84 |
| 300--5 | 15,69 | 15,47 | 14,67 | 14,56 | 14,98 | 16,24 | 15,35 | 15,45 |
| 600--1 | 15,19 | 15,22 | 15,23 | 14,36 | 15,31 | 15,09 | | |
| Fe (wt-%) | | | | | | | | |
| 20--2 | 54,21 | 54,05 | 54,64 | 55,21 | 53,19 | 53,98 | 53,61 | |
| 20--3 | 57,16 | 55,28 | 57,09 | | | | | |
| 30--2 | 52,86 | 53,31 | 52,89 | 53,14 | 53,89 | 53,72 | 54,12 | 54,4 |
| 30--3 | 54,17 | 54,38 | 54,13 | 54,16 | 53,26 | 53,5 | 52,91 | 53,5 |
| 60--2 | 51,85 | 52,09 | 52,88 | 53,32 | 51,92 | 52,28 | 52,38 | 52,05 |
| 60--3 | 51,34 | 51,55 | 51,36 | 51,72 | 51,82 | 51,64 | 51,67 | 51,43 |
| 150--1 | 50,87 | 50,9 | 51,36 | 52,01 | 52,24 | 52,32 | 51,82 | 52,11 |
| 150--2 | 51,34 | 51,78 | 51,96 | 51,65 | 50,78 | 51,31 | 51,05 | 51,49 |
| 150--4 | 49,92 | 49,78 | 49,72 | 49,8 | 49,06 | 49,41 | 49,37 | |
| 150--5 | 52,15 | 51,93 | 53,89 | 51,96 | 46,08 | 51,23 | 50,92 | |
| 300--1 | 51,97 | 52,09 | 51,81 | 52,37 | 51,73 | 51,18 | 52,62 | 52,68 |
| 300--2 | 50,98 | 51,18 | 51,08 | 51,16 | 50,61 | 51,08 | 50,85 | 50,94 |
| 300--3 | 48,78 | 49,42 | 49,78 | 49,74 | 49,53 | 49,63 | 49,79 | 49,39 |
| 300--4 | 52,86 | 52,18 | 53,08 | 53,01 | 53,04 | 52,68 | 53,69 | 52,94 |
| 300--5 | 51,53 | 51,74 | 53,7 | 53,8 | 52,01 | 50,31 | 51,53 | 51,17 |
| 600--1 | 50,47 | 50,44 | 51,07 | 51,07 | 50,56 | 50,62 | | |

Table 15. SEM-EDS data for silicon and iron in slag in argon atmosphere (in wt-%).

| Si (wt-%) | | | | | | | | |
|---|---|---|---|---|---|---|---|---|
| 5--1 | 14,86 | 14,78 | 14,72 | 14,66 | 14,71 | 14,74 | 14,8 | 14,8 |
| 5--2 | 14,73 | 14,76 | 14,79 | 14,77 | 14,78 | 14,76 | 14,95 | 14,84 |
| 10--1 | 14,49 | 14,53 | 14,37 | 14,61 | 14,65 | 14,58 | 14,59 | 14,44 |
| 10--2 | 14,96 | 14,37 | 14,4 | 14,37 | 14,37 | 14,32 | 14,48 | 14,48 |
| 20--2 | 14,32 | 14,54 | 14,68 | 14,63 | 14,9 | 15,38 | 14,84 | 14,43 |
| 40--1 | 15,04 | 15,05 | 14,97 | 14,88 | 14,84 | 15,08 | 15,12 | |
| 40--2 | 14,87 | 14,86 | 14,36 | 14,65 | 14,58 | 14,52 | 14,3 | 14,31 |
| Fe (wt-%) | | | | | | | | |
| 5--1 | 48,18 | 48,08 | 48,5 | 47,91 | 48,18 | 48,49 | 48,18 | 48,4 |
| 5--2 | 48,68 | 48,42 | 48,58 | 47,8 | 48,41 | 48,78 | 48,61 | 48,6 |
| 10--1 | 49,66 | 49,72 | 50,8 | 50,78 | 50,26 | 49,37 | 49,49 | 50,18 |
| 10--2 | 48,98 | 48,87 | 48,92 | 48,81 | 49,21 | 49,3 | 50,09 | 49,92 |
| 20--2 | 51,3 | 51,18 | 50,89 | 50,96 | 50,35 | 49,77 | 49,46 | 50,49 |
| 40--1 | 50,73 | 50,22 | 50,12 | 50,81 | 50,47 | 50,91 | 50,38 | |
| 40--2 | 48,94 | 49,47 | 49,72 | 51,42 | 49,9 | 49,49 | 50,02 | 50,68 |